Technische Universität München
TUM School of Engineering and Design

Strategies for the Realisation of Geocentric Regional Epoch Reference Frames

Dipl.-Ing. Alexander Marian Frederik Nicholas Kehm

Vollständiger Abdruck der von der TUM School of Engineering and Design der Technischen Universität München zur Erlangung eines

Doktors der Ingenieurwissenschaften (Dr.-Ing.)

genehmigten Dissertation.

Vorsitz: Prof. Dr.-Ing. Christoph Holst

Prüfer der Dissertation:

1. Prof. Dr.-Ing. habil. Florian Seitz
2. Prof. Dr. Urs Hugentobler
3. Adjunct Prof. Dr. Richard Gross

Die Dissertation wurde am 24.06.2022 bei der Technischen Universität München eingereicht und durch die TUM School of Engineering and Design am 23.10.2022 angenommen.

Abstract

Terrestrial reference frames are the basis for numerous applications such as the determination of positions and movements, for navigation on the ground, at sea, and in the air, as well as for the referencing of geophysical processes, as they give access to the geodetic datum defined by the origin of the coordinate axes, their orientation with respect to the Earth's body, and the scale of the unit of length. They are provided in the form of networks of reference stations whose positions are determined with high precision. Measurements involving the reference stations enable users to relate local observations to the geodetic datum of the reference frame. In this context, regional reference frames, which provide dense networks of reference stations for certain regions, are of particular importance. Reference frames can be parameterised in different ways: Multi-year reference frames are given in the form of station positions at a reference epoch with linear velocities that can be extrapolated to any epoch, including epochs outside the observation period. It should be noted that the linear models usually do not represent the true station movement which means that further correction models are required. Epoch reference frames are realised on an epoch-wise basis (e.g., weekly) and provided in the form of station position time series. The station positions usually reflect the local conditions much better, which makes epoch reference frames particularly interesting for the study of geophysical processes, but they cannot be reliably extrapolated to arbitrary epochs outside the observation period.

The International Terrestrial Reference System (ITRS) defines a geocentric, i.e., the origin coinciding with the Earth's centre-of-mass, three-dimensional cartesian coordinate system, whereby the z-axis coincides with the Earth's mean rotation axis, the x-axis is located in the plane of the Greenwich meridian and the y-axis complements the other two axes to form a right-handed coordinate system. The orientation is based on a definition of the Bureau International de l'Heure 1984 and is maintained via a no-net-rotation condition. The scale of the ITRS is defined as the realisation of the metre via the Geocentric Coordinate Time (SI second).

The realisation of the ITRS in terms of station coordinates in a terrestrial reference frame is done by combining several space-geodetic techniques. These are SLR (Satellite Laser Ranging), VLBI (Very Long Baseline Interferometry), GNSS (Global Navigation Satellite Systems) and DORIS (Doppler Orbitography and Radiopositioning Integrated by Satellite), whereby each technique contributes to the datum realisation with specific strengths. In this context, SLR is of particular importance, as it is the only technique that enables the realisation of the origin with high accuracy, while the other two satellite techniques GNSS and DORIS do not contribute to the realisation of the origin due to

technique-specific deficiencies. For the same reason, the scale has so far been realised by combination of SLR and VLBI only. Due to their good global coverage, the GNSS and DORIS station networks usually contribute to the realisation of the mathematically defined orientation of the coordinate axes with respect to the Earth's body.

The International Terrestrial Reference Frame (ITRF) is parameterised as a multi-year reference frame. Therefore, the datum of the ITRF is a secular realisation of the ITRS, which means in particular that the origin of the ITRF within the observation period agrees only on average with the Earth's instantaneous centre-of-mass and gradually decreases in accuracy when extrapolated outside the observation period. These variations of the ITRF origin with respect to the Earth's centre-of-mass are often denoted as geocentre variation.

The datum of regional reference frames is usually realised by aligning a regional station network to the global ITRF station network. For epoch reference frames, this has the consequence that short-term and periodic variations of station positions do not relate to the Earth's centre-of-mass but to the geometric centre of the station network, which approximately coincides with the Earth's centre-of-figure. The position time series therefore reflect only a part of the actual geophysical signal and must be corrected for the part of the variation of the Earth's centre-of-figure with respect to the Earth's centre-of-mass. This is particularly relevant for applications in (near-)real time, where the observation epochs are naturally outside the observation period of the ITRF, which means that the reference coordinates have to be extrapolated.

This thesis describes a method for direct geocentric realisation of the datum of regional epoch reference frames, which is demonstrated on the example of the Latin American reference frame consisting of a dense GNSS station network. The datum realisation is done by combining the observations of global SLR, VLBI, and GNSS networks, whereby SLR and VLBI are used to realise the origin and the scale, and GNSS is used to realise the orientation. The combination of the respective networks is done via terrestrial measurements of local ties at co-location sites. Due to the fact that the station networks of SLR and VLBI are subject to permanent changes, a filtering approach is implemented to stabilise the estimated geodetic parameters. In the context of the relevance of SLR for the determination of the origin of terrestrial reference frames, further studies show to what extent extending existing solutions by observations to additional satellites contributes to the stabilisation of the geodetic parameters determined by SLR. Simulation studies on a future evolution of the space and ground segments of SLR demonstrate the importance of high-performing global station networks for the reliability of the datum realisation.

Zusammenfassung

Terrestrische Referenzrahmen bilden die Grundlage für zahlreiche Anwendungen wie zum Beispiel die Bestimmung von Positionen und Bewegungen, für die Navigation am Boden, zur See und in der Luft sowie für die Referenzierung geophysikalischer Prozesse, indem sie einen Zugriff auf das geodätische Datum bieten, welches durch den Ursprung der Koordinatenachsen, ihre Orientierung in Bezug auf den Erdkörper und den Maßstab der Längeneinheit definiert ist. Sie werden in Form von Netzen von Referenzstationen, deren Positionen hochgenau bestimmt sind, bereitgestellt. Durch Messungen unter Einbezug der Referenzstationen erhalten Anwender die Möglichkeit, lokale Beobachtungen auf das geodätische Datum des Referenzrahmens zu beziehen. Eine besondere Bedeutung kommt in diesem Zusammenhang regionalen Referenzrahmen zu, welche für bestimmte Regionen dichte Netze von Referenzstationen zur Verfügung stellen. Referenzrahmen können auf verschiedene Weisen parametrisiert werden: Mehrjahresreferenzrahmen sind in Form von Stationspositionen zu einer Referenzepoche mit linearen Geschwindigkeiten gegeben, welche auf jede beliebige Epoche, auch auf Zeitpunkte außerhalb des Beobachtungszeitraums, extrapoliert werden können. Hierbei ist zu beachten, dass die linearen Modelle in der Regel nicht die wahre Stationsbewegung abbilden und somit weitere Korrekturmodelle erforderlich sind. Epochenreferenzrahmen werden epochenweise realisiert (beispielsweise wöchentlich) und in Form von Stationspositionszeitreihen bereitgestellt. Die Stationspositionen spiegeln hierbei im Regelfall wesentlich besser die lokalen Gegebenheiten wider, womit Epochenreferenzrahmen insbesondere für das Studium geophysikalischer Prozesse von Interesse sind, jedoch nicht zuverlässig auf beliebige Epochen außerhalb des Beobachtungszeitraums extrapoliert werden können.

Das Internationale Terrestrische Referenzsystem (ITRS) definiert ein geozentrisch, also mit Ursprung im Massenzentrum der Erde, gelagertes dreidimensionales rechtwinkliges Koordinatensystem, dessen z-Achse mit der mittleren Erdrotationsachse übereinstimmt, dessen x-Achse in der Ebene des Greenwich-Meridians verläuft und dessen y-Achse die beiden anderen Achsen zu einem rechtshändigen Koordinatensystem ergänzt. Die Orientierung beruht auf einer Festlegung des Bureau International de l'Heure 1984 und wird über eine No-Net-Rotation-Bedingung fortgeschrieben. Der Maßstab des ITRS ist als Realisierung des Meters über die geozentrische Koordinatenzeit (SI-Sekunde) definiert.

Die Realisierung des ITRS in Form von Stationskoordinaten in einem terrestrischen Referenzrahmen erfolgt durch Kombination mehrerer geodätischer Weltraumverfahren. Dies sind SLR (Satellite Laser Ranging, Laserentfernungsmessungen zu Satelliten),

VLBI (Very Long Baseline Interferometry, Interferometrie mit sehr langen Basislinien), GNSS (Globale Navigations-Satellitensysteme) und DORIS (Doppler Orbitography and Radiopositioning Integrated by Satellite, Doppler-Orbitbestimmung und Radiopositionierung integriert per Satellit), wobei jedes Verfahren mit technikspezifischen Stärken zur Realisierung des Datums beitragen kann. Eine besondere Bedeutung kommt hierbei SLR zu, da es als einziges Verfahren die Realisierung des Ursprungs mit hoher Genauigkeit ermöglicht, während die anderen beiden Satellitenverfahren GNSS und DORIS aufgrund technikspezifischer Defizite nicht zur Realisierung des Ursprungs beitragen. Aus dem gleichen Grund wird der Maßstab bisher ausschließlich durch die Kombination von SLR und VLBI realisiert. Die GNSS- und DORIS-Stationsnetze tragen aufgrund ihrer guten globalen Verteilung in der Regel zur Realisierung der mathematisch definierten Orientierung der Koordinatenachsen in Bezug auf den Erdkörper bei.

Der Internationale Terrestrische Referenzrahmen (International Terrestrial Reference Frame, ITRF) ist als Mehrjahresreferenzrahmen parametrisiert. Dies bedeutet, dass das Datum des ITRF eine säkulare Realisierung des ITRS darstellt, womit insbesondere der Ursprung des ITRF innerhalb des Beobachtungszeitraums nur im Mittel mit dem wahren Massenzentrum der Erde übereinstimmt und bei Extrapolation außerhalb des Beobachtungszeitraums graduell in der Genauigkeit abnimmt. Die Abweichungen des ITRF-Ursprungs vom Massenzentrum der Erde werden oft als Geozentrumsvariation bezeichnet.

Das Datum regionaler Referenzrahmen wird meist durch Lagerung eines regionalen Stationsnetzes auf dem globalen ITRF-Stationsnetz realisiert. Für Epochenreferenzrahmen hat dies zur Folge, dass kurzzeitige und periodische Variationen von Stationspositionen nicht auf das Massenzentrum der Erde sondern auf das geometrische Zentrum des Stationsnetzes, welches ungefähr mit dem geometrischen Erdmittelpunkt übereinstimmt, bezogen sind. Die Positionszeitreihen spiegeln daher nur einen Teil des tatsächlichen geophysikalischen Signals wider und müssen um den Anteil der Variation des geometrischen Erdmittelpunktes gegenüber dem Massenzentrum korrigiert werden. Dies ist insbesondere für Anwendungen in (Nahe-)Echtzeit relevant, wo die Beobachtungszeitpunkte naturgemäß außerhalb des ITRF-Beobachtungszeitraums liegen, womit die Referenzkoordinaten extrapoliert werden müssen.

Diese Arbeit beschreibt eine Methode zur direkten geozentrischen Realisierung des Datums regionaler Epochenreferenzrahmen, welche am Beispiel des lateinamerikanischen Referenzrahmens, gebildet aus einem dichten GNSS-Stationsnetz, demonstriert wird. Die Datumsrealisierung erfolgt durch Kombination der Beobachtungen globaler SLR-, VLBI- und GNSS-Stationsnetze, wobei SLR und VLBI zur Realisierung von Ursprung und Maßstab und GNSS zur Realisierung der Orientierung dienen. Die Kombination der jeweiligen Netze erfolgt über terrestrische Verbindungsmessungen an Kolokationsstationen. Aufgrund der Tatsache, dass die Stationsnetze von SLR und VLBI ständigen Veränderungen unterliegen, wird zur Stabilisierung der mit ihnen bestimmten geodätischen Parameter ein Filteransatz implementiert. Im Kontext der

Relevanz von SLR für die Bestimmung des Ursprungs terrestrischer Referenzrahmen zeigen weitere Studien, in welchem Umfang die Erweiterung bestehender Lösungen um Beobachtungen zu weiteren Satelliten zur Stabilisierung der mittels SLR bestimmten geodätischen Parameter beiträgt. Simulationsstudien zur zukünftigen Weiterentwicklung des Weltraum- und Bodensegments von SLR demonstrieren die Wichtigkeit leistungsfähiger globaler Stationsnetze für die Zuverlässigkeit der Datumsrealisierung.

Contents

Preface

The content of the present doctoral thesis is structured into an introductory block (Chapt. 1–4) motivating the studies and outlining the basic questions and concepts, two main subject blocks related to the scientific work and results (Chapt. 5–6), and a section providing a summary of the conclusions and an outlook into potential future research (Chapt. 7). Thereby, the thesis frequently refers to three scientific publications first-authored and one scientific publication co-authored by the author of this work, each of them in the context of one of the two subject blocks that build the scientific part of this thesis:

Block 1 (Chapt. 5): Determination of a regional geocentric epoch reference frame for Latin America.

Kehm et al. (2022b■): *Combination Strategy for the Geocentric Realization of Regional Epoch Reference Frames.* Journal of Geophysical Research: Solid Earth, 127(10): e2021JB02388, DOI: 10.1029/2021JB023880. Citations in this work refer to a preprint, DOI: 10.1002/essoar.10511202.1.

Block 2 (Chapt. 6): Satellite Laser Ranging and its relevance for the stable determination of geodetic parameters.

Kehm et al. (2018■): *Future global SLR network evolution and its impact on the terrestrial reference frame.* Journal of Geodesy, 92(6):625–635, DOI: 10.1007/s00190-017-1083-1.

Kehm et al. (2019■): *Future TRFs and GGOS – where to put the next SLR station?* Advances in Geosciences, 50:17–25, DOI: 10.5194/adgeo-50-17-2019.

Bloßfeld et al. (2018■): *Consistent estimation of geodetic parameters from SLR satellite constellation measurements.* Journal of Geodesy, 92(9):1003–1021, DOI: 10.1007/s00190-018-1166-7.

The results presented within this thesis are the outcome of a project that aimed to develop a combination strategy for a geocentric epoch reference frame for Latin America. Besides the published work, the present doctoral thesis provides more information

on the theoretical background, the implemented algorithms, further results which have not yet been published as well as additional discussion of the results.

While subject **Block 1** of this thesis develops a strategy to combine regional epoch reference frames from space-geodetic observations that are routinely available, subject **Block 2** investigates the potential of future enhancements of the space and ground segments of Satellite Laser Ranging (SLR), as this is the space-geodetic technique that is most relevant to realise the datum of terrestrial reference frames. Thereby, the focus is put not only on the stability of the derived datum parameters but also on the consequences for the determination of different geodetic parameter groups in one common adjustment, among them the datum parameters of terrestrial reference frames, the coefficients of the Earth's gravity field model, and the Earth rotation parameters.

The findings from subject **Block 1** and **2** also contributed to a project that aimed to develop a processing strategy to consistently combine final and rapid Earth rotation parameters from space-geodetic techniques, whereby the combined time series served as basis for predictions involving geophysical fluid models. In this context, the findings from subject **Block 2** are of special relevance not only in the view of a more reliable determination of Earth rotation parameters alone but also in view of their joint and consistent determination together with terrestrial reference frames. The realised strategy to combine and predict Earth rotation parameters from multiple space-geodetic techniques, however, is beyond the scope of the present thesis, so the reader may refer to the following three scientific publications with contribution by the author:

Kehm et al. (2022a): *Combination strategy for the consistent final, rapid and predicted Earth rotation parameters.* Submitted to Journal of Geodesy.

Dill et al. (2020): *Evaluating Processing Choices for the Geodetic Estimation of Earth Orientation Parameters with Numerical Models of Global Geophysical Fluids.* Journal of Geophysical Research: Solid Earth, 125(9):e2020JB02002, DOI: `10.1029/2020JB020025`.

Hellmers et al. (2019): *Combination of VLBI Intensive Sessions with GNSS for generating Low Latency Earth Rotation Parameters.* Advances in Geosciences, 50:49–56, DOI: `10.5194/adgeo-50-49-2019`.

The conceptual design of this doctoral thesis is a monographic representation of the scientific work and results. For the sake of readability, those parts of the present text which are directly taken from the publications related to the subject **Block 1** and **2** are placed between symbols marking their beginning (▸) and their end (◂) in the respective colour (see publication list above). The marked blocks cite the original text from the publications but have been harmonised to a common orthography, style (e.g., hyphenation), and referencing (citation style and numbering of figures, tables, and equations, as well as a consistent usage of scientific terms). If smaller parts of these text blocks have been reworded or extended, the modified passages are placed within

squared brackets [...]. Full-text citations stem from those parts of the publications that have been primarily contributed by the author of the present doctoral thesis, while other parts of these works, or parts that have been reformulated to a larger extent, are referenced in the classical way. The captions of figures cited from the above-listed publications start with a mark (▪) in the respective colour (the caption itself thereby may be modified).

Chapter 1 motivates the studies (Sect. 1.1) and outlines the scientific research questions that are addressed within this thesis (Sect. 1.2).

Chapter 2 introduces into the concept of geodetic reference systems and frames. After providing an overview of the historical evolution of the understanding of the Earth's geometry and orientation in space (Sect. 2.1), we introduce the modern concepts of terrestrial reference systems and frames (Sect. 2.2). Afterwards, the main motivation for these studies, the question of the geocentricity of regional reference frames, is discussed (Sect. 2.3).

Chapter 3 is dedicated to the processing and combination of space-geodetic techniques. First, we introduce the space-geodetic techniques and outline their contribution to the realisation of geodetic reference systems (Sect. 3.1). We continue introducing the algorithms of geodetic parameter estimation via the Gauß-Markov model (Sect. 3.2) and motivate the approach chosen for the intra- and inter-technique combination (Sect. 3.3). Having motivated our approach, the algorithms relevant to combine equation systems (Sect. 3.4) and examples for parameter transformations applied to the equation systems (Sect. 3.5) are described in detail.

Chapter 4 introduces the implementation of the algorithms to combine and solve the equation systems. First, we introduce the software packages which are used to create the results of this study (Sect. 4.1), followed by a more detailed introduction into the software packages which are used within the framework of this study to process SLR observations (Sect. 4.2) and to combine and solve the equation systems (Sect. 4.3). The author of the present doctoral thesis is continuously contributing to the development of these two software packages that are also used within the framework of DGFI-TUM's involvement within the Scientific Services of the International Association of Geodesy.

Related to the subject **Block 1**, Chapter 5 outlines the approach developed to realise a regional geocentric epoch reference frame for Latin America, starting with a short introduction of the general idea (Sect. 5.1) followed by a description of the chosen approach in relation to the goals of the study (Sect. 5.2). The following section describes the reprocessing of the space-geodetic input data (Sect. 5.3) that is used as input to the combination. Afterwards, we describe our approach for the inter-technique combination (Sect. 5.4), which includes strategies developed to filter the input data, to assign relative weights to the technique-specific contributions and to perform a datum transfer between the technique-specific networks via local ties. Finally, we discuss the results of this study by contrasting our approach and the geodetic datum realised against independent

solutions and by comparing derived station displacement time series against geophysical loading models (Sect. 5.5). Section 5.6 summarises the findings.

Related to the subject **Block 2**, Chapter 6 is dedicated to SLR as the space-geodetic technique that is most relevant to realise the datum of terrestrial reference frames. First, we provide an overview of the current status and prospects of the SLR space and ground segments (Sect. 6.1) and outline the consequences for the estimation of geodetic parameters. Afterwards, the measurement principle and the applied models for the analysis of SLR observations are explained (Sect. 6.2). We continue with studies on the potential of exploiting more of the observations to the already-existing space segment (Sect. 6.3), followed by introducing a simulation approach (Sect. 6.4) developed to investigate the impact of potential future enhancements of the space (Sect. 6.5) and ground segments of SLR (Sect. 6.6). Section 6.7 summarises the findings from these studies.

Chapter 7 summarises the results, concludes with final remarks, and provides an outlook into potential future research.

1 Introduction

1.1 Background and motivation

Geodesy (from Ancient Greek γεωδαισία "division of the Earth") is the science of measuring and mapping the Earth's surface (Helmert, 1880), which includes the determination of the Earth's shape and orientation in space as well as of its gravity field (Bruns, 1878), and of their temporal changes. As a consequence, the major disciplines of geodesy are commonly structured into the so-called "three pillars of geodesy", namely

(1) Geokinematics, i.e., the description of the geometry of the Earth's surface and its changes,

(2) Earth rotation, i.e., the description of the evolution of the orientation of the Earth's rotation axis and its angular velocity, and

(3) Gravity field, including its temporal variations.

Plag and Pearlman (2009) outline that these three pillars are "intrinsically linked to each other, and [that] they jointly change as a consequence of dynamical processes in the Earth system as a whole." Consequently, the reliable long-term monitoring of, e.g., global change effects and variations in the Earth's rotation via geometric and gravitational measurement systems requires that any measurements, the data processing procedures, and the estimated geodetic or geophysical parameters must relate to a consistent and stable reference that is common to all observation types. This common reference is defined by geodetic reference systems (Fig. 1.1).

For geometric measurements, one differentiates between two types of reference systems: Earth-fixed and space-fixed. Earth-fixed, or terrestrial, reference systems (TRSs) are – as the name already suggests – fixed to the Earth's body, which means that they are co-rotating with the Earth. They serve to describe positions or velocities with respect to the Earth's crust and are commonly used for navigation and positioning purposes, but also serve as the reference for surveying, mapping, or monitoring of processes in the Earth system (Plag and Pearlman, 2009). The TRS adopted by the International Union of Geodesy and Geophysics (IUGG) is the International Terrestrial Reference System (ITRS), which defines a rectangular coordinate axes system with an *origin*, i.e., the reference point of the coordinate axes, an *orientation*, i.e., the direction of the coordinate axes, and a *scale*, i.e., the defined unit of length (Sect. 2.2). The implementation is provided in the International Earth Rotation and Reference Systems Service (IERS) Conventions 2010 (Petit and Luzum, 2010). Space-fixed, or celestial,

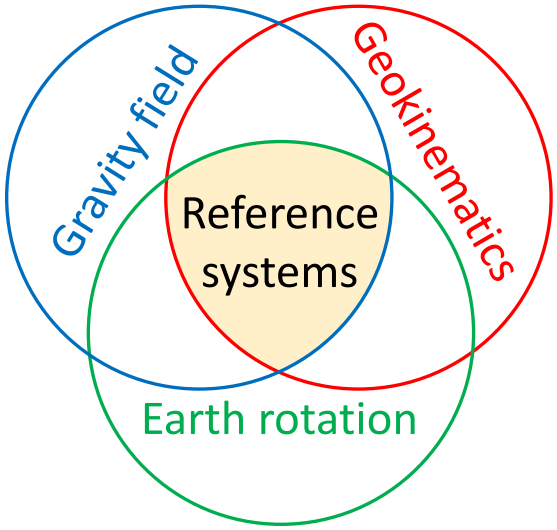

Figure 1.1: The three pillars of geodesy (cf. Rummel, 2000).

reference systems (CRSs), on the other hand, do not co-rotate with the Earth but have an orientation fixed with respect to the (quasi-)inertial space. They are used to model positions and velocities in space and are commonly applied to navigate in space or to describe satellite orbits. The official CRS adopted by the International Astronomical Union (IAU) is the International Celestial Reference System (ICRS; Arias et al., 1995; Petit and Luzum, 2010). While a reference system comprises the theoretical concept that defines the coordinate axis system, its realisation in the form of a set of reference coordinates (cf. Sect. 2.2) is called a reference frame. A realisation of a TRS is thus a terrestrial reference frame (TRF) and a realisation of a CRS is a celestial reference frame (CRF).

The link between a TRS and a CRS is a transformation that necessarily involves the Earth's instantaneous orientation in space, described by the Earth orientation parameters (EOPs; Petit and Luzum, 2010). The EOPs describe the orientation of the Earth's rotation axis with respect to the inertial space in terms of precession and nutation and with respect to the Earth's body in terms of polar motion (PM) and the Earth's angular velocity, namely the absolute offset between the Universal Time UT1 and the Coordinated Universal Time UTC (UT1 – UTC) and its negative time derivative length-of-day (LOD). The latter sub-group, namely PM, UT1 – UTC, and LOD, is called the Earth rotation parameters (ERPs). The ERPs undergo permanent irregular variations and are monitored by various space-geodetic techniques. To ensure a reliable transformation between a CRF and a TRF at any epoch, the ERPs must be determined accurately not only retrospectively and in (near) real time, but also prospectively, in the form of predictions based on deterministic signals derived from the observations and/or geophysical models (e.g., Kehm et al., 2022a).

Due to the fact that most geodetic observations in some way relate to the Earth's gravity field, the natural origin of a TRS is located in the geocentre, i.e., the Earth's centre-of-mass. In this way, a scientific usage of TRFs is to observe and quantify processes related to the Earth system. Examples for these processes of interest are geophysical processes like tectonic deformations including episodic events like earthquakes, seasonal loading, or anthropogenic changes like subsidence due to groundwater withdrawal. In order to be able to relate local observations to a global TRS, two conditions must be fulfilled: first, the station distribution of the TRF must be dense enough to provide a sufficient number of reference stations in or near the region of interest, and second, the TRF datum must be realised in a way that the observed processes can be related to the Earth system in a reliable way. Because of the fact that the station distribution of the global TRF often is too sparse to fulfil the first condition, regional reference frames allow access to the global TRF datum by providing a dense network of reference stations in the region of interest (Sect. 2.3). The fact that the datum of these regional reference frames is usually aligned to a global multi-year TRF solution that realises a secular geocentre – via fiducial coordinates that often have to be linearly extrapolated beyond their actual observation period – raises the issue that derived displacement time series of individual stations in the regional network are not strictly geocentric and, consequently, are limited in their geophysical information content.

In this context, the DFG-funded project *DIrect GEocentric Realisation of the American reference frame by combination of geodetic observation TechnIques* (DIGERATI) asked whether it is possible to realise a geocentric regional epoch reference frame for the Latin America that is

(1) geocentric at any epoch,

(2) realised epoch-wise for short periods,

(3) and stable.

The focus of the present doctoral thesis is to investigate whether a reliable epoch-wise geocentric realisation of the datum for such a regional TRF is possible, exploiting the capabilities of the three space-geodetic techniques Satellite Laser Ranging (SLR), Very Long Baseline Interferometry (VLBI), and Global Navigation Satellite Systems (GNSS). Thereby, SLR is the only space-geodetic technique that allows to determine the TRF origin with high accuracy, while SLR and VLBI jointly realise the scale. The Latin American regional GNSS network is extended by globally well distributed stations in order to perform the datum transfer with the SLR and VLBI networks via measured local tie vectors at co-located sites. Moreover, the global GNSS stations serve to realise the orientation of the network with respect to the Earth's body (Chapt. 5). Afterwards, special focus is put on current deficiencies of the SLR network that reduce the reliability of the datum parameters realised, and how enhancements of the space and ground segments can improve the stability of the SLR-derived TRF datum parameters as well as their joint determination with other geodetic parameters of the Earth system like the Stokes coefficients of the Earth's gravity field model and the ERPs (Chapt. 6).

1.2 Research goals

The motivation outlined above leads us to posing the following two research questions **(RQs)** that relate to the two subject blocks that have been outlined in the Preface:

RQ 1 To what extent do currently available space-geodetic observations allow to realise a regional reference frame that is geocentric at any epoch, epoch-wise for short periods, and has a stable datum?

RQ 2 To what extent can further enhancements in the SLR space and ground segments improve the reliability of SLR-derived geodetic parameters with relation to the TRF datum?

These research questions will be addressed within the remainder of this doctoral thesis.

2 Geodetic reference systems and frames

2.1 Historical background

Attempts to determine the shape of the Earth and its position within the cosmos are probably as old as mankind. While assumptions about the Earth's spherical shape have been documented since the ancient era (Aristoteles, *Περὶ οὐρανοῦ* "On the Heavens", also known as *De caelo*, Book II, Chapt. 4; cf. Stocks, 1922), it was the Greek polymath Eratosthenes (c. 276 BC–c. 195 BC), chief librarian at the renowned Library of Alexandria, to be the first one known to determine the Earth's circumference with remarkable accuracy. By an arc measurement between the Egyptian cities of Alexandria and Syene, he computed an Earth's circumference of 250 000 stadia, 50 times the distance he measured between the two cities. Assuming his measurement to reflect the distance between the two cities of 835 km in modern units, one results in a circumference of 41 750 km. Thus, Eratosthenes' result is less than 5 % off the value of 40 075 km we know today. Eratosthenes also determined the tilt of the Earth's axis with an accuracy unachieved before and used a global projection introducing a system of meridians and parallels. Unfortunately, large parts of Eratosthenes' work have been lost and are only accessible via secondary sources which are concisely collected by Berger (1880). Eratosthenes is seen as one of the founders of modern geography, and his basic findings about the Earth's shape and surface remained state of the art in the European sphere throughout the ancient and medieval times until the early modern era. Based on Eratosthenes' findings, Claudius Ptolemy (c. 100–c. 170) collected the knowledge of the then-known world and published his *Cosmographia* (or *Γεωγραφικὴ Ὑφήγησις* "Geographical Guidance") around AD 150. In Europe, this work has been re-edited over more than a thousand years and belongs to the first world maps that are preserved in larger editions of incunabula (early prints; e.g., Ptolemaeus, 1482). To describe coordinates for more than 8000 places all over the then-known world, Ptolemy introduces a consistent system of meridians and parallels, the degrees of latitude being counted from the equator and the degrees of longitude counted from a prime meridian through the Fortunate Islands, the westernmost land recorded in his maps. By the 9th century, Ptolemy's map has been further improved by cartographers in the Muslim world, most notably by the Persian polymath Muhammad ibn Musa al-Khwarizmi (c. 780–c. 850), later head of the House of Wisdom in Baghdad. Al-Khwarizmi is responsible for introducing the modern Hindu-Arabic numeral system to the western world (his name al-Khwarizmi survives in the word "algorithm") and described the modern concept of formula-based mathematics published in his work *The Compendious Book on Calcu-*

lation by Completion and Balancing (also known by the short version *Al-Jabr* of its Arab title, from which the word "Algebra" is derived). By this, al-Khwarizmi laid the fundamental basis of modern mathematics, without which modern geodetic science and application would be unthinkable.

Starting with gravitational studies by Newton (1687) suggesting the Earth's oblate shape, it was not until the first half of the 18th century that measurement campaigns conducted by the French Academy of Sciences could prove that the Earth is actually not circular in shape but has an oblateness of about 1:210, introducing the ellipsoid as reference for the Earth's geometrical shape. In this context, Clairaut (1743) confirms Newton's assumption by being the first one to develop a theory for the direct relation between the Earth's shape (i.e., its geometry) and its gravity field (i.e., its physics), while Bouguer (1749) confirms Newton's assumptions by a geometric arc measurement in conjunction with gravimetric observations (thereby, Bouguer also develops the gravity reduction today named after him).

A heliocentric system has already been suggested by the ancient Greek astronomer and mathematician Aristarchus of Samos (c. 310 BC–c. 230 BC). While Aristarchus' original work has been lost, Archimedes (c. 287 BC–212 BC) makes reference to the Aristarchian theory in an attempt to calculate an upper bound for the number of grains of sand required to fill the universe (Archimedes, *Ψαμμίτης* "The Sand Reckoner"; cf. Heath, 1897, pp. 221–232). However, it took until the 16th century until Copernicus (1543) elaborated the heliocentric theory in a detailed way, describing the Earth's and other then-known planets' revolution about the Sun – assuming circular orbits – and the precession of the Earth's rotation axis. With that, Copernicus laid one of the fundamental bases of modern Astronomy and the description of the Earth's rotation. Kepler (1609, 1619) improved Copernicus' theory based on planetary observations, formulating the three Keplerian laws of planetary motion. The first two laws (Kepler, 1609) describe (1) the elliptical nature of a planet's orbit with the Sun in one of the ellipse's focal points and (2) the respective planet's revolution along the orbit with a constant area speed, the third law (Kepler, 1619) establishes the relation between the orbit's semi-major axis and the planet's orbital period. Newton (1687) generalises Kepler's laws to any object in space by showing that they are in accordance with his theory of gravitation. Consequently, the Keplerian laws are commonly applied for the description of the motion of natural as well as artificial objects in space, and serve as the mathematical foundation for satellite-based surveillance and navigation.

Helmert (1880, 1884) unified all previous findings to the full concept of geodesy we know today. With the foundation of the Mitteleuropäische Gradmessung (Central European Arc Measurement) in 1862, geodetic measurements started to become harmonised and coordinated on a supra-national level (Drewes et al., 2020). Extended by member states from all continents, today's International Association of Geodesy (IAG) as part of the IUGG is responsible for defining standards and coordinating all work related to the geodetic observation techniques operating on a global scale. Since the availability of satellite techniques from the 1960s and of VLBI from the 1980s on, space geodesy al-

lows us to accurately realise the theoretical concepts of geocentric terrestrial reference systems by establishing terrestrial reference frames, starting with the Bureau International de l'Heure (BIH) Terrestrial System 1984 (BTS84; Boucher and Altamimi, 1985) that has been the first one to be combined from space-geodetic techniques. Since 1988, the IERS is responsible for providing realisations of the ITRS in the form of the International Terrestrial Reference Frame (ITRF; Petit and Luzum, 2010).

2.2 Definition and realisation of terrestrial reference systems

In (higher[1]) geodesy, a *reference system* defines the reference for representing geometric measurements of absolute or relative positions and velocities by means of 3-dimensional position or velocity vectors. Thereby, the reference system is the concept providing the theory how the geodetic datum is defined, which means to define the origin of the coordinate axes (x-, y- and z-axis), their orientation with respect to the Earth's body, and the scale of the unit of length. Once one has agreed on numbers (e.g., the physical constants valid within the system) and models for the physical structure (e.g., Earth and pole tide models), one talks of a *conventional reference system* (Kovalevsky et al., 1989). Conventional reference systems can be defined globally, i.e., related to the whole Earth's body, or regionally, for example aligned to a continental plate. National or local reference systems, for example local level systems, are rather relevant in surveying disciplines and are outside the scope of this thesis.

To be accessible to the users, global and regional conventional reference systems are materialised by networks of reference stations with precisely determined coordinates, called *(conventional) reference frames* (Kovalevsky et al., 1989). These reference coordinates allow a user to refer any other observations that involve the reference stations to the reference frame as the common, superordinate system.

According to the IERS Conventions 2010 (Petit and Luzum, 2010), "a terrestrial reference system (TRS) is a spatial reference system co-rotating with the Earth in its diurnal motion in space. In such a system, positions of points attached to the solid surface of the Earth have coordinates which undergo only small variations with time, due to geophysical effects (tectonic or tidal deformations)". The ITRS is the official TRS applied by the IERS (Petit and Luzum, 2010). The IUGG[2] and IAG[3] 1991 Resolutions define the ITRS to be a TRS fulfilling the following conditions (Fig. 2.1):

[1] The term "higher geodesy", as introduced by Helmert (1880, 1884), refers to the geodetic disciplines that deal with the Earth's figure, rotation, and gravity field on a global scale and is often associated with the stand-alone term "geodesy" (e.g., Torge, 2001). In contrast to this, the term "lower" or "applied geodesy" refers to the geodetic disciplines related to land surveying and engineering, often summarised under the term "surveying".

[2] IUGG Resolution N°2 (1991). URL: `https://iag.dgfi.tum.de/fileadmin/IAG-docs/IUGG_Resolutions_1991.pdf` (2022-06-15).

[3] IAG Resolution N°1 (1991). URL: `https://iag.dgfi.tum.de/fileadmin/IAG-docs/IAG_Resolutions_1991.pdf` (2022-06-15).

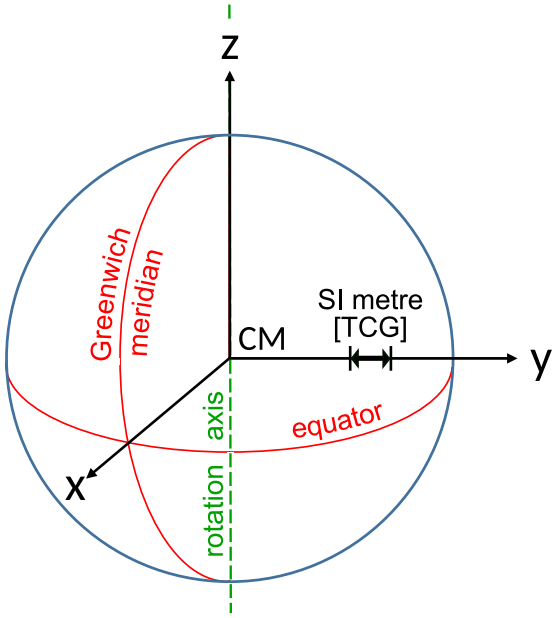

Figure 2.1: The International Terrestrial Reference System. CM denotes the Earth's centre-of-mass.

(1) The origin of the ITRS is defined geocentric, i.e., coinciding with the centre-of-mass of the whole Earth system including oceans and atmosphere.

(2) The orientation of the ITRS with respect to the Earth's body is defined equal to the orientation defined by the Bureau International de l'Heure (BIH) 1984.0, meaning that the z-axis corresponds to the Earth's mean rotation axis, the x-axis in the equatorial plane points towards the zero meridian (also called Greenwich meridian) and the y-axis completes a right-handed system. Over time, the orientation of the ITRS shall fulfil a no-net-rotation (NNR) condition with regard to horizontal tectonic motions over the whole Earth's surface.

(3) The scale of the ITRS is defined equal to the SI metre as unit of length, consistent with the TCG (Temps Coordonné Géocentrique/Geocentric Coordinate Time) time coordinate according to the IAU[4] and IUGG 1991 Resolutions for a geocentric local frame.

The realisation of the ITRS is the ITRF. The ITRF is determined by combining observations of the four space-geodetic techniques SLR, VLBI, GNSS, and Doppler Orbitography and Radiopositioning Integrated by Satellite (DORIS). Thereby, one exploits the different technique-specific strengths to realise subsets of the datum-relevant geodetic parameters, which are outlined in detail in Section 3.1. The ITRF origin is realised from SLR only, which is due to the fact that SLR observations are highly sensitive

[4]IAU Resolution No. A4 (1991): *Recommendations from the Working Group on Reference Systems.* URL: `https://www.iau.org/static/resolutions/IAU1991_French.pdf` (2022-06-15).

to the Earth's gravity field but less affected by modelling deficiencies than GNSS and DORIS. VLBI is not capable to determine the origin as its observations are not sensitive to the Earth's gravity field, but together with SLR, it contributes to the realisation of the ITRF scale. GNSS and DORIS have globally well distributed station networks that can contribute to realising the orientation of the ITRF with respect to the Earth's surface. Recent ITRF solutions realise the orientation by applying no-net-rotation (NNR) constraints with respect to positions and velocities that maintain the orientation of a new ITRF solution in accordance with its predecessor (Altamimi et al., 2016).

Realisations of the ITRS are computed by three ITRS Combination Centres. The most recent official ITRF release at the time of these studies is the ITRF2014 (Altamimi et al., 2016) provided by the Institut national de l'information géographique et forestrière (IGN). Along with the ITRF2014, two other independent ITRS realisations exist, namely the DTRF2014 (Seitz et al., 2022) provided by the Deutsches Geodätisches Forschungsinstitut (DGFI-TUM) at the Technical University of Munich (TUM) and the JTRF2014 (Abbondanza et al., 2017) provided by the National Aeronautics and Space Administration (NASA) Jet Propulsion Laboratory (JPL) at the California Institute of Technology (Caltech). Two out of the three ITRS realisations, namely the ITRF2014 and the DTRF2014, are conventional solutions with constant station velocities according to the definition provided in the IERS Conventions 2010. The JTRF2014, in contrast, is a subsecular frame based on a Kalman filter and smoother approach realising geocentric non-linear station position time series (cf. Sect. 5.5.2). Since April 15, 2022, the newest official ITRF release is the ITRF2020[5].

2.3 Regional reference frames and the problem of geocentricity

The close-by accessibility to the Terrestrial Reference System is ensured by regional reference frames. These regional reference frames are realised deliberately for certain regions on the globe, in order to ensure a sufficient number of close-by reference stations for various purposes related to navigation, surveying, or the monitoring of processes in the Earth system. Usually, these regional reference frames are realised as densifications of the ITRF by aligning the datum of a regional dense GNSS station network to the global ITRF datum. Depending on the geophysical activity of the region of interest, a regional reference frame can be determined either as a multi-year reference frame that parameterises station positions and constant velocities, or as series of epoch reference frame (ERF) realisations that can mirror geophysical effects such as loading displacements or deformations due to earthquakes. An example for the first approach is the European reference frame EUREF/ETRS89 (Altamimi, 2018), which is aligned to the ITRF datum at the epoch 1989.0 and fixed to the European plate, while an example

[5] *General Announcements: The ITRF2020 is available online.* IAG Newsletter, April 2022, URL: `https://www.iag-aig.org/iag-newsletters/April2022` (2022-06-15).

for the second approach is the Latin American reference frame Sistema de Referencia Geodésico para las Américas (SIRGAS; Sánchez et al., 2016), which is realised weekly and aligned to the ITRF datum. In any case, the alignment to the datum of the ITRF is done by applying NNR, no-net-translation (NNT), or no-net-scale (NNS) constraints to a selection of regionally or globally distributed fiducial stations.

As outlined by Kehm et al. (2022b), the linear parameterisation of the station coordinates implies that the ITRF origin reflects the Earth's centre-of-mass (CM) in a mean sense (i.e., on secular time scales) only. The consequence of aligning regional networks to the ITRF datum via NNT constraints is that station displacement time series on seasonal and short time scales refer to the geometric centre of the Earth, usually called the Earth's centre-of-figure (CF; Dong et al., 2003). Although this holds in particular for the interpretation of seasonal and short-term displacement effects, from now on we denote coordinates as "CM-related" if they are given in a reference frame referring to an instantaneously-realised geocentre and as "CF-related" if they are given in a reference frame aligned to the ITRF datum.

An ITRF solution is always computed from space-geodetic observations over a limited time span. The constant station velocities imply that short-term and periodic mass variations, for example caused by atmospheric, oceanic, or hydrological loading variations (Seitz and Krügel, 2009; Seitz et al., 2014; Glomsda et al., 2021a), are not reflected in the ITRF coordinates. Consequently, the ITRF origin performs seasonal variations with respect to the instantaneous geocentre (Drewes et al., 2013), an effect often called "geocentre motion" (e.g., Collilieux and Altamimi, 2009; Collilieux et al., 2009). Recent ITRF realisations benefit from longer space-geodetic observation time series and improved geophysical background models. Moreover, they provide station-specific models to correct for post-seismic deformation (Altamimi et al., 2016). However, after the end of the observation period, the reference coordinates can neither reflect episodic events like earthquakes that lead to sudden position or velocity changes (Sánchez and Drewes, 2016, 2020), nor anthropogenic influence like subsidence caused by the withdrawal of groundwater (e.g., Bevis et al., 2005), nor, for example, the impact of changes in the technical equipment of individual sites on the determined positions and velocities. Consequently, it is unavoidable that the ITRF coordinates become less accurate over time, meaning a gradual decrease in the accuracy of their geocentricity until a new ITRF release is computed. In regions with high geophysical activity, the aforementioned geophysical effects may result in a substantial loss of valid fiducial stations over time. As an example, Fig. 2.2 shows recent changes in the station velocities induced by strong earthquakes at selected sites in Latin America.

Regional networks aligned to the ITRF datum, in particular regional epoch reference frames realised at short latencies (up to several weeks), practically exclusively rely on fiducial coordinates in the extrapolation period of the ITRF. The consequence is that the datum of the regional network cannot be realised strictly geocentric: neither in an instantaneous sense, which is always true due to the secular nature of the ITRF origin, nor in a mean sense, which is due to the fact that the accuracy of the geocentricity of

the ITRF unavoidably decreases after the end of the observation period. Once a new ITRF solution is released, the regional networks are aligned to the new ITRF datum, resulting in discontinuous or, due to reprocessing, retrospectively changing time series. This significantly reduces the information value of the derived coordinate time series for the study of geophysical effects like loading-induced site displacements on both short and long time scales.

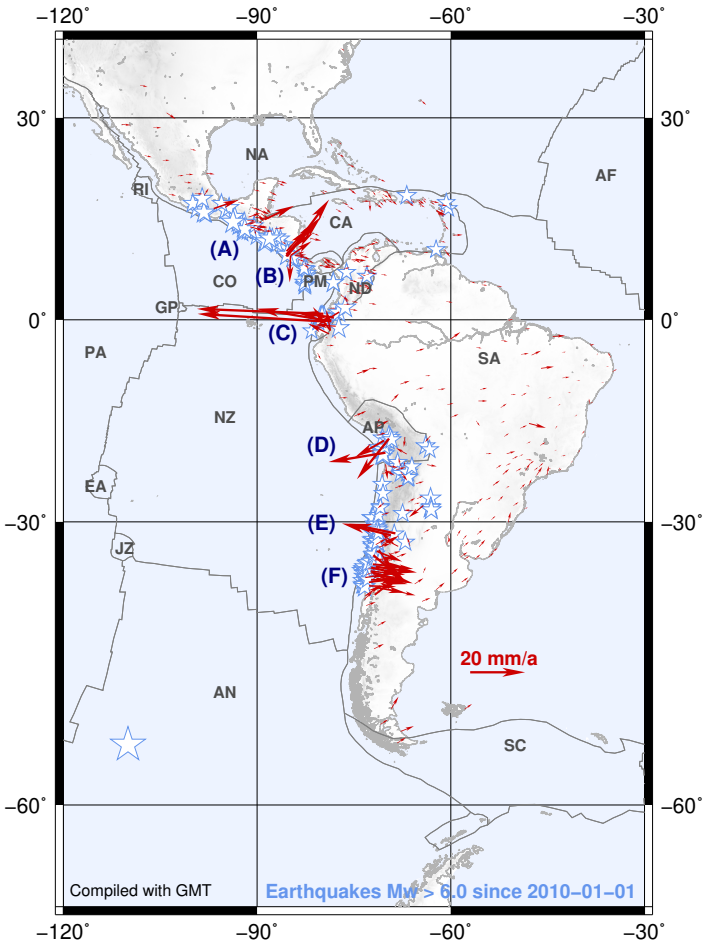

Figure 2.2: ▪Changes in the Latin American reference frame kinematics induced by strong earthquakes. They are inferred from the difference between the two latest multi-year solutions SIR15P01 (Sánchez and Drewes, 2016) and SIR17P01 (Sánchez and Drewes, 2020). Stars represent earthquakes with Mw > 6.0 since Jan 1, 2010. The large discrepancies appear close to the epicentre of strong earthquakes: (A) Guatemala (Mw: 7.4, 2012-11-11), (B) Nicoya (Mw: 7.6, 2012-09-05), (C) Pedernales (Mw: 7.8, 2016-04-16), (D) Iquique (Mw: 8.2, 2014-04-01), (E) Illapel (Mw: 8.3, 2015-09-16), (F) El Maule (Mw: 8.8, 2010-02-27).

As Latin America is a region of high geophysical activity, the direct study of effects related to the Earth system over long and short time scales, as well as the availability of reference coordinates at short latencies, are of vital interest. To overcome the aforementioned deficiencies of non-geocentric reference coordinates, our study aims to realise a regional reference frame that is CM-related, i.e., has a geocentric datum, at any epoch.

While a long-term geocentric TRF datum can already be realised with high accuracy (Altamimi et al., 2016; Seitz et al., 2022), also instantaneously geocentric reference frame solutions filtered from long-term observation time series have already been realised with high accuracy (Abbondanza et al., 2017). The drawback of both approaches is that they rely on a common processing of space-geodetic observations over a limited time span. Short-term realisations of the ITRS that rely on observation data that is available at short latencies up to several weeks, however, suffer from deficiencies in the observation networks due to several technical and administrative reasons which decrease the reliability of the datum parameters realised. The consequences of these deficiencies are that the realisation of the origin and the scale are affected by permanently changing station networks of SLR or VLBI (Chapt. 6; Bloßfeld et al., 2014b, 2015b; Kehm et al., 2018▪, 2019▪). As the realisation of the orientation relies on NNR constraints with respect to a multi-year reference frame, insufficiently distributed station networks may also result in correlations between the orientation and the origin (Bloßfeld et al., 2014b).

Based on the example of the Latin American reference frame, the present study investigates the feasibility of direct geocentric short-term realisations of the datum of a regional reference frame by combining global networks of SLR and VLBI with the regional GNSS network extended by global stations (Chapt. 5). The approach implements a filtering strategy to cope with current technique-specific deficiencies reducing the reliability of the SLR- and VLBI-derived datum parameters, and realises the orientation via a globally well distributed network of GNSS stations. On the example of SLR, further studies investigate the potential of enhanced networks for the estimation of geodetic parameters related to the TRF datum (Chapt. 6).

3 Space-geodetic techniques and combination

3.1 Space-geodetic techniques and their contribution to the determination of parameters of the Earth system

The IAG maintains technique-specific Scientific Services that are responsible to develop the space-geodetic networks, to coordinate the work between different public and private contributing institutions, to analyse the data, and to provide scientific as well as operational products. For SLR, this is the International Laser Ranging Service (ILRS; Pearlman et al., 2019), for VLBI, this is the International VLBI Service for Geodesy and Astrometry (IVS; Nothnagel et al., 2017), for GNSS, this is the International GNSS Service (IGS, Johnston et al., 2017), and for DORIS, this is the International DORIS Service (IDS; Willis et al., 2015).

Table 3.1: The sensitivity of space-geodetic techniques to selected parameters of the Earth system. Bracketed marks indicate parameters that cannot yet be determined with sufficient accuracy.

		VLBI	SLR	GNSS	DORIS
CRF	source coordinates	■			
	orbit parameters		■	■	■
EOPs	nutation	■	(■)	(■)	(■)
	polar motion	■	■	■	■
	UT1 – UTC	■			
	LOD	■	■	■	■
TRF	station coordinates	■	■	■	■
TRF datum and gravity field	**scale** (GFC degree 0)	■	■	(■)	(■)
	origin (CM; GFC degree 1)		■	(■)	(■)
	orientation (GFC degree 2)		(■)	(■)	(■)
	GFC > degree 2		■	(■)	(■)
Atmosphere	thermosphere	■	■	■	■
	ionosphere	■		■	■

Tab. 3.1 shows the most important geodetic parameters of the Earth system and how the four space-geodetic techniques serve to determine them. Within the present doctoral thesis, we put special focus on the realisation of the TRF datum. In this context, it is important to note that the list provided by Tab. 3.1 is non-exhaustive and could be extended by far more parameter groups that are relevant to describe the Earth system, for example relativistic parameters or corrections to ocean tidal models which are directly or indirectly accessible via space-geodetic observations.

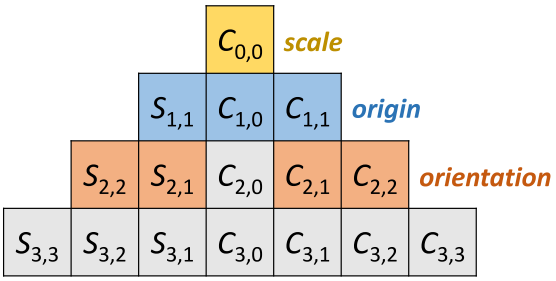

Figure 3.1: The equivalence between low-degree Stokes coefficients and the TRF datum.

By nature, the (geometrical) TRF datum is directly linked to the (physical) properties of the Earth's gravity field. This means that the TRF datum is equivalently represented by low-degree spherical harmonic gravity field coefficients (GFCs, Stokes coefficients) of the Earth's gravity field model (cf. Hofmann-Wellenhof and Moritz, 2006; Bloßfeld, 2015), namely the Stokes coefficients of degrees 0 (scale), 1 (origin), and the tesseral and sectoral Stokes coefficients of degree 2 (orientation; cf. Fig. 3.1). Assuming a TRF datum given, its geometrical representation in the form of a TRF, i.e., a set of station coordinates, can be determined via all four space-geodetic techniques. Rank deficiencies of the normal equation matrix thereby have to be eliminated by introducing corresponding datum constraints in the form of pseudo-observations. However, only those space-geodetic techniques that are sensitive to the low-degree coefficients of the Earth's gravity field model are able to determine whether that given TRF datum coincides with the ITRS, namely by determining the datum-related low-degree Stokes coefficients.

As a result, a TRS can be defined physically by pre-defining values for the low-degree Stokes coefficients of the Earth's gravity field model, while the geometric realisation of the corresponding TRF (in terms of constraint-free estimated station coordinates) is possible only if the observations are sufficiently sensitive to the corresponding coefficients of the Earth's gravity field model.

The scale of the ITRS is defined through the TCG time coordinate (cf. Sect. 2.2), which is equivalent to setting

$$C_{0,0} \coloneqq 1, \tag{3.1}$$

and, consequently, is accessible via converting measured signal running times into distances. Scaling of $C_{0,0}$ would be the equivalent to scaling the geocentric gravitational constant GM, which, as a result of Einstein's general theory of relativity (Einstein, 1916), would scale the TCG time coordinate, and with that any measured distance. This means that, in principle, all four space-geodetic techniques are able to determine the scale of a reference frame, as all of these techniques exploit the relationship between timing and range determination.

The origin of the ITRS is defined equal to the Earth's centre-of-mass, which is equivalent to setting

$$C_{1,0} = C_{1,1} = S_{1,1} \coloneqq 0, \tag{3.2}$$

and, consequently, is accessible in a geometrical way only via observations to objects that are under direct influence of the Earth's gravity field: The aforementioned condition forces orbits determined for objects in space to be geocentric, meaning that the centre-of-mass is forced to the coordinates $\begin{bmatrix} 0 & 0 & 0 \end{bmatrix}^{\mathrm{T}}$ of the TRF. In principle, all satellite-based space-geodetic techniques (SLR, GNSS, and DORIS) are sensitive to these Stokes coefficients.

The tesseral and sectoral Stokes coefficients of degree 2 of the Earth's gravity field model are directly linked to the Earth's principle axes of inertia. Thereby, $C_{2,1}$ and $S_{2,1}$ describe the discrepancy between the z-axis and the Earth's principle axis of maximum inertia, which closely approximates the Earth's mean rotation axis (Hofmann-Wellenhof and Moritz, 2006; Göttl, 2013). Setting

$$C_{2,1} = S_{2,1} \coloneqq 0 \tag{3.3}$$

forces the z-axis to coincide with the Earth's principle axis of maximum inertia. The two Stokes coefficients $C_{2,2}$ and $S_{2,2}$ describe the rotation of the TRS in the equatorial plane. Aligning the conventional equatorial axes x and y with the equatorial principle axes of inertia is equivalent to setting the angle Λ between those (Liu and Chao, 1991)

$$\Lambda = \frac{1}{2}\arg(C_{2,2} + iS_{2,2}) \coloneqq 0. \tag{3.4}$$

Consequently, also a physical realisation of the TRF orientation aligned to the Earth's principle axes of inertia, in principle, is possible with all satellite-based space-geodetic techniques. For the equatorial axes, it is important to note that this orientation aligned to the Earth's equatorial principle axes of inertia does not coincide with the conventional BIH 1984.0 orientation. Transforming from a conventional reference system to a system aligned to the Earth's equatorial principle axes of inertia requires a rotation by about 14.93° to the West (Liu and Chao, 1991), with remaining first-order corrections

due to the insensitivity of the conventional reference frames to the second-order Stokes coefficients (Barkin and Ferrandiz, 2000; Modiri, 2021).

Although theoretically sensitive to the TRF origin and scale, GNSS and DORIS observations do not contribute to their realisation. This is because there are system-inherent systematic errors due to mis-modelling of non-gravitational forces acting on the satellites, and due to uncertainties caused by the orbital altitudes (e.g., Männel and Rothacher, 2017). Origin and scale time series from DORIS, moreover, show significant constellation-related drift and discontinuity effects in the realised origin and scale time series (e.g., Bloßfeld et al., 2016). For GNSS, the scale realisation is highly dependent on the applied phase center variation (PCV) models for GNSS antennas (e.g., Steigenberger et al., 2009). Usually, these have been derived by comparing GNSS observations to the reference positions of the stations, which means that an ITRF solution has already been required in order to determine the corresponding PCV models. Future PCV models are derived from laboratory calibrations, i.e., independent from a pre-existing TRF solution, allowing GNSS to contribute to the realisation of the TRF scale (Villiger et al., 2020). Extended GNSS constellations with satellites in different orbital heights shall also enable GNSS to contribute to long- and short-term realisations of the TRF origin in the future (e.g., Günther, 2018, Glaser et al., 2020). To date, none of the satellite techniques is accurate enough to allow for a physical realisation of the TRF orientation, as their observations are poorly sensitive to the tesseral and sectoral Stokes coefficients of degree 2, as well as due to unresolved correlations among the parameters and erroneous observation models (e.g., Bloßfeld et al., 2015a; Sośnica et al., 2015; Chen et al., 2016; Couhert et al., 2020; Rosat et al., 2020). Consequently, the degrees of freedom related to the TRF orientation must be removed in an alternative way, which is the application of purely mathematical NNR constraints maintaining the orientation of a new TRF in correspondence with the BIH 1984.0 orientation.

3.2 Parameter estimation

A common characteristic of all geodetic problems is that they rely on observations, i.e., measurements of physical quantities that are in a functional relationship with the parameter that shall be determined. None of these functional relationships is in perfect correspondence with reality because the applied background models, as well as the observations, have inherent systematic and stochastic errors. The performance of a measurement system is thus described by two quantities, namely the *accuracy* describing the absolute correspondence of the expected value of the measurement with the reality, and the *precision* as an internal measure of the repeatability of a measurement, i.e., the scatter of the observations about the expected value. Consequently, the accuracy of a measurement predominantly relies on the absence of systematic errors which can be detected once the precision of the measurement is high enough to determine systematic deviation from a reference.

The commonly applied approach for the solution of geodetic problems is the least-squares adjustment according to the Gauß-Markov model which has been developed by Gauss (1823) via proving that least-squares adjustment leads to a best estimate. For detailed deductions of the model in modern notation, the reader may refer to Koch (2004) and Niemeier (2008); the notation used in the following is a compromise between those two publications. The goal is to estimate values for a set of u parameters (unknowns) $\mathbf{x}$ from a set of n observations $\mathbf{L}$ that are assumed to be stochastic variables following a normal distribution. The observations are functions of the parameters, following the relationship

$$\mathbf{L} + \mathbf{v} = f(\hat{\mathbf{x}}), \tag{3.5}$$

whereby $\mathbf{v}$ is the vector of corrections to the observations and $\hat{\mathbf{x}}$ is the vector of parameter estimates. The stochastic model is given by a variance-covariance matrix of the observations

$$\mathbf{\Sigma}_{ll} = \sigma_0^2 \mathbf{Q}_{\mathbf{ll}}, \tag{3.6}$$

with σ_0^2 is the a priori variance factor (in the following assumed to be chosen as 1.0), and $\mathbf{Q}_{\mathbf{ll}}$ is the cofactor matrix of the observations.

In general, the relationship according to Eq. 3.5 is not linear. Taylor decomposition yields

$$\mathbf{L} + \mathbf{v} = f(\mathbf{x}_0) + \left.\frac{\partial f}{\partial \mathbf{x}}\right|_{\mathbf{x}=\mathbf{x}_0} \cdot \Delta\hat{\mathbf{x}} + \mathcal{O}, \tag{3.7}$$

with $\mathbf{x}_0$ being the a priori values of the parameters and $\Delta\hat{\mathbf{x}}$ being the first-order corrections to the a priori values of the parameters. We assume the a priori values to be known accurately enough so that the higher-order correction terms $\mathcal{O}$ can be omitted, meaning that the Taylor decomposition is truncated after the first-order term. Consequently, we can reduce Eq. 3.5 by the deterministic terms dependent only from the a priori values $\mathbf{x}_0$, and result in a linear relationship between a reduced observation vector

$$\mathbf{l} = \mathbf{L} - f(\mathbf{x}_0) \tag{3.8}$$

(*observed minus computed* from the a priori values of the parameters, $O - C$) and the vector of (unknown) corrections to the a priori values of the parameters $\Delta\hat{\mathbf{x}}$ according to

$$\mathbf{l} + \mathbf{v} = \mathbf{A}\Delta\hat{\mathbf{x}}. \tag{3.9}$$

Thereby, $\mathbf{A}$ is the *design matrix* (dimension $n \times u$) containing the first-order partial derivatives of the functional model from Eq. 3.7. The parameter estimation according to the Gauß-Markov model is based on this linearised (reduced) relationship.

The method of least squares implies to minimise the squared weighted sum of observation residuals

$$\mathbf{v}^{\mathrm{T}}\mathbf{P}_{\mathbf{ll}}\mathbf{v} \rightarrow \min, \tag{3.10}$$

whereby $\mathbf{P}_{\mathbf{ll}} = \mathbf{Q}_{\mathbf{ll}}{}^{-1}$ is the weight matrix of the observations. This yields a relationship between the observations and the parameters

$$\mathbf{N}\Delta\hat{\mathbf{x}} = \mathbf{y}, \tag{3.11}$$

with $\mathbf{N} = \mathbf{A}^{\mathrm{T}}\mathbf{P}_{\mathbf{ll}}\mathbf{A}$ being the normal equation matrix and $\mathbf{y} = \mathbf{A}^{\mathrm{T}}\mathbf{P}_{\mathbf{ll}}\mathbf{l}$ being the right-hand side vector of the normal equation system, and $\mathbf{l}^{\mathrm{T}}\mathbf{P}_{\mathbf{ll}}\mathbf{l}$ being the weighted sum over the vector of $O - C$.

The system is solved for $\Delta\hat{\mathbf{x}}$ by multiplication with the cofactor matrix of the estimated parameters

$$\mathbf{Q}_{\hat{\mathbf{x}}\hat{\mathbf{x}}} = \mathbf{N}^{-1}, \tag{3.12}$$

yielding the vector of estimated parameter corrections

$$\Delta\hat{\mathbf{x}} = \mathbf{N}^{-1}\mathbf{y} \tag{3.13}$$

to be restored to the a priori values of the parameters $\mathbf{x}_0$ to obtain the parameter estimates

$$\hat{\mathbf{x}} = \mathbf{x}_0 + \Delta\hat{\mathbf{x}}. \tag{3.14}$$

The a posteriori variance factor

$$\hat{\sigma}_0^2 = \frac{\mathbf{v}^{\mathrm{T}}\mathbf{P}_{\mathbf{ll}}\mathbf{v}}{n - u} \tag{3.15}$$

can be interpreted as a measure for the agreement between the functional and stochastic models – which have been chosen a priori – and the actual observations. If this agreement is given, the a priori and a posteriori variance factors are expected to be equal (or close to each other). In the ideal case, this means that

$$\mathbf{Q}_{\hat{\mathbf{x}}\hat{\mathbf{x}}} = \mathbf{\Sigma}_{\hat{\mathbf{x}}\hat{\mathbf{x}}}, \tag{3.16}$$

where $\mathbf{\Sigma}_{\hat{\mathbf{x}}\hat{\mathbf{x}}}$ is the variance-covariance matrix of the estimated parameters. Otherwise, the variance-covariance matrix of the estimated parameters can be calculated by multiplying the cofactor matrix with the a posteriori variance factor.

In our main study (Chapt. 5), we deal with normal equation systems of which the stochastic information content shall be deliberately modified to realise a filtering (Sect. 5.4.2) and to compensate for known stochastic mis-modellings (Sect. 5.4.3). Consequently, we use externally-derived information to appropriately scale the input normal equations (i.e., the inverse cofactor/covariance matrices of the data sets contributing to the solutions) beforehand, meaning that we assume the scaled inherent stochastic model to be correct. In this case, the a posteriori variance factor is meaningless for us (as it would compensate for modifications deliberately applied to the stochastic model), and Eq. 3.16 is considered valid.

3.3 Approach for the intra- and inter-technique combination

Intra-technique combination means the combination of data sets of the same technique into one common equation system, e.g., the combination of different satellite-specific SLR equation systems into one multi-satellite equation system or the combination of different session-specific VLBI equation systems into one multi-session equation system. Intra-technique combination is performed to exploit different data sets of the same technique to obtain a more reliable solution. For SLR, for example, the combination of different satellite-specific data sets allows to decorrelate different parameter groups (cf. Chapt. 6). Inter-technique combination means the combination of different technique-specific equation systems into one multi-technique equation system. Inter-technique combination is performed to exploit the different strengths of all techniques, like sensitivities to different parameters of the Earth system, to obtain one combined solution for all parameters (cf. Chapt. 5).

The intra- and inter-technique combination of independently-generated space-geodetic data sets can be performed at three different levels of the Gauß-Markov model, namely at the observation level, at the normal equation level, or at the solution level (Fig. 3.2) with different advantages and disadvantages (e.g., Seitz et al., 2015).

A combination at the *observation level* would be the most rigorous way to combine space-geodetic data. Thereby, a common system of observation equations would be set up to be solved in a single adjustment. The big advantage would be that, first, all observations could be processed using common background models automatically and, second, also the treatment of the observations, e.g., the outlier detection, could follow common standards in one common, combined solution to which all techniques contribute. Correlations between the different technique-specific contribution could

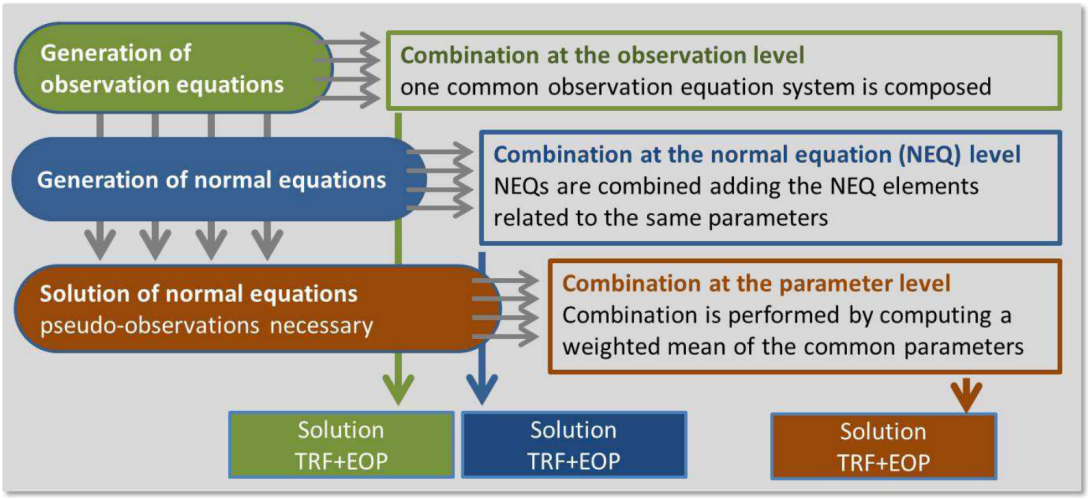

Figure 3.2: Combination of space-geodetic techniques at different levels of the Gauß-Markov model. The grey arrows stand for the four space-geodetic techniques SLR, VLBI, GNSS, and DORIS. Figure taken from Seitz et al. (2015).

directly be taken into account. The datum of a TRF could be realised consistently for all techniques applying common constraints. However, this would mean that all input data must be processed in a single software package setting up the observation equations and solving one common normal equation matrix. This would, by nature, exclude combining data sets that are routinely provided by the IAG Scientific Services or the processing centres of regional networks. As we focus on the combination of data sets that already are, or could, be provided by the IAG Scientific Services, the approach is not suitable for our studies.

A combination at the *solution level*, or at the level of parameters, uses technique-specific solutions as input. These solutions are calculated beforehand and independent from each other, and can be derived from separate technique-specific software packages. Consequently, each technique-specific solution is computed stand-alone (ignoring any inter-technique correlations) and has an independently-realised datum that is derived either from the observations, given that the technique is sensitive to TRF datum parameters, or is introduced via datum constraints applied to each technique-specific data set individually. Combining these solutions would always require the removal of these (potentially unknown) constraints which would imply the estimation of empirical bias and drift parameters, which decreases the physical significance of the realised combined TRF datum. Although the IAG Scientific Services and the processing centres of regional networks provide technique-specific solutions, the aforementioned imponderables lead us to the conclusion that the approach is not optimal for our studies aiming to realise a consistent TRF datum for all technique-specific networks contributing to the solution.

The combination at the *normal equation level* uses pre-processed datum-free normal equations as input. Given that the processing standards, most relevant the applied background models and the parameterisation, are harmonised, and that, apart from their sensitivity to common parameters, the technique-specific observations are uncorrelated, the approach can be considered as "a close approximation" (Seitz et al., 2015) to a combination at the observation level. After combining the datum-free normal equations by stacking common parameters like the ERPs and introducing local ties as constraints for the station coordinates at co-located sites, a common TRF datum can be realised for all techniques in a single adjustment. The combination at the normal equation level thus is a comparably rigorous, but still flexible, approach to combine data provided by independent sources like the IAG Scientific Services. This is the reason why we choose this level of the Gauß-Markov model for our combination procedures.

To date, one drawback of the combination at the normal equation level is that the parameters in the normal equations provided by the IAG Scientific Services are not harmonised yet. This is of special relevance for the determination of ERPs, as non-parameterised ERPs in a normal equation are fixed to their a priori values (e.g., Kehm et al., 2022a).

Section 3.4 outlines the algorithms that realise a combination at the normal equation level, Section 3.5 describes the different transformations applied to the normal equation system. All algorithms relate to the normal equation level of the Gauß-Markov model. The equivalences (or non-equivalences) of these operations with operations at other levels of the Gauß-Markov model are concisely described by, e.g., Bloßfeld (2015). Chapter 4 describes how these algorithms are implemented within the combination software used for this study.

3.4 Combination algorithms

This section provides the mathematical algorithms that are used to combine normal equations, to add constraint equation systems, and to perform an iterative relative weighting of individual data sets contributing to the combined solution.

3.4.1 Combination of normal equation systems

Combining two normal equation systems implies adding the elements that correspond to common parameters in the normal equation matrices. The order of the parameters (i.e., rows and columns) and the size of the two normal equation systems must be the same. The size of the two matrices is harmonised by introducing zero rows and columns for parameters missing in a system.

The combined normal equation system $\mathbf{N}_c$, $\mathbf{y}_c$, $\left(\mathbf{l}^{\mathrm{T}}\mathbf{P}_{\mathbf{ll}}\mathbf{l}\right)_c$ with the a pre-defined a priori variance factor $\sigma^2_{0,c}$ reads

$$\mathbf{N}_c = \lambda_1 \frac{\sigma_{0,c}^2}{\sigma_{0,1}^2}\mathbf{N}_1 + \lambda_2 \frac{\sigma_{0,c}^2}{\sigma_{0,2}^2}\mathbf{N}_2, \tag{3.17}$$

$$\mathbf{y}_c = \lambda_1 \frac{\sigma_{0,c}^2}{\sigma_{0,1}^2}\mathbf{y}_1 + \lambda_2 \frac{\sigma_{0,c}^2}{\sigma_{0,2}^2}\mathbf{y}_2, \tag{3.18}$$

$$\left(\mathbf{l}^{\mathrm{T}}\mathbf{P}_{\mathbf{ll}}\mathbf{l}\right)_c = \frac{\sigma_{0,c}^2}{\sigma_{0,1}^2}\left(\mathbf{l}^{\mathrm{T}}\mathbf{P}_{\mathbf{ll}}\mathbf{l}\right)_1 + \frac{\sigma_{0,c}^2}{\sigma_{0,2}^2}\left(\mathbf{l}^{\mathrm{T}}\mathbf{P}_{\mathbf{ll}}\mathbf{l}\right)_2 \tag{3.19}$$

with $\mathbf{N}_1$, $\mathbf{y}_1$, $\left(\mathbf{l}^{\mathrm{T}}\mathbf{P}_{\mathbf{ll}}\mathbf{l}\right)_1$ and $\mathbf{N}_2$, $\mathbf{y}_2$, $\left(\mathbf{l}^{\mathrm{T}}\mathbf{P}_{\mathbf{ll}}\mathbf{l}\right)_2$ being the normal equation systems to be combined with their respective weights λ_1 and λ_2 and their respective a priori variance factors $\sigma_{0,1}^2$ and $\sigma_{0,2}^2$.

3.4.2 Set-up and addition of condition equations

Parameters are constrained by introducing a set of n_c pseudo-observations $\mathbf{c}$ in the form

$$\mathbf{c} + \mathbf{v_c} = \mathbf{C}\Delta\mathbf{x}, \tag{3.20}$$

whereby $\mathbf{v_c}$ is the vector of pseudo-observation residuals and $\mathbf{C}$ describes the linear functional relationship between the pseudo-observations and the parameters. The weight matrix of the constraint equations $\mathbf{P_{cc}}$ is obtained by assigning standard deviations $\sigma_{\mathbf{c}}$ to each of these pseudo-observations, whereby a zero standard deviation would force the constraint equation to be fulfilled exactly.

The addition of the constraint equations to the normal equation system results in the constrained normal equation system

$$\tilde{\mathbf{N}} = (\mathbf{N} + \mathbf{C}^{\mathrm{T}}\mathbf{P_{cc}}\mathbf{C}), \tag{3.21}$$

$$\tilde{\mathbf{y}} = \mathbf{y} + \mathbf{C}^{\mathrm{T}}\mathbf{P_{cc}}\mathbf{c}, \tag{3.22}$$

$$\widetilde{\mathbf{l}^{\mathrm{T}}\mathbf{P}_{\mathbf{ll}}\mathbf{l}} = \mathbf{l}^{\mathrm{T}}\mathbf{P}_{\mathbf{ll}}\mathbf{l} + \mathbf{c}^{\mathrm{T}}\mathbf{P_{cc}}\mathbf{c}. \tag{3.23}$$

3.4.3 Variance component estimation

Assuming a system combined from m individual normal equation systems (data groups), variance component estimation (VCE) serves to determine the weight with which each of the data groups contributes to the combined solution. This implies iterative solutions of the combined normal equation system to calculate weights λ_k for each of the individual data groups $\mathbf{N}_k$ (Niemeier, 2008; Böckmann et al., 2010).

For the iteration step (j), the combined normal equation system reads (cf. Eq. 3.17–3.19)

$$\mathbf{N}_c^{(j)} = \sum_{k=1}^{m} \lambda_k^{(j)} \mathbf{N}_k, \tag{3.24}$$

$$\mathbf{y}_c^{(j)} = \sum_{k=1}^{m} \lambda_k^{(j)} \mathbf{y}_k, \tag{3.25}$$

$$(\mathbf{l}^{\mathrm{T}}\mathbf{P}_{\mathbf{ll}}\mathbf{l})_c^{(j)} = \sum_{k=1}^{m} \lambda_k^{(j)} (\mathbf{l}_k^{\mathrm{T}}\mathbf{P}_{\mathbf{ll},k}\mathbf{l}_k), \tag{3.26}$$

with $\lambda_k^{(j)}$ being the weight of the individual contribution $\mathbf{N}_k$. The equation system is solved according to Eq. 3.12–3.15.

The VCE algorithm requires initial values for the data group weights in the first iteration step; for the sake of simplicity, these weights are often chosen to be equal. After each of the following iterations, the weighted square sum of the residuals of the individual data group within the combined solution

$$\left(\mathbf{v}^{\mathrm{T}}\mathbf{P}_{\mathbf{ll}}\mathbf{v}\right)_{c,k}^{(j)} = \left(\Delta\hat{\mathbf{x}}_c^{(j)}\right)^{\mathrm{T}} \mathbf{N}_k \Delta\hat{\mathbf{x}}_c^{(j)} - 2\mathbf{y}_k^{\mathrm{T}} \Delta\hat{\mathbf{x}}_c^{(j)} + \mathbf{l}_k^{\mathrm{T}}\mathbf{P}_{\mathbf{ll},k}\mathbf{l}_k, \tag{3.27}$$

and a corresponding partial redundancy

$$r_{c,k}^{(j)} = n + n_c - \lambda_k^{(j)} \mathrm{tr}\left(\mathbf{N}_k \left(\mathbf{N}_c{}^{(j)}\right)^{-1}\right) \tag{3.28}$$

are computed (n is the number of observations, n_c the number of constraints), resulting in the a posteriori variance factor

$$\left(\hat{\sigma}_{0,k}^2\right)^{(j)} = \frac{\left(\mathbf{v}^{\mathrm{T}}\mathbf{P}_{\mathbf{ll}}\mathbf{v}\right)_{c,k}^{(j)}}{r_{c,k}^{(j)}} \tag{3.29}$$

defining the weight of the individual data group in the next iteration $(j+1)$

$$\lambda_k{}^{(j+1)} = \frac{1}{\left(\hat{\sigma}^2_{0,k}\right)^{(j)}}. \tag{3.30}$$

The calculation according to Eq. 3.24–3.30 is iterated until all data-group-specific differences $\left(\hat{\sigma}^2_{0,k}\right)^{(j+1)} - \left(\hat{\sigma}^2_{0,k}\right)^{(j)}$ between an iteration (j) and the following iteration $(j+1)$ converge below a chosen threshold.

3.5 Transformations of the normal equation system

This section provides the mathematical algorithms to transform the parameters within a normal equation system (e.g., transformations of the parameter epoch), and to reduce or eliminate parameters from, or to introduce new parameters into a normal equation system.

We can divide the operations applied to the normal equation system into *translations of the a priori values* (case 1):

$$\begin{aligned} \mathbf{x}_0 &\rightarrow \tilde{\mathbf{x}}_0 + \mathbf{t}, \\ \Delta\tilde{\mathbf{x}} &\rightarrow \Delta\hat{\mathbf{x}} - \mathbf{t}, \end{aligned} \tag{3.31}$$

and into *affine transformations of the parameter vector* (case 2):

$$\hat{\mathbf{x}} \rightarrow \mathbf{R}\hat{\mathbf{x}} + \mathbf{d}, \tag{3.32}$$

specified by the translation vector of the a priori values $\mathbf{t}$ (case 1) or the regular transformation matrix $\mathbf{R} = \mathbf{T}^{-1}$ and the translation vector $\mathbf{d}$ of the affine transformation (case 2).

The following three equations (Eq. 3.33–3.35) describe the possible operations on the normal equation system by a transformation of the normal equation matrix

$$\tilde{\mathbf{N}} = \mathbf{T}^{\mathrm{T}}\mathbf{N}\mathbf{T}, \tag{3.33}$$

a transformation of the right-hand side of the normal equation system

$$\tilde{\mathbf{y}} = \mathbf{T}^{\mathrm{T}}(\mathbf{y} - \mathbf{N}\mathbf{t}), \tag{3.34}$$

and a transformation of the weighted sum over the $O - C$ vector

$$\widetilde{\mathbf{l}^{\mathrm{T}}\mathbf{P}_{\mathbf{ll}}\mathbf{l}} = \mathbf{l}^{\mathrm{T}}\mathbf{P}_{\mathbf{ll}}\mathbf{l} - \mathbf{t}^{\mathrm{T}}(2\mathbf{y} - \mathbf{N}\mathbf{t}), \tag{3.35}$$

with (case 1)

$$\begin{aligned} \mathbf{t} &= \mathbf{T}(\tilde{\mathbf{x}}_0 - \mathbf{d}) - \mathbf{x}_0, \\ \tilde{\mathbf{x}}_0 &\text{ defined,} \end{aligned} \tag{3.36}$$

or (case 2)

$$\begin{aligned} \mathbf{t} &= 0, \\ \tilde{\mathbf{x}}_0 &= \mathbf{T}^{-1}\mathbf{x}_0 + \mathbf{d} \\ &= \mathbf{R}\mathbf{x}_0 + \mathbf{d}. \end{aligned} \tag{3.37}$$

If a transformation affects only a subset of parameters, the transformation matrix

$$\mathbf{R} = \begin{bmatrix} \mathbf{I}_{u-r} & \mathbf{0} \\ \mathbf{0} & \mathbf{R}_i \end{bmatrix} \tag{3.38}$$

is composed of a unity matrix block $\mathbf{I}_{u-r}$ for the $u - r$ unaffected parameters and a transformation matrix block $\mathbf{R}_i$ for the r transformed parameters.

3.5.1 Reduction of parameters

Reducing (or "pre-eliminating") parameters from a system means to remove them from the explicitly-estimated parameters without constraining or fixing them to their a priori values, i.e., the estimates for the parameters that remain in the system are not affected.

We assume the list of parameters $\mathbf{x}$ to be composed of two subsets of parameters $\mathbf{x}_1$ and $\mathbf{x}_2$

$$\mathbf{x} = \begin{pmatrix} \mathbf{x}_1 \\ \mathbf{x}_2 \end{pmatrix} \tag{3.39}$$

with $\mathbf{x}_1 \in \mathbb{R}^{n_1}$ being the parameter set to be reduced from the normal equation system and $\mathbf{x}_2 \in \mathbb{R}^{n_2}$ being the parameter set to remain in the normal equation system.

Decomposing the normal equation system correspondingly yields

$$\begin{pmatrix} \mathbf{y}_1 \\ \mathbf{y}_2 \end{pmatrix} = \begin{bmatrix} \mathbf{N}_{11} & \mathbf{N}_{12} \\ \mathbf{N}_{12}^{\mathrm{T}} & \mathbf{N}_{22} \end{bmatrix} \begin{pmatrix} \Delta\hat{\mathbf{x}}_1 \\ \Delta\hat{\mathbf{x}}_2 \end{pmatrix}. \tag{3.40}$$

The reduced normal equation system is derived by applying the Gaussian elimination method to Eq. 3.40, resulting in

$$\tilde{\mathbf{N}} = \mathbf{N}_{22} - \mathbf{N}_{12}^{\mathrm{T}}\mathbf{N}_{11}^{-1}\mathbf{N}_{12}, \tag{3.41}$$

$$\tilde{\mathbf{y}} = \mathbf{y}_2 - \mathbf{N}_{12}^{\mathrm{T}}\mathbf{N}_{11}^{-1}\mathbf{y}_1, \tag{3.42}$$

$$\widetilde{\mathbf{l}^{\mathrm{T}}\mathbf{P}_{\mathrm{ll}}\mathbf{l}} = \mathbf{l}^{\mathrm{T}}\mathbf{P}_{\mathrm{ll}}\mathbf{l} - \mathbf{y}_1^{\mathrm{T}}\mathbf{N}_{11}^{-1}\mathbf{y}_1, \tag{3.43}$$

with $\tilde{\mathbf{N}}$ being the reduced normal equation matrix, $\tilde{\mathbf{y}}$ being the reduced right-hand side of the normal equation system, and $\widetilde{\mathbf{l}^{\mathrm{T}}\mathbf{P}_{\mathrm{ll}}\mathbf{l}}$ being the weighted sum of $O-C$ of the reduced normal equation system.

3.5.2 Elimination or stacking of parameters

Eliminating or stacking (equalising) u_e parameters $\Delta\hat{\mathbf{x}}_1$ in a normal equation system so that a vector of parameters $\Delta\hat{\mathbf{x}}_2$ remains according to the relation

$$\Delta\hat{\mathbf{x}} = \begin{pmatrix} \Delta\hat{\mathbf{x}}_1 \\ \Delta\hat{\mathbf{x}}_2 \end{pmatrix} \rightarrow \Delta\hat{\tilde{\mathbf{x}}} = \Delta\hat{\mathbf{x}}_2 \tag{3.44}$$

is performed by formulating the transformation

$$\mathbf{C}_1\Delta\hat{\mathbf{x}}_1 + \mathbf{C}_2\Delta\hat{\mathbf{x}}_2 = \mathbf{z}. \tag{3.45}$$

Thereby, in the case of eliminating the parameters $\Delta\hat{\mathbf{x}}_1$ from the system,

$$\begin{aligned} \mathbf{C}_1 &= \mathbf{I}_{[u_e]}, \\ \mathbf{C}_2 &= \mathbf{0}, \\ \mathbf{z} &= \mathbf{0}, \end{aligned} \tag{3.46}$$

while in case of stacking (equalising) the parameters in $\Delta\hat{\mathbf{x}}_1$ with the first u_e parameters in $\Delta\hat{\mathbf{x}}_2$,

$$\begin{aligned} \mathbf{C}_1 &= \mathbf{I}_{[u_e]}, \\ \mathbf{C}_2 &= \begin{bmatrix} -\mathbf{I}_{[u_e]} & \mathbf{0}_{[u-2u_e]} \end{bmatrix}, \\ \mathbf{z} &= \mathbf{x}_{0,2} - \mathbf{x}_{0,1}. \end{aligned} \tag{3.47}$$

The elements of Matrix $\mathbf{C}_2$ correspond to the order of the parameters to be stacked within $\Delta\hat{\mathbf{x}}_2$.

The relationship between the original parameter vector $\begin{bmatrix} \Delta\hat{\mathbf{x}}_1 & \Delta\hat{\mathbf{x}}_2 \end{bmatrix}$ and the reduced parameter vector $\Delta\tilde{\hat{\mathbf{x}}}$ reads

$$\begin{pmatrix} \Delta\hat{\mathbf{x}}_1 \\ \Delta\hat{\mathbf{x}}_2 \end{pmatrix} = \begin{bmatrix} -\mathbf{C}_1^{-1}\mathbf{C}_2 \\ \mathbf{I}_{[u-u_e]} \end{bmatrix} \Delta\tilde{\hat{\mathbf{x}}} + \begin{pmatrix} \mathbf{C}_1^{-1}\mathbf{z} \\ \mathbf{0} \end{pmatrix} \tag{3.48}$$

which provides us the functional model of the transformation

$$\begin{aligned} \mathbf{T} &= \begin{bmatrix} -\mathbf{C}_1^{-1}\mathbf{C}_2 \\ \mathbf{I}_{[u-u_e]} \end{bmatrix}, \\ \mathbf{d} &= 0, \\ \mathbf{t} &= \begin{pmatrix} \mathbf{C}_1^{-1}\mathbf{z} \\ \mathbf{0} \end{pmatrix} \end{aligned} \tag{3.49}$$

to be inserted into Eq. 3.33–3.37.

3.5.3 Introduction of additional parameters

Introducing additional parameters into a system of u parameters that are in an affine relation with parameters that do already exist in the equation system is the inverse procedure to eliminating parameters. The functional model to introduce a set of u_a parameters $\hat{\mathbf{q}}_j$ that is in affine relation with an existing subset of u_t parameters $\hat{\mathbf{x}}_j$ of the parameter vector (e.g., introducing velocity parameters or infinitesimal Helmert parameters into an equation system containing station positions) would read

$$\hat{\mathbf{x}}_j \rightarrow \begin{pmatrix} \tilde{\hat{\mathbf{x}}}_j \\ \hat{\mathbf{q}}_j \end{pmatrix} \tag{3.50}$$

(note that this transformation is not unique, as the dimension of the vector of solved parameters is increased).

Starting with the inverse relationship, the transformation is formulated

$$\begin{aligned} \hat{\mathbf{x}}_j &= \mathbf{T}_j(\tilde{\hat{\mathbf{x}}}_j - \mathbf{d}_j) + \mathbf{S}_j\hat{\mathbf{q}}_j \\ &= \begin{bmatrix} \mathbf{T}_j & \mathbf{S}_j \end{bmatrix} \begin{pmatrix} \tilde{\hat{\mathbf{x}}}_j \\ \hat{\mathbf{q}}_j \end{pmatrix} - \mathbf{T}_j\mathbf{d}_j, \end{aligned} \tag{3.51}$$

$$\begin{aligned} \Delta\hat{\mathbf{x}}_j &= \mathbf{T}_j\Delta\tilde{\hat{\mathbf{x}}}_j + \mathbf{S}_j\Delta\hat{\mathbf{q}}_j + \mathbf{t}_j \\ &= \begin{bmatrix} \mathbf{T}_j & \mathbf{S}_j \end{bmatrix} \begin{pmatrix} \Delta\tilde{\hat{\mathbf{x}}}_j \\ \Delta\hat{\mathbf{q}}_j \end{pmatrix} + \mathbf{t}_j, \end{aligned} \tag{3.52}$$

where $\mathbf{T}_{j\,[u_t \times u_t]}$ is the transformation matrix for the existing set of parameters and $\mathbf{S}_{j\,[u_a \times u_a]}$ describes the functional relationship between the parameters to be introduced and the parameters that do already exist within the system. For parameters that are not affected by the transformation, the transformation matrices $\mathbf{T}$ and $\mathbf{S}$ as well as the vectors $\mathbf{d}$ and $\mathbf{t}$ are padded with zero elements. To introduce a set of u_a parameters $\hat{\mathbf{q}}_j$ into an equation system of which a subset $\hat{\mathbf{x}}_1$ of $u - u_a - u_t$ parameters are unaffected by the transformation, the transformation to a new set of u parameters is described in the following way:

$$\begin{pmatrix} \hat{\mathbf{x}}_1 \\ \hat{\mathbf{x}}_j \end{pmatrix}_{[u-u_a \times 1]} \rightarrow \begin{pmatrix} \hat{\mathbf{x}}_1 \\ \hat{\tilde{\mathbf{x}}}_j \\ \hat{\mathbf{q}}_j \end{pmatrix}_{[u \times 1]} \tag{3.53}$$

with

$$\begin{aligned} \mathbf{T} &= \begin{bmatrix} \mathbf{I}_{[u-u_a-u_t]} & \mathbf{0} \\ \mathbf{0} & \mathbf{T}_j \end{bmatrix}, \\ \mathbf{S} &= \begin{bmatrix} \mathbf{0} \\ \mathbf{S}_j \end{bmatrix}, \\ \mathbf{d} &= \begin{pmatrix} \mathbf{0} \\ \mathbf{d}_j \end{pmatrix}, \\ \mathbf{t} &= \begin{pmatrix} \mathbf{0} \\ \mathbf{t}_j \end{pmatrix}, \end{aligned} \tag{3.54}$$

which extend the transformation equations given in Eq. 3.33–3.37 to derive the extended normal equation matrix

$$\tilde{\mathbf{N}} = \begin{bmatrix} \mathbf{T}^{\mathrm{T}}\mathbf{N}\mathbf{T} & \mathbf{T}^{\mathrm{T}}\mathbf{N}\mathbf{S} \\ \mathbf{S}^{\mathrm{T}}\mathbf{N}\mathbf{T} & \mathbf{S}^{\mathrm{T}}\mathbf{N}\mathbf{S} \end{bmatrix}, \tag{3.55}$$

the extended right-hand side of the normal equation system

$$\tilde{\mathbf{y}} = \begin{pmatrix} \mathbf{T}^{\mathrm{T}}(\mathbf{y} - \mathbf{N}\mathbf{t}) \\ \mathbf{S}^{\mathrm{T}}(\mathbf{y} - \mathbf{N}\mathbf{t}) \end{pmatrix}, \tag{3.56}$$

and the weighted square sum of $O - C$ of the extended normal equation system

$$\widetilde{\mathbf{l}^{\mathrm{T}}\mathbf{P}_{\mathbf{ll}}\mathbf{l}} = \mathbf{l}^{\mathrm{T}}\mathbf{P}_{\mathbf{ll}}\mathbf{l} - \mathbf{t}^{\mathrm{T}}(2\mathbf{y} - \mathbf{N}\mathbf{t}), \tag{3.57}$$

separating again the cases of predefined new a priori values $\tilde{\mathbf{x}}_0$ (1) and of an affine transformation of the parameter vector (2) with

$$\begin{aligned} \mathbf{t} &= \mathbf{T}(\tilde{\mathbf{x}}_0 - \mathbf{d}) + \mathbf{S}\mathbf{q}_0 - \mathbf{x}_0, \\ &\tilde{\mathbf{x}}_0 \text{ defined (case 1)}, \end{aligned} \tag{3.58}$$

or

$$\begin{aligned} \mathbf{t} &= 0, \\ \tilde{\mathbf{x}}_0 &= \mathbf{T}^{-1}(\mathbf{x}_0 - \mathbf{S}\mathbf{q}_0) + \mathbf{d} \\ &= \mathbf{R}(\mathbf{x}_0 - \mathbf{S}\mathbf{q}_0) + \mathbf{d} \text{ (case 2)}. \end{aligned} \tag{3.59}$$

In our study, this algorithm is used to remove a priori datum information contained in normal equation systems by introducing infinitesimal Helmert transformation parameters. For an equation system parameterising the three-dimensional positions of N stations, one must introduce $u_a = 7$ infinitesimal Helmert transformation parameters, namely three translations (origin) $\mathbf{t} = \begin{pmatrix} t_1 & t_2 & t_3 \end{pmatrix}^{\mathrm{T}}$, three rotations (orientation) $\mathbf{r} = \begin{pmatrix} r_1 & r_2 & r_3 \end{pmatrix}^{\mathrm{T}}$, and one excess scale parameter $\Delta\mu$. For each station s, the relationship between the station coordinates $\mathbf{x}_s = \begin{pmatrix} x_s & y_s & z_s \end{pmatrix}^{\mathrm{T}}$ and the infinitesimal Helmert transformation parameters is derived by a Taylor series expansion that is truncated after the first-order correction term (cf. Gerstl et al., 2008)

$$\begin{aligned} \mathbf{x}_s &= \tilde{\mathbf{x}}_s + \begin{bmatrix} 1 & 0 & 0 & 0 & -\tilde{z}_s & \tilde{y}_s & \tilde{x}_s \\ 0 & 1 & 0 & \tilde{z}_s & 0 & -\tilde{x}_s & \tilde{y}_s \\ 0 & 0 & 1 & -\tilde{y}_s & \tilde{x}_s & 0 & \tilde{z}_s \end{bmatrix} \cdot \begin{pmatrix} -\mathbf{t} \\ -\mathbf{r} \\ -\Delta\mu \end{pmatrix} \\ &= \tilde{\mathbf{x}}_s + \mathbf{S}_s \cdot \mathbf{q}, \end{aligned} \tag{3.60}$$

with $\tilde{\mathbf{x}}_s = \begin{pmatrix} \tilde{x}_s & \tilde{y}_s & \tilde{z}_s \end{pmatrix}^{\mathrm{T}}$ being the starting points of the Taylor expansion (e.g., the a priori values of the station coordinates). The negative signs of the infinitesimal Helmert parameters relate to the direction of the transformation.

The functional model to be inserted into Eq. 3.55–3.57 reads

$$\begin{aligned} \mathbf{T} &= \mathbf{I}_u, \\ \mathbf{S} &= \begin{bmatrix} \mathbf{0}_{[(u-3N)\times 7]} \\ \mathbf{S}_1 \\ \vdots \\ \mathbf{S}_N \end{bmatrix}, \\ \mathbf{d} &= \mathbf{0}, \\ \mathbf{t} &= \mathbf{0}. \end{aligned} \tag{3.61}$$

Thereby, the zero block of $\mathbf{S}$ relates to the $u - 3N$ parameters of the equation system that are not in a functional relationship with the seven infinitesimal Helmert parameters (e.g., parameters other than station coordinates).

3.5.4 Transformation of a priori values

The operation serves to transform the vector of a priori values $\mathbf{x}_0$ to a new vector of a priori values $\tilde{\mathbf{x}}_0 = \mathbf{x}_0 + \mathbf{t}$. It is often applied to transform the a priori values of identical parameters in different normal equations to the same values before combining the equation systems and stacking the parameters.

The functional model to be inserted into Eq. 3.33–3.37 reads

$$\begin{aligned} \mathbf{R} &= \mathbf{T} = \mathbf{I}_u, \\ \mathbf{d} &= 0, \\ \mathbf{t} &= \tilde{\mathbf{x}}_0 - \mathbf{x}_0, \end{aligned} \tag{3.62}$$

resulting in a transformed normal equation system

$$\tilde{\mathbf{N}} = \mathbf{N}, \tag{3.63}$$

$$\tilde{\mathbf{y}} = \mathbf{y} - \mathbf{N}\mathbf{t}, \tag{3.64}$$

$$\widetilde{\mathbf{l}^{\mathrm{T}}\mathbf{P}_{\mathbf{ll}}\mathbf{l}} = \mathbf{l}^{\mathrm{T}}\mathbf{P}_{\mathbf{ll}}\mathbf{l} - \mathbf{t}^{\mathrm{T}}(2\mathbf{y} - \mathbf{N}\mathbf{t}). \tag{3.65}$$

3.5.5 Linear epoch transformation

The operation serves to transform the a pair of parameters in an offset/drift notation from an epoch t_1 to an epoch t_2 according to the relationship

$$\begin{pmatrix} p(t_1) \\ \dot{p}(t_1) \end{pmatrix} \rightarrow \begin{pmatrix} p(t_2) \\ \dot{p}(t_2) \end{pmatrix}, \tag{3.66}$$

with a constant drift $\dot{p}(t_2) = \dot{p}(t_1)$.

The relationship between the parameters follows

$$\begin{aligned} \hat{\tilde{\mathbf{x}}}_i &= \begin{pmatrix} p(t_2) \\ \dot{p}(t_2) \end{pmatrix} = \begin{bmatrix} 1 & t_2 - t_1 \\ 0 & 1 \end{bmatrix} \begin{pmatrix} p(t_1) \\ \dot{p}(t_1) \end{pmatrix} \\ &= \mathbf{T}_i^{-1}\hat{\mathbf{x}}_i = \mathbf{R}\hat{\mathbf{x}}_i, \end{aligned} \tag{3.67}$$

resulting in the functional model for the transformation

$$\begin{aligned} \mathbf{R}_i &= \begin{bmatrix} 1 & t_2 - t_1 \\ 0 & 1 \end{bmatrix}, \\ \mathbf{d}_i &= 0, \\ \mathbf{t_i} &= 0 \end{aligned} \tag{3.68}$$

to be inserted into Eq. 3.33–3.37.

3.5.6 Linear epoch transformation with regularisation

The operation serves to transform a pair of parameters ΔUT1 and LOD = $-d/dt\Delta$UT1 from an epoch t_1 to an epoch t_2.

A three-step procedure is applied for each pair of parameters

$[p(t_i), \dot{p}(t_i)] = [\Delta\text{UT1}(t_i), -\text{LOD}(t_i)]$,

namely

(1) regularisation
$[p(t_1), \dot{p}(t_1)] \rightarrow [\bar{p}(t_1), \bar{\dot{p}}(t_1)]$,

(2) linear transformation of the regularised pair of parameters
$[\bar{p}(t_1), \bar{\dot{p}}(t_1)] \rightarrow [\bar{p}(t_2), \bar{\dot{p}}(t_2)]$,

(3) de-regularisation
$[\bar{p}(t_2), \bar{\dot{p}}(t_2)] \rightarrow [p(t_2), \dot{p}(t_2)]$.

The non-regularised parameters $p = \Delta\text{UT1}, \dot{p} = -\text{LOD}$ and their regularised counterparts $\bar{p}$ and $\bar{\dot{p}}$ are related according to

$$p(t_i) = \bar{p}(t_i) + r(t_i),\ \dot{p}(t_i) = \bar{\dot{p}}(t_i) + \dot{r}(t_i), \tag{3.69}$$

with r and $\dot{r}$ being the regularisation of p and $\dot{p}$, respectively. Conventionally, the regularisation is calculated according to Chapter 8.1 of Petit and Luzum (2010).

For one pair $p(t_i), \dot{p}(t_i)$, the relationship reads

$$\begin{pmatrix} p(t_1) \\ \dot{p}(t_1) \end{pmatrix} \rightarrow \begin{pmatrix} p(t_2) \\ \dot{p}(t_2) \end{pmatrix}. \tag{3.70}$$

Inserting Eq. 3.69 into Eq. 3.67 results in the functional model

$$\begin{aligned}\mathbf{R}_i &= \begin{bmatrix} 1 & t_2 - t_1 \\ 0 & 1 \end{bmatrix}, \\ \mathbf{d}_i &= \begin{pmatrix} r(t_2) - r(t_1) - (t_2 - t_1)\dot{r}(t_1) \\ \dot{r}(t_2) - \dot{r}(t_1) \end{pmatrix}, \\ \mathbf{t_i} &= 0\end{aligned} \tag{3.71}$$

to be inserted into Eq. 3.33–3.37.

3.5.7 Re-parameterisation from offset/drift to two offsets

The transformation serves to re-parameterise a set of parameters in offset/drift notation (epoch t_i) linearly to two offsets (epochs t_1, t_2). It is mostly applied to transform pole coordinates and their rates from an epoch during the day to the neighbouring day boundaries. For one parameter p, the transformation reads

$$\begin{pmatrix} p(t_i) \\ \dot{p}(t_i) \end{pmatrix} \rightarrow \begin{pmatrix} p(t_1) \\ p(t_2) \end{pmatrix}. \tag{3.72}$$

The relationship between the parameters is

$$\begin{aligned}\hat{\tilde{\mathbf{x}}}_i &= \begin{pmatrix} p(t_1) \\ p(t_2) \end{pmatrix} = \begin{bmatrix} 1 & t_1 - t_i \\ 1 & t_2 - t_i \end{bmatrix} \begin{pmatrix} p(t_i) \\ \dot{p}(t_i) \end{pmatrix} \\ &= \mathbf{T}_i^{-1}\hat{\mathbf{x}}_i = \mathbf{R}\hat{\mathbf{x}}_i,\end{aligned} \tag{3.73}$$

resulting in the functional model for the transformation

$$\begin{aligned}\mathbf{R}_i &= \begin{bmatrix} 1 & t_1 - t_i \\ 1 & t_2 - t_i \end{bmatrix}, \\ \mathbf{d}_i &= 0, \\ \mathbf{t_i} &= 0\end{aligned} \tag{3.74}$$

to be inserted into Eq. 3.33–3.37.

3.5.8 Re-parameterisation from offset/drift to two offsets with regularisation

The transformation serves to re-parameterise a set of parameters ΔUT1 and LOD = $-d/dt\Delta$UT1 (epoch t_i) to two ΔUT1 offsets at the day boundaries (epochs t_1, t_2).

A three-step procedure is applied for each pair of parameters

$[p(t_i),\dot{p}(t_i)] = [\Delta\mathrm{UT1}(t_i), -\mathrm{LOD}(t_i)]$,

namely

(1) regularisation
$[p(t_i), \dot{p}(t_i)] \rightarrow [\bar{p}(t_i), \bar{\dot{p}}(t_i)]$,

(2) linear transformation of the regularised pair of parameters
$[\bar{p}(t_i), \bar{\dot{p}}(t_i)] \rightarrow [\bar{p}(t_1), \bar{p}(t_2)]$,

(3) de-regularisation
$[\bar{p}(t_1), \bar{p}(t_2)] \rightarrow [p(t_1), p(t_2)]$.

The non-regularised parameters $p = \Delta\mathrm{UT1}$, $\dot{p} = -\mathrm{LOD}$ and their regularised counterparts $\bar{p}$ and $\bar{\dot{p}}$ are related according to Eq. 3.40

For one pair $[p(t_i),\dot{p}(t_i)]$, the transformation reads

$$\begin{pmatrix} p(t_i) \\ \dot{p}(t_i) \end{pmatrix} \rightarrow \begin{pmatrix} p(t_1) \\ p(t_2) \end{pmatrix}. \tag{3.75}$$

Inserting Eq. 3.75 into Eq. 3.73 results in the functional model

$$\begin{aligned} \mathbf{R}_i &= \begin{bmatrix} 1 & t_1 - t_i \\ 1 & t_2 - t_i \end{bmatrix}, \\ \mathbf{d}_i &= \begin{pmatrix} r(t_1) - r(t_i) - (t_1 - t_i)\dot{r}(t_i) \\ r(t_2) - r(t_i) - (t_2 - t_i)\dot{r}(t_i) \end{pmatrix}, \\ \mathbf{t_i} &= 0 \end{aligned} \tag{3.76}$$

to be inserted into Eq. 3.33–3.37.

4 Implementation of the analysis and combination strategies

4.1 Software overview

With the **D**GFI **O**rbit and **G**eodetic parameter estimation **S**oftware (DOGS), DGFI-TUM maintains a software to process space-geodetic observation data (SLR, DORIS, and VLBI) and to integrate data sets from internal and/or external sources into combined solutions. All branches of the DOGS software have been developed within the institute for a long time and are in operational use within the framework of DGFI-TUM's involvement as an ITRS Combination Centre (Angermann et al., 2020) as well as within its contribution to the IAG Scientific Services, namely as Analysis Centre (AC) within the ILRS (Bloßfeld and Kehm, 2020) and the IVS (Glomsda et al., 2021b), respectively, and as Associate Analysis Centre (AAC) within the IDS (Rudenko et al., 2021). DGFI-TUM and the Federal Agency for Cartography and Geodesy (BKG) jointly operate an IVS Combination Centre (Bachmann et al., 2021). Moreover, DGFI-TUM in its function as IGS SIRGAS Regional Network Associate Analysis Centre (IGS SIRGAS RNAAC; Sánchez and Kehm, 2021) uses the Bernese GNSS Software v. 5.2 (Dach et al., 2015) to process GNSS data.

Tab. 4.1 provides an overview of the software packages used at DGFI-TUM and their involvement within the present studies, Fig. 4.1 outlines the involvement of the software packages in our main study (Chapt. 5) in a graphical way. The usage of the DOGS software branches DOGS-OC and DOGS-CS in the simulation studies presented in Section 6.4 is shown in detail in Fig. 6.8.

Table 4.1: Software packages used at DGFI-TUM. Activities in parentheses were conducted outside of this study but the resulting data have been used.

Software	techniques	usage within this study
DOGS-OC	SLR	reprocessing of SLR observations, simulation studies
	DORIS	–
DOGS-RI	VLBI	(reprocessing of VLBI observations for ITRF2020)
Bernese	GNSS	reprocessing of GNSS observations
DOGS-CS	all	combination, normal equation operations, solution

The DOGS software comprises three branches, namely

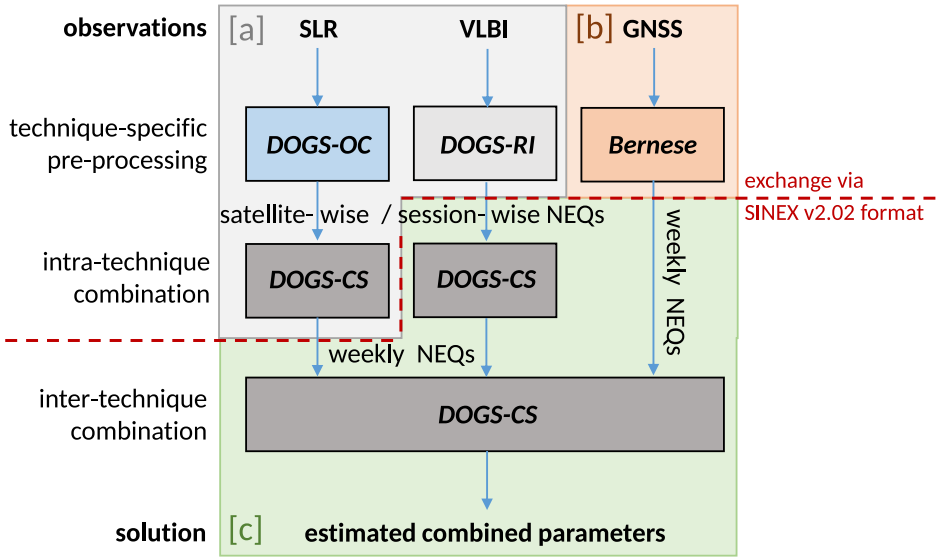

Figure 4.1: Usage of the software packages for the realisation of a regional geocentric reference frame. [a] Reprocessing of SLR and VLBI, cf. Sect. 5.3.2; [b] Reprocessing of the SIRGAS GNSS network, cf. Sect. 5.3.1; [c] Inter-technique combination, cf. Sect. 5.4.

(1) an **O**rbit **C**omputation software (DOGS-OC, Gerstl, 1997, current version 5.5) to process SLR and DORIS data,

(2) a **R**adio **I**nterferometry software (DOGS-RI, Kwak et al., 2017, current version 1.3) to process VLBI data, and

(3) a **C**ombination and **S**olution library (DOGS-CS, Gerstl et al., 2008, current version 5.1) to combine, constrain, transform, and solve normal equation systems.

While DOGS-RI is being developed within the institute but independently from this study and the Bernese GNSS Software is being developed externally at the University of Berne, DOGS-OC and DOGS-CS have undergone a significant development with contribution by the author of this doctoral thesis.

4.2 The orbit computation software DOGS-OC

DOGS-OC (Gerstl, 1997) is DGFI-TUM's software to process satellite observations from SLR and DORIS. DOGS-OC is written in Fortran 2008[1]. The software provides four processing modi, namely an *orbit integration modus*, a *simulation modus*, a *normal equation generation modus*, and a *parameter estimation modus*. While the orbit integration modus serves to dynamically integrate a satellite orbit based on a given ini-

[1]ISO/IEC 1539-1:2010, URL: `https://www.iso.org/standard/50459.html` (2022-06-15).

tial state vector and dynamical models, a simulation modus has been implemented in order to simulate SLR observations from an integrated orbit. The two remaining modi allow to process (real or simulated) SLR observations to generate normal equations or other output files which are used to evaluate the data or to be forwarded into further processing steps (e.g., binary normal equation files for combination and solution with DOGS-CS, or binary solution equation files for analysis with DOGS-CS; cf. Fig. 4.2). While the normal equation generation modus serves to directly set up a normal equation system, the parameter estimation modus performs an iterative optimisation of the square sum of observation residuals $\mathbf{v}^{\mathrm{T}}\mathbf{P}\mathbf{v}$ (cf. Sect. 3.2) in connection with an automatic outlier detection. The parameter estimation modus is used to iteratively pre-process single-satellite arcs until all observation outliers are identified. Thereby, the parameter estimates from one iteration (e.g., initial orbital elements) are used as a priori values of the parameters for the next iteration. Finally, an arc that has been iterated in such a way is used to generate the normal equations that are the input to the subsequent intra- and/or inter-technique combination steps.

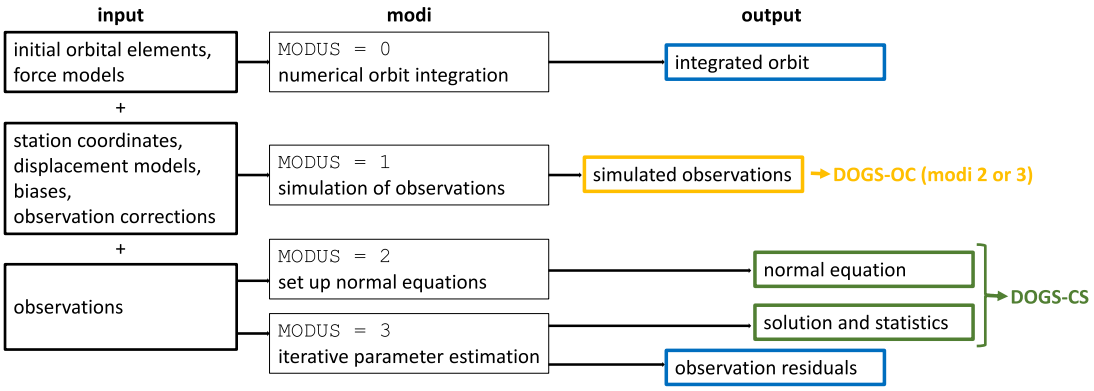

Figure 4.2: Structure of the DOGS-OC software.

Table 4.2: Orbit integration settings for SLR processing.

Model	description
Orbit integration frame	Geocentric Celestial Reference System
Integrator	Gauß-Jackson predictor-corrector algorithm of 7th order
Relative error bound	10^{-9}
Integrator step size	satellite-dependent
Arc length	7 days
Observation weight	1 cm (core stations$^{(a)}$) or 1 m (other stations)
Elevation cut-off angle	5°

$^{(a)}$according to the ILRS Discontinuities File

Tab. 4.2 gives an overview of the orbit integration procedure implemented in DOGS-OC. The software applies a Gauß-Jackson algorithm of 7th order to integrate satellite orbits in a Geocentric Celestial Reference System. The integrator step size can be chosen satellite-dependent, the observational model of SLR is implemented according to Section 6.2. For the processing of spherical satellites after 1993, the ILRS-defined standard arc length is 7 days (i.e., one week), which is the processing standard applicable to our studies. All observations are assigned a weight equivalent to a standard deviation of 1 cm, and the elevation cut-off angle is set to 5° for all stations. Within the framework of these studies, the simulation modus of DOGS-OC was made operational, complemented by an environment of script programs that allow a free choice of the conditions assumed in a simulation scenario (tracking scheme, noise assumptions, etc.). Moreover, the software was updated to the most recent standards and conventions for a full and consistent reprocessing of the SLR observations.

4.3 The combination and solution library DOGS-CS

DOGS-CS (Gerstl et al., 2008) is DGFI-TUM's library to combine (Sect. 3.4), manipulate (Sect. 3.5), and solve (Sect. 3.2) normal equation systems. Like DOGS-OC, the DOGS-CS software is written in Fortran 2008. The software uses an internal binary format where a file stores a full equation system including its metadata (Fig. 4.3). Thereby, the *file header* contains bookkeeping information about the processing history (i.e., the file tree), the equation's type, dimension and statistics, the observation/data type contained in the equation, the applied background models, the active, reduced, or eliminated parameters, as well as station, eccentricity, and VLBI source inventories. The *file body* contains the actual equation system in a matrix/vector notation, i.e., either a set of normal equations, (pseudo-)observation equations, or solution equations, including its right-hand side, its (pseudo-)observation vector, or its solution vector, respectively, and relevant statistical parameters, namely $\mathbf{l}^{\mathrm{T}}\mathbf{P}\mathbf{l}$ for normal equation or (pseudo-)observation equation systems and $\mathbf{v}^{\mathrm{T}}\mathbf{P}\mathbf{v}$ for solutions (cf. Bloßfeld et al., 2021).

The equation system in the file body is stored in one of the following ways:

Normal equation system

$\mathbf{x}_{0\,[1\times u]}^{\mathrm{T}}$	$\mathbf{l}^{\mathrm{T}}\mathbf{P}_{\mathbf{ll}}\mathbf{l}$
$\mathbf{N}_{[u\times u]}$	$\mathbf{y}_{[u\times 1]}$

Observation equation system

$\left[\mathbf{x}_{0\,[1\times u]}^{\mathrm{T}}, \mathbf{l}^{\mathrm{T}}\mathbf{P}_{\mathbf{ll}}\mathbf{l}\right]$		–
$\mathbf{p}_{[n\times 1]}$	$\mathbf{A}_{[n\times u]}$	$\mathbf{l}_{[n\times 1]}$

Solution equation system

$\mathbf{x}_{0\,[1\times u]}^{\mathrm{T}}$	$\mathbf{v}^{\mathrm{T}}\mathbf{P}_{\mathbf{ll}}\mathbf{v}$
$\mathbf{Q}_{[u\times u]}$	$\Delta\hat{\mathbf{x}}_{[u\times 1]}$

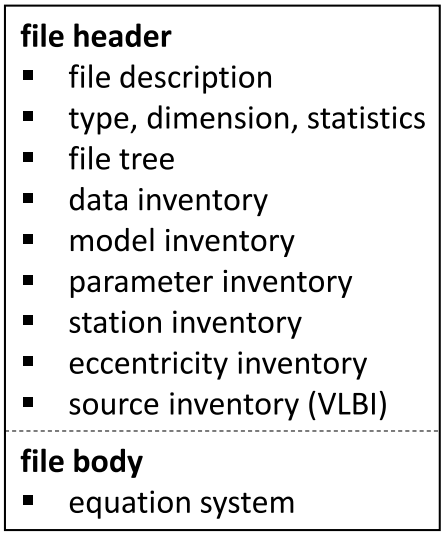

Figure 4.3: Structure of a binary DOGS equation file.

The principle usage of DOGS-CS is to combine and manipulate equation systems at the normal equation level before calculating a solution. To a limited extent, also manipulations of solution equation systems are possible (e.g., epoch transformations). Normal equations can be imported either directly in the software-internal binary format (e.g., the output from DOGS-OC and DOGS-RI), or they can be converted from the Solution INdependent EXchange version 2.02 (SINEX v2.02, or earlier) format[2]. The latter functionability allows us to process normal equation systems independently from their origin, for example provided routinely by the IAG Scientific Services.

The library contains 20 standalone programs, each of them dedicated to performing specific groups of operations. The routines can be classified into five groups, namely

(1) DOGS-CS interfaces with external data formats or human-readable output formats

(1.1) **cs_glscod**: convert an equation system and/or selected related metadata from the internal binary format to a human-readable format.

(1.2) **cs_solview**: output the estimates of a solution equation system in a human-readable solution format.

(1.3) **cs_sinexgls**: convert an equation system from SINEX v2.02 (or earlier) format into a normal equation system in the internal binary format. If the SINEX file contains a solution, the constraint-free normal equation is reconstructed automatically if all required information is given in the SINEX file.

[2]cf. IERS Message No. 103, 2006. URL: `https://datacenter.iers.org/data/2/message_103.txt` (2022-06-15).

(1.4) **cs_glssinex**: convert an equation system (normal equation or solution) from the internal binary format to SINEX v2.02 format.

(2) DOGS-CS routines to modify the content of equation systems

(2.1) **cs_headmod**: modify the metadata in the header of an equation system.

(2.2) **cs_vasort**: re-sort the parameters within an equation system.

(2.3) **cs_renam**: rename parameters in an equation system.

(3) DOGS-CS routines to combine normal equation systems or to set up and add constraints (cf. Sect. 3.4)

(3.1) **cs_add**: add two normal equation systems (Eq. 3.17–3.19).

(3.2) **cs_cond**: set up a system of (pseudo-)observation/condition equations (Eq. 3.20–3.23).

(3.3) **cs_bgl2ngl**: convert a (pseudo-)observation equation system into a normal equation system (the functionality is also performed automatically by **cs_add**). Relevant to generate a normal equation of constraints to be written into a SINEX file.

(4) DOGS-CS routines to transform parameters within equation systems (cf. Sect. 3.5)

(4.1) **cs_reduc**: reduce parameters from a normal equation system (Eq. 3.39–3.43).

(4.2) **cs_elim**: eliminate parameters from a normal equation system (Eq. 3.44–3.49).

(4.3) **cs_inpar**: introduce parameters into a normal equation system (Eq. 3.50–3.59).

(4.4) **cs_trafo**: parameter transformations with regular transformation matrix (general formulation in Eq. 3.31–3.38; examples in Sect. 3.5.4–3.5.8).

(4.5) **cs_trasi**: parameter transformations with singular transformation matrix (applicable to solution equation systems only, cf. Bloßfeld, 2015).

(4.6) **cs_wicht**: re-weight (scale) a given equation system (the functionality is also implemented in **cs_add**).

(5) DOGS-CS routines to solve (cf. Sect. 3.2) **and evaluate equation systems**

(5.1) **cs_invert**: solve a normal equation system (Eq. 3.12–3.15).

(5.2) **cs_eiwe**: calculate the eigenvalues of the equation matrix.

(5.3) **cs_helmert**: estimate parameters of a Helmert transformation between two sets of station coordinates (in the DOGS solution format or in the SINEX format). If velocities are given, the parameter epochs can be harmonised automatically.

(5.4) **cs_resid**: calculate the weighted square sum of observation residuals of individual sub-equation systems that were introduced into a given solution.

Each DOGS-CS routine is an independent program. A chain of operations on an equation system is realised by sequential calls of DOGS-CS routines via configuration files, whereby the workflow may be implemented in an arbitrary programming language. In the present studies, all workflows were implemented in the free Unix shell and command language BASH (Bourne Again SHell[3]). The DOGS-CS routines have been extended by additional functionalities enabling the filtering approach realised within the framework of these studies. Moreover, the interfaces with external formats as well as the internal binary format were extended to enable a consistent bookkeeping of all relevant information related to combined equation systems.

[3] `https://www.gnu.org/software/bash/` (2022-06-15).

5 Determination of a regional geocentric epoch reference frame for Latin America

5.1 Idea and overview

This chapter describes a strategy that has been developed by Kehm et al. (2022b▪) to achieve an improved datum realisation for a regional epoch reference frame for Latin America. Starting with the issues raised in Section 2.3, the study aims to realise a regional epoch reference frame that is geocentric at any epoch, whereby our area of interest covers the regional GNSS network of SIRGAS (Sect. 5.2) while the datum is realised by a combination of global space-geodetic networks, namely SLR, VLBI, and a globally extended GNSS network. We continue by outlining the corresponding reprocessing of the space-geodetic input data (Sect. 5.3) and the developed combination and filtering strategy (Sect. 5.4). All combination and filtering steps are performed at the level of normal equations (NEQs). Finally, we evaluate our approach by comparison and validation against the JTRF2014, a subsecular geocentric realisation of the ITRS, and against geophysical fluid loading models for non-tidal loading (NT-L; Sect. 5.5). We conclude with a summary and discussion of the results (Sect. 5.6).

5.2 Realisation of the datum

Currently, the operational weekly SIRGAS solutions are based on a GNSS network of which positions of a subset of selected core stations are constrained to the IGS weekly solutions, which themselves are aligned to the ITRF datum via NNR, NNT, and NNS constraints (cf. left panel of Fig. 5.1 and Chapter 2 of Kehm et al., 2022b▪).

▸Depending on the focus of interest, there are two possible ways of realising the datum of regional ERFs: The first would be to maintain the strategy as it is but improve the datum realisation via fiducial coordinates for a more accurate alignment with the ITRF datum. By these means, one could stick to the concept of processing GNSS-only-solutions, but consequently, coordinate variations would still be CF-related, i.e., the CM-minus-CF content of NT-L signals would still be missing in the station-specific displacement time series, as it is removed by the application of NNT constraints with respect to the ITRF. This would allow for a direct interpretation with respect to geophysics only after a correction of the CM-minus-CF variation from external geophysical

models. Because of the growing interest in exploiting geodetic data for geophysical investigations, the second possibility would be a direct epoch-wise geocentric realisation of the datum of the ERFs, resulting in CM-related coordinates at each epoch. This would imply the processing not only of a globally-extended GNSS network but also of global SLR and VLBI networks. The great advantage of such a solution would be the direct interpretability of station displacement time series in a geophysical sense, without having to rely on external information on the motion of a multi-year reference frame with respect to the geocentre. By these means, geodetic observations could contribute directly to interpreting geophysical processes and the improvement and validation of geophysical models. Within this study, we investigate the second approach and have developed a strategy for a direct realisation of the datum of weekly regional geocentric ERF solutions based on the reference frame for Latin America.

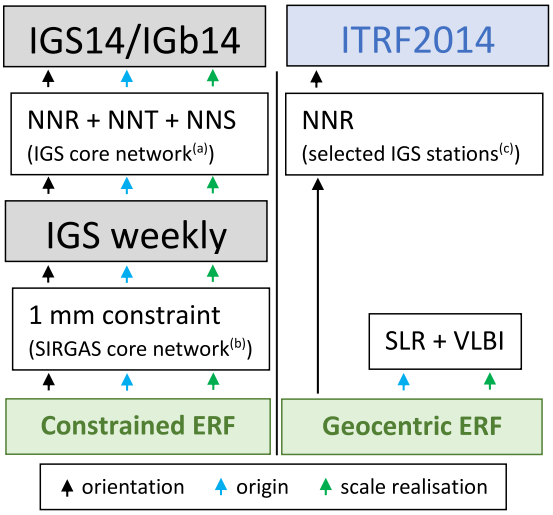

Figure 5.1: Concepts of datum realisation for the SIRGAS regional ERFs (left) and a direct geocentric realisation of ERFs (right). (a) cf. Rebischung et al. (2016); (b) cf. Sánchez and Kehm (2021); (c) cf. Sect. 5.3.1. The colours of the arrows refer to the different datum parameters. The datum of the IGS14/IGb14 and the ITRF2014 reference frames is considered identical.

Goal of this study are series of ERF solutions for Latin America, whereby the datum of each epoch-wise solution is defined consistently with the ITRS. The datum realisation is performed by combining the three space-geodetic techniques of SLR, VLBI, and GNSS. The origin is realised by SLR – the only technique permitting its realisation with highest accuracy –, and the scale is realised as a weighted mean by SLR and VLBI. Because these two techniques are responsible for the physically-defined datum parameters (in contrast to the orientation, which is defined by a mathematical constraint), we later denote these techniques as the "datum-relevant techniques". [...] The orientation is realised via a NNR constraint over the global GNSS (IGS stations) network (Fig. 5.1). [The NNR constraint over a well-distributed network compensates for the rank deficiency related to the orientation only and does not impact the geocentricity

or deform the network. This means that the solution fulfils the condition of "minimum constraints" (e.g., Kotsakis, 2012).] The datum transfer between the techniques is performed by introduction of local ties (LTs) at co-located sites, i.e., sites equipped with more than one of the space-geodetic techniques used, and locally measured difference vectors (ties) between the technique-specific reference points. Because, in our case, the target parameters are the positions of the GNSS stations contained in the regional network covered by SIRGAS, we do not include DORIS into the combination as this technique serves to densify the global ITRF station network [(cf. Sect. 3.1)] though it does not contribute to the datum parameters origin and scale.

One major issue in the realisation of ERFs is the so-called "network effect", i.e., apparent variations in the observed origin and scale caused by variations in the observing networks (e.g., Collilieux et al., 2009; Bloßfeld et al., 2014b). Unfortunately, this effect is of special importance for the datum-relevant techniques SLR and VLBI, which both suffer from sparse and inhomogeneous network distributions. As demonstrated in various simulation studies (e.g., Pavlis and Kuźmicz-Cieślak, 2009; Otsubo et al., 2016; Glaser et al., 2017, 2019a, b; Kehm et al., 2018▪, 2019▪), a substantial extension of the global SLR and VLBI networks would significantly stabilise the datum parameters realised. [In this context, Chapter 6 of this doctoral thesis presents various studies on the importance of exploiting the SLR observations to additional satellites and on the potential of future enhancements of the network.]

Table 5.1: ▪Ratio of gaps ≥ 1 week in observation time series of VLBI and SLR stations between 2000 and 2014. Corresponding to our combination approach, the investigation is based on GPS weeks. In other words, a gap of one week means a full GPS week without a single observation.

Gap length	SLR	VLBI
1 week	50.0 %	46.7 %
2 weeks	17.4 %	16.5 %
3 weeks	8.6 %	10.3 %
4 weeks	4.5 %	5.7 %
5–8 weeks	8.5 %	11.7 %
> 8 weeks	11.0 %	9.1 %

However, for the time being, we must deal with the existing networks and their apparent variations due to the observational gaps of individual stations. Tab. 5.1 gives an overview of the gaps within the observation time series of VLBI and SLR stations. As can be seen, approximately 50 % of the gaps extend over one single week whereas about 10 % of the gaps extend over more than 8 weeks. Another approximately 10 % of the gaps have a length of between 4 and 8 weeks. To increase the stability of the networks, one major point of our study has thus been to investigate the way in which a filter approach allows sufficient bridging of these observational gaps to reduce the network effect, without systematically distorting the datum parameters realised

(cf. Sect. 5.4.2).◂ The involvement of the different software packages in the processing steps is outlined in Section 4.1.

5.3 Reprocessing of the input data

This section describes the reprocessing of the space-geodetic input data according to the most recent standards and conventions as well as the modifications in the procedures that have been applied to achieve the goals of this study. Section 5.3.1 describes the reprocessing of the GNSS data, while Section 5.3.2 describes the reprocessing of the SLR and VLBI observations.

5.3.1 Reprocessing SIRGAS normal equations for combination with SLR and VLBI

▸An appropriate combination of global SLR, VLBI, and GNSS networks is required to implement an epoch-wise datum realisation for regional networks. In our case, the regional GNSS network must be extended beyond the area covered by the SIRGAS network to include SLR/GNSS and VLBI/GNSS co-located stations and enough GNSS stations to realise the orientation via a NNR constraint. Therefore, one main objective of the study was to identify the GNSS network configuration required for a reliable datum realisation. Different scenarios were evaluated in this context. The first considered only those GNSS sites co-located with SLR and VLBI (blue circles and green dots in Fig. 5.2). As most of these stations are in the northern hemisphere, this station distribution did not turn out to be favourable for the GNSS data pre-processing. Consequently, additional GNSS sites have been included to ensure a more homogeneous global network distribution, which is also favourable for a reliable realisation of the orientation. After a series of empirical experiments, our main conclusion is to include the core stations of the IGS14/IGb14 reference frame into the GNSS data processing.

Further research concentrated on the simultaneous determination of GNSS satellite orbits, satellite clock offsets, EOPs and station positions within the GNSS data processing. Although we use a global network in the computations, simultaneous inclusion of all SIRGAS regional stations reduces the reliability of the EOPs and GNSS orbits due to the dense station distribution in one specific region (see Fig. 5.2). Therefore, we apply a two-step procedure: (a) orbit and EOP determination based on a global and homogeneous network, and (b) processing of the GNSS data (global + regionally densified network), whereby the previously determined orbits and EOPs are fixed. A priori datum information introduced into the GNSS NEQs by fixing the orbits and the EOPs is removed before combining them with the SLR and VLBI NEQs. This is performed by introducing and reducing (pre-eliminating) seven Helmert parameters (3 translations, 3 rotations, and 1 scale parameter; cf. Bloßfeld, 2015). Thus, the GNSS NEQs introduced into the combination process are free from datum information.

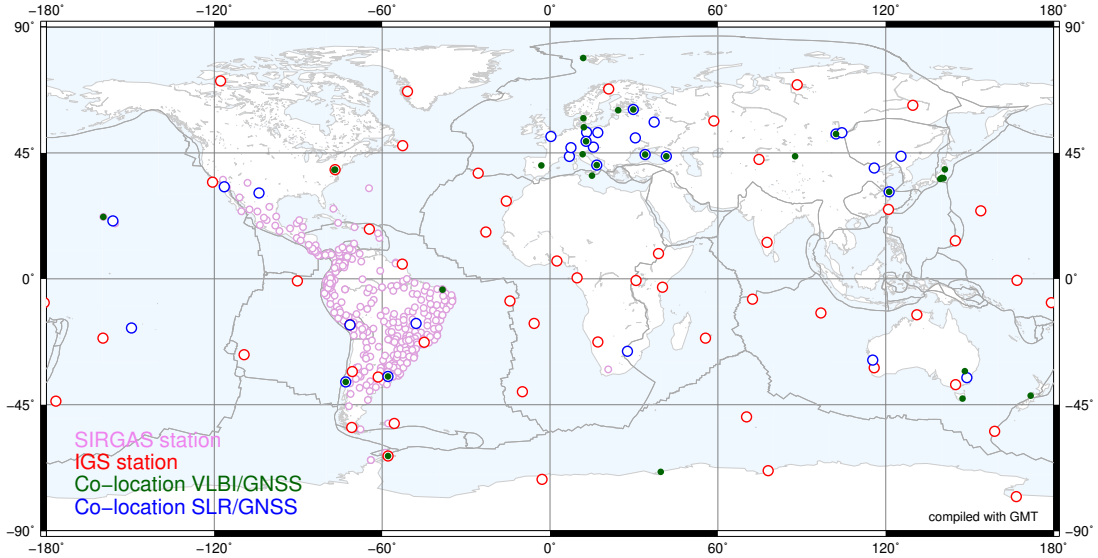

Figure 5.2: ▪Extension of the SIRGAS network by global IGS stations.

The SIRGAS data reprocessing for this study covers January 2000 to December 2020. It is based on the IGS14/IGb14 reference frame and includes 530 SIRGAS and 135 IGS reference stations (30 co-located with SLR and 31 co-located with VLBI). This reprocessed global GNSS network is called the SIRGAS extended network hereafter.◂ The GNSS data processing was performed with the Bernese GNSS Software Version 5.2. The weekly NEQs are provided in the SINEX v2.02 format as input to the further processing steps.

5.3.2 Reprocessing of the SLR and VLBI data

▸Besides a full reprocessing of the SIRGAS GNSS network, the SLR and VLBI input data also underwent a full reprocessing to comply with the most recent standards and conventions (Petit and Luzum, 2010, including updates until v. 1.3.0).

For SLR, we performed reprocessing specifically for this study. We extended the current standard 4-satellite-constellation [...], namely LAGEOS-1/2 (LAser GEOdynamics Satellite-1/2) and Etalon-1/2, by a fifth satellite, LARES (LAser RElativity Satellite). This is planned to be the future ILRS standard setup to ensure a higher stability of the SLR-derived origin (Bloßfeld et al., 2018▪). The satellites have been combined into weekly NEQs applying a [VCE (cf. Sect. 3.4.3)]. Satellite-specific parameters and orbits have been pre-reduced from the NEQs, leaving station positions and range biases as explicit parameters.

For VLBI, we rely on the VLBI contribution of DGFI-TUM to ITRF2020 (Glomsda et al., 2020). This data set has no NT-L correction applied and is thus consistent

with the routine processing standards of the other techniques. This contrasts with DGFI-TUM's routine contribution [to the IVS], "dgf2020a", which contains a priori corrections for non-tidal atmospheric loading (Glomsda et al., 2021b). We use the twice-weekly CORE/NEOS (until 2001) and R1/R4 (from 2002 on) sessions, as these are available on a permanent twice-weekly basis and contain sufficient co-location sites for datum realisation. VLBI-specific parameters like troposphere and clock are pre-reduced and thus not explicitly contained in the NEQs. The properties of all technique-specific contributions are summarised in Tab. 5.2.

Table 5.2: ▪Input data to the ERF combination.

Technique	temporal resolution	processing setup *SINEX NEQ content*	datum constraints
SLR	weekly	future ILRS 5-satellite setup *station coordinates* *range biases* *EOPs*	no
VLBI	session-wise	CORE/NEOS/R1/R4 sessions *station coordinates* *source coordinates* *EOPs*	no
GNSS	weekly	SIRGAS + global IGS network *station coordinates*	yes (to be removed)

The SLR and VLBI NEQs are free from datum constraints and thus only contain the datum information to which the respective observations are sensitive.◂ The processing of SLR and VLBI was performed with DOGS-OC and DOGS-RI, respectively. The weekly (SLR) or session-wise (VLB) NEQs are provided in the SINEX v2.02 format as input to the further processing steps.

5.4 Inter-technique combination strategy

This section describes the combination approach (Sect. 5.4.1) as well as the strategies for the filtering (Sect. 5.4.2), the technique-specific weighting (Sect. 5.4.3), and the treatment of local ties in the epoch-wise solutions (Sect. 5.4.4).

5.4.1 Combination approach

▸Weekly NEQs ($\mathbf{N}^i_{\text{tech}}$) from SLR and GNSS and session-wise NEQs from VLBI are the input data for the combination. The processing for an epoch t_i comprises the following steps (Fig. 5.3):

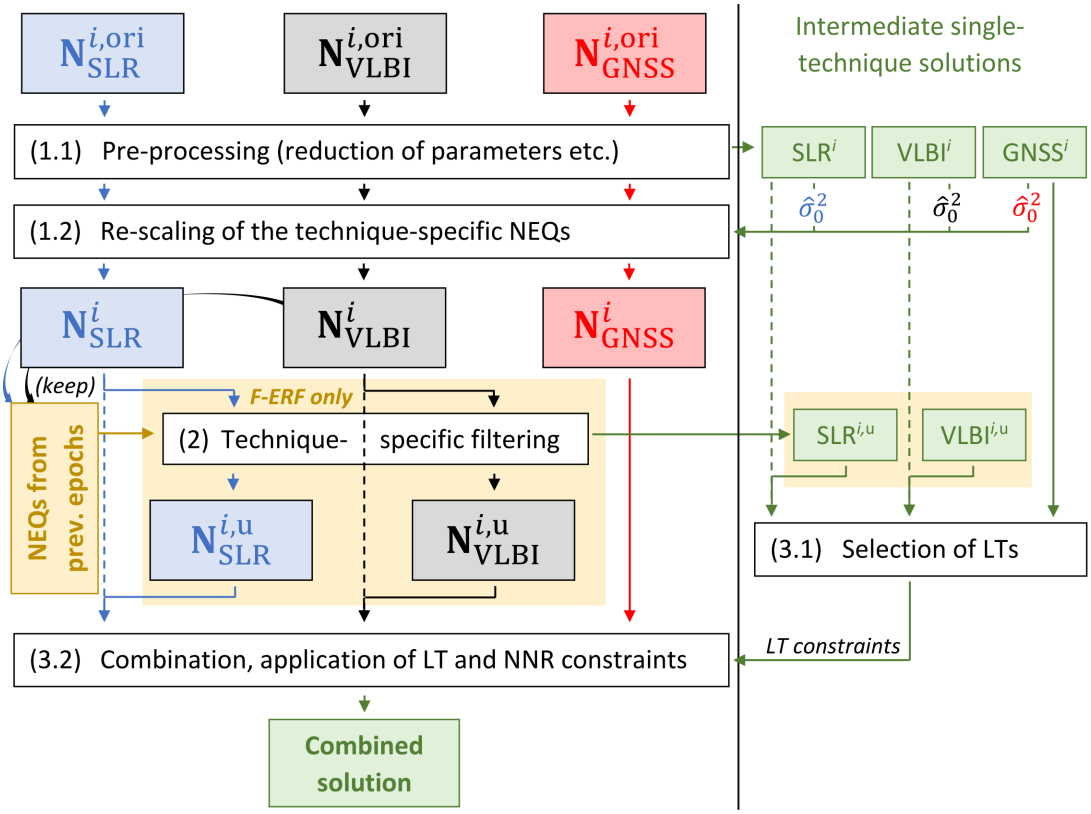

Figure 5.3: Concept of the technique-specific filtering (SLR and VLBI) and the inter-technique combination for epoch t_i. Dashed lines denote the unfiltered processing chain (U-ERF); light yellow boxes contain the additional steps performed only within the filtered processing chain (F-ERF).

(1.1) Pre-processing of the technique-specific NEQs. Calculation of intermediate single-technique (U-ST; "U" stands for "unfiltered") solutions.

(1.2) Rescaling of the technique-specific NEQs with their respective a posteriori variance factors from the U-ST solutions.

(2) Filtering the SLR and VLBI NEQs (F-ERF solution only). Calculation of intermediate filtered single-technique (F-ST) solutions.

(3.1) LT selection and weighting procedure based on the single-technique solutions.

(3.2) Inter-technique combination, the introduction of LT and NNR constraints and the subsequent solution of the combined NEQ.

In Step (1.1), incoming single-technique NEQs $\mathbf{N}^{i,\mathrm{ori}}_{\mathrm{tech}}$ are pre-processed for the combination. This includes accumulating the sessions of a week into one common NEQ for VLBI, reducing EOPs for SLR and VLBI, reducing range bias parameters for SLR, and eliminating source coordinates, i.e., fixing the celestial reference frame (CRF), for

VLBI. [For GNSS, infinitesimal Helmert parameters are introduced in order to remove the datum information contained in the NEQs due to fixing the satellite orbits (for the reprocessing of the GNSS NEQs, cf. Sect. 5.3.1)]. As a result, each NEQ is free from artificial datum information and only contains station coordinates as explicitly-estimated parameters. Afterwards, the intermediate U-ST solution is calculated with minimal constraints (i.e., NNR for SLR, NNR + NNT for VLBI, NNR + NNT + NNS for GNSS). The system is solved according to Eq. 3.12 and Eq. 3.15. The derived a posteriori variance factor $\hat{\sigma}_0^2$ (Eq. 3.15) is used to rescale the NEQ in Step (1.2). The U-ST solutions will be used for the LT selection and weighting procedure performed in Step (3.1). Moreover, they are used to validate the datum realisation (cf. Sect. 5.5).

Step (1.2) performs the rescaling of the NEQ with its reciprocal a posteriori variance factor $1/\hat{\sigma}_0^2$ to fulfil Eq. 3.16. The resulting pre-processed and rescaled technique-specific NEQ $\mathbf{N}_{\text{tech}}^{i}$ will be the actual input to the subsequent filtering and combination steps.

Step (2) performs the filtering for SLR and VLBI (F-ERF solution only): The single-technique NEQs are filtered before the combination (cf. Sect. 5.4.2) to guarantee an enhanced stability of the physically-derived datum parameters origin and scale. The outcome is a NEQ $\mathbf{N}_{\text{tech}}^{i,\text{u}}$ (where "u" stands for "updated") for this week, which is later used for the combination. Afterwards, the intermediate F-ST solution is calculated with minimal constraints. The SLR and VLBI F-ST solutions are introduced into the LT selection and weighting procedure performed in Step (3.1). [In case of the F-ERF solution, $\mathbf{N}_{\text{tech}}^{i,\text{u}} = \mathbf{N}_{\text{tech}}^{i}$.]

Step (3.1) performs the LT selection and weighting procedure (cf. Sect. 5.4.4). For the U-ERF solution, we use the GNSS solution and the U-ST solutions of SLR and VLBI from Step (1.1), while for the F-ERF solution, we use the GNSS solution from Step (1.1) and the F-ST solutions of SLR and VLBI from Step (2). The outcome is a set of LT constraint equations introduced into the combination and solution procedure performed in Step (3.2).

Step (3.2) performs the actual inter-technique combination. The technique-specific NEQs are combined into one NEQ

$$\mathbf{N}_{\text{comb}}^{i} = \lambda_{\text{SLR}} \cdot \mathbf{N}_{\text{SLR}}^{i,\text{u}} + \lambda_{\text{VLBI}} \cdot \mathbf{N}_{\text{VLBI}}^{i,\text{u}} + \lambda_{\text{GNSS}} \cdot \mathbf{N}_{\text{GNSS}}^{i}, \tag{5.1}$$

applying the technique-specific relative weights λ_{tech} (cf. Sect. 5.4.3). After introducing the LT constraint equations set up in Step (3.1) and adding a NNR constraint over a global selection of IGS stations (cf. Sect. 5.3.1), the solution is computed from the combined NEQ $\mathbf{N}_{\text{comb}}^{i}$ according to Eq. 3.12 and Eq. 3.15.◂

5.4.2 Filtering

▸All the pre-processing and combination steps are performed at the NEQ level. Consequently, we implement an information filter approach, a transfer of the Kalman filter

(Kalman, 1960) approach from the solution level to the NEQ level (e.g., Chin, 2001; Assimakis et al., 2012). The approach thus enables us to apply relevant modifications directly to the NEQ systems without a need to solve the system beforehand. The filter generally implements a kinematic model that shall predict displacements of the stations within the network and a stochastic model that shall predict the evolution of their accuracy, or, in other words, the reliability of the predicted state.

As SLR and VLBI are the critical techniques for realising the physically-defined datum parameters for the regional GNSS network, their availability for each weekly ERF solution is crucial. Thereby, a network geometry that is as stable as possible must be achieved to minimise the network effect on the datum parameters realised. The developed filtering strategy needs to be a compromise between

(1) the optimal filling of observational gaps for single stations and

(2) the fact that the physical relevance of observations for the datum realisation is only given for a limited time span.

The information content to be derived from the NEQs of the datum-relevant techniques is uniquely related to their implicitly-contained datum information. This information is provided by the observing networks as a whole, and single stations at co-location sites serve to transfer the datum information [between the GNSS, SLR, and VLBI networks] within the combined solution. Therefore, we are not interested in modelling motions of individual non-observing stations over long periods: The artificial information thereby introduced (based on assumptions) would potentially distort the realised datum. The contribution of a single station to the datum realisation shall be based solely on its observations. Consequently, the chosen kinematic filter model assumes positions of individual stations to be constant for a certain period without observations. Our filter's prediction step is thus intended to modify the stochastic information contained in the NEQ so that the decreasing reliability of the datum information due to unknown displacements is considered.

As a result of the considerations described above, we realise the prediction step by consistently modifying the complete stochastic information contained in the NEQ. Thereby, the prediction of a NEQ $\mathbf{N}_{\text{tech}}^{i-1}$ from epoch t_{i-1} to a NEQ $\mathbf{N}_{\text{tech}}^{i,\text{p}}$ at epoch t_i is performed by rescaling the NEQ with a factor κ:

$$\mathbf{N}_{\text{tech}}^{i,\text{p}} = \kappa \cdot \mathbf{N}_{\text{tech}}^{i-1} \tag{5.2}$$

Afterwards, the update step is performed, resulting in an updated NEQ

$$\mathbf{N}_{\text{tech}}^{i,\text{u}} = \begin{cases} \mathbf{N}_{\text{tech}}^{i,\text{p}} + \mathbf{N}_{\text{tech}}^{i} & \dots \text{ if } \mathbf{N}_{\text{tech}}^{i} \text{ exists,} \\ \mathbf{N}_{\text{tech}}^{i,\text{p}} & \dots \text{ otherwise,} \end{cases} \tag{5.3}$$

with $\mathbf{N}^{i}_{\text{tech}}$ being the incoming information update for epoch t_i. Usually, an information update for SLR and VLBI is available every week (especially in our reprocessing scenario), so the second case is somewhat relevant for rare occasions of processing delays in the routine processing.

Because of the above requirement (2), we choose to filter the information from a specific epoch only over a limited period of $w + 1$ weeks into the future (i.e., for all further prediction steps, the weighting factor κ is zero). Consequently, the filtered NEQ of epoch t_i is equal to a weighted sum of the NEQs from epoch t_{i-w} to epoch t_i. Each summand is only present if a NEQ for the respective epoch exists:

$$\mathbf{N}^{i,\text{u}}_{\text{tech}} = \sum_{n=0}^{w} \kappa^n \cdot \mathbf{N}^{i-n}_{\text{tech}} \tag{5.4}$$

The two filter parameters to be set are the filter weight κ to be applied within each prediction step and the "cut-off" number of prediction steps w after which the weight of a NEQ is set to zero.

For the determination of κ, auto-correlation functions have been computed for several stations that have observed continuously for multiple years and have not been affected by earthquakes. These functions follow a common pattern for both SLR and VLBI in all three coordinate components. This lets us compute an average auto-correlation function that roughly follows an exponential pattern for the first couple of weeks (Fig. 5.4). For both SLR and VLBI, the average auto-correlation $r(\Delta t)$ of the station position time series decreases weekly to about 0.5 after three weeks. From this, we deduce an approximate decrease factor of 0.8 per week. Introducing this into Eq. 5.2 as a rescaling factor $\kappa = 0.8$ means that the overall variance level of a NEQ is raised by a factor of $1/\kappa$ per prediction step, increasing the standard deviations for non-observing stations by about 12 %.

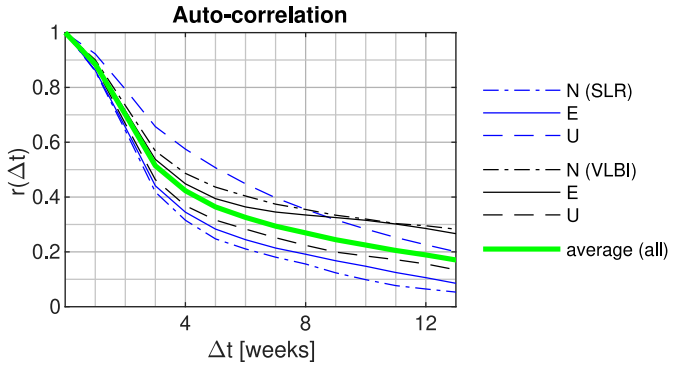

Figure 5.4: Average auto-correlation behaviour of selected SLR and VLBI site displacement time series.

The cut-off number of prediction steps w has been chosen after three weeks (each prediction step is equivalent to a step of one week), meaning that a station will be present in the solution for no more than three weeks after its last observation. Concerning the above requirement (1), this yields approximately 75 % of the observational gaps within both the SLR and VLBI time series being bridged, leaving only the remaining 25 % of gaps that are longer than 3 weeks (cf. Sect. 5.2, Tab. 5.1). In this way, we significantly reduce the network effect (cf. Sect. 5.5.1). The cut-off prediction step yields a downweighting of the respective NEQ to a factor of $\kappa^3 = 0.51$ by applying the rescaling factor of $\kappa = 0.8$. The resulting standard deviations are scaled by a factor of 1.4 for stations that did not provide an observation update after this epoch.◂

5.4.3 Technique-specific weights

▸It is well known that the standard deviations of GNSS estimates are too optimistic due to neglected correlations (Schön and Kutterer, 2007; Schön and Brunner, 2008). This means that, although internally fulfilling the condition formulated in Eq. 3.16, the relative weight of the GNSS NEQ is too high compared to SLR and VLBI and could systematically distort the combined solution while simultaneously yielding too accurate standard deviations. Therefore, technique-specific a priori weights are determined by calculating the ratio between an empirically-derived weighted root mean square (WRMS) deviation and the average formal error (estimated standard deviation) of several representative and continuous coordinate time series. Thereby, the WRMS has been calculated from the time series content that can be considered noise rather than signal. The noise part of the time series has been extracted by applying a band-pass filter that sets the amplitudes of all periods above a threshold of 13 weeks (a quarter year) to zero, leaving only the short periods below the threshold. The coordinate time series have been chosen from stations that do not show significant peaks in the coordinate spectra for periods below the threshold.

Table 5.3: ▪Ratio between average estimated standard deviations and empirically-derived WRMS values (3D station coordinates; upper line) and technique-specific weights applied within the combination (lower line).

	SLR	VLBI	GNSS
$WRMS/\sigma$	1.3 ± 0.2	1.1 ± 0.3	9.7 ± 3.1
Weight applied	1.0	1.0	0.01

Tab. 5.3 gives the empirically-derived ratios between estimated standard deviations and the WRMS of the three-dimensional (3D) coordinate time series. The resulting ratio between WRMS and formal error is close to 1 for SLR and VLBI while it is close to 10 for GNSS. Consequently, the GNSS NEQs are introduced into the combination with an a priori scaling factor of $\lambda_{\mathrm{GNSS}} = 0.01$ while the scaling factor for SLR and VLBI is set up to $\lambda_{\mathrm{SLR}} = \lambda_{\mathrm{VLBI}} = 1.0$.◂

5.4.4 Treatment of local ties

To realise a common datum for all techniques, measured LTs are introduced on an epoch-wise basis as constraints at co-located sites. The fact that the SIRGAS extended network includes global IGS sites thereby makes sure that we can exploit all available co-locations between the GNSS, SLR, and VLBI networks.

▸In this study, the LT treatment is based on the procedure described in detail by Seitz et al. (2012). The basis is the LT table initially compiled to realise the DTRF2014 [(Seitz et al., 2022)]. Concerning the techniques combined here, the table contains LTs for 95 inter-technique station pairs (49 GNSS–SLR pairs, 38 GNSS–VLBI pairs, 8 SLR–VLBI pairs) and 24 intra-technique station pairs (15 GNSS–GNSS pairs, 6 SLR–SLR pairs, and 3 VLBI–VLBI pairs). Here, multiple measurements of the same LT are counted only once. The LT selection and weighting are performed independently for each epoch-wise ERF solution. The LT constraints are selected and weighted according to the discrepancy between the measured LT and the coordinate difference derived from the single-technique solutions. In the process, only LTs below a certain discrepancy threshold are considered. For the U-ERF solution, this threshold is chosen as 50 mm to achieve enough LTs per week (38 on average). A larger threshold of 70 mm would not yield a significant increase in the number of available LTs, but experiments showed that solutions might suffer from the introduction of single LTs which do not fit the local situation. This effect becomes worse when the threshold is further increased. For the F-ERF solution, the threshold for LT introduction can be tightened to a discrepancy of 30 mm (cf. Tab. 5.4). Additional stations from the filtering enable the use of more LTs which fulfil a stricter discrepancy criterion. This yields a more stable datum realisation in the F-ERF solution than U-ERF solution (cf. Sect. 5.5.1).

Table 5.4: ▪Average weekly number of LTs selected for the U-ERF and F-ERF solutions, resp., depending on the discrepancy criterion. The selected criterion is marked bold.

Solution	discrepancy criterion	GNSS –SLR	GNSS –VLBI	SLR –VLBI	intra-tech.	total
U-ERF	30 mm	14.0	9.6	1.5	8.6	33.7
	50 mm	16.4	11.0	1.8	8.7	37.9
	70 mm	17.1	11.3	1.9	8.7	39.0
F-ERF	20 mm	14.0	11.5	2.2	7.4	35.1
	30 mm	18.1	13.9	2.8	8.7	43.5
	50 mm	20.3	15.6	3.0	8.8	47.7

To avoid systematic network deformations, some LTs must be excluded, especially at those stations affected by severe earthquakes (Tab. 5.5). This is necessary because LTs might still pass the selection procedure despite systematic errors. As a result, we consider it necessary to re-measure the LTs at affected stations after major seismic events.◂

Table 5.5: ▪Sites co-located with GNSS with local ties that have been excluded after major seismic events.

Site	DOMES No.	technique	from	event
Concepción	41719M001	SLR	2010-02-27	Chile Earthquake
Concepción	41719S001	VLBI	2010-02-27	Chile Earthquake
Monument Peak	40497M001	SLR	2010-04-04	Baja Earthquake
Tsukuba	21730S007	VLBI	2011-03-11	Tōhoku Earthquake
Arequipa	42202M003	SLR	2017-07-18	Peru Earthquake

5.5 Validation of the results

This section presents the validation of the combination and filtering procedure. Section 5.5.1 compares translation time series of the SLR single-technique solutions as well as of the technique-specific subnetworks of the U-ERF and F-ERF solutions with respect to the ITRF2014, while Section 5.5.2 contrasts the F-ERF solution against the JTRF2014, a sub-secular geocentric realisation of the ITRS. Finally, Section 5.5.3 contrasts station-specific displacement time series derived from the F-ERF solution against geophysical loading models in CM- and CF-frames.

5.5.1 Impact of combination and filtering on the datum realisation

▸Tab. 5.6 summarises the impact of combination and filtering on the single-technique and combined solutions. Tab. 5.7 summarises the weighted mean and RMS deviations along the transformation time series of the U-ST and F-ST solutions of VLBI and SLR, respectively, with respect to ITRF2014; shown are the non-constrained datum parameters. Tab. 5.8 presents the weighted mean and RMS values along the transformation time series of the technique-specific subnetworks of the U-ERF and F-ERF solutions with respect to ITRF2014.

For the U-ERF solution, we can state that the datum realisation via the introduced LTs has no systematic effects on the datum-relevant technique-specific subnetworks. The comparison between the SLR U-ST solution and the combined U-ERF solution shows no significant impact on the SLR origin and scale; the same holds for the VLBI-derived scale (Tab. 5.6, U-ERF w.r.t. U-ST). The comparison of the solutions with respect to ITRF2014 (Fig. 5.5; Tab. 5.7, U-ST; Tab. 5.8, U-ERF) confirms that the transfer of the origin from SLR to the VLBI and GNSS networks is well-performed, although with a systematic effect of about $-3.5\,\mathrm{mm}$ in t_z for GNSS. A drift is observed in the scales of SLR and VLBI after 2015 [(cf. upper right panel of Fig. 5.6)], the end of the observation period of the ITRF2014. The scale of the GNSS subnetwork lies between the scales from SLR and VLBI. This confirms that the combined scale is realised as a weighted mean of the SLR and VLBI scales.

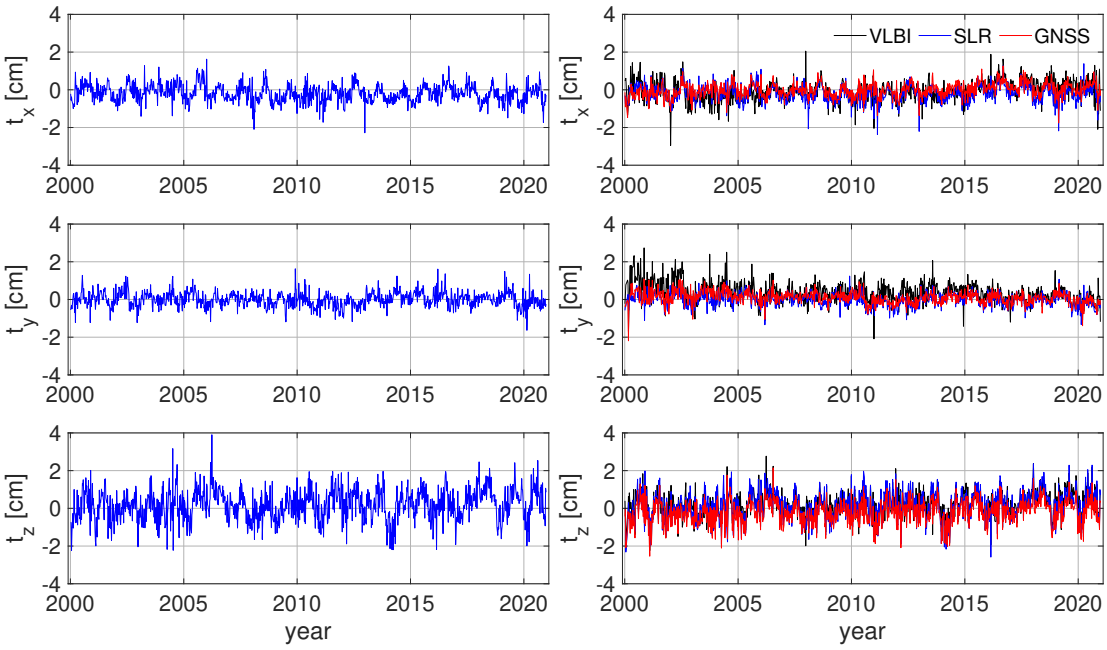

Figure 5.5: Translations with respect to ITRF2014 of the SLR U-ST solution (left) and the technique-specific subnetworks of the U-ERF solution (right).

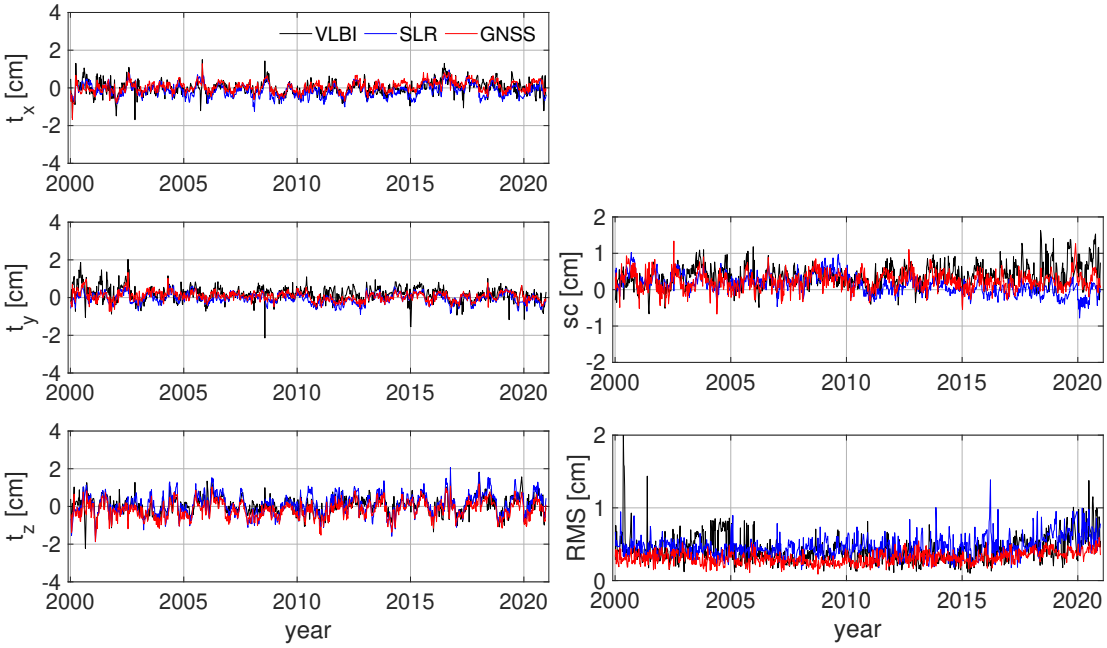

Figure 5.6: Translations (left), scale difference, and RMS of the residuals of the Helmert transformation (right) of the technique-specific subnetworks of the F-ERF solution with respect to ITRF2014.

Table 5.6: ▪Impact of filtering and combination on the datum parameters derived by SLR and VLBI in terms of Helmert transformation parameters between the solutions. Smaller RMS values mean a better agreement between the solutions.

Technique	datum parameter	U-ERF w.r.t. U-ST mean [mm]	U-ERF w.r.t. U-ST RMS [mm]	F-ST w.r.t. U-ST mean [mm]	F-ST w.r.t. U-ST RMS [mm]	F-ERF w.r.t. F-ST mean [mm]	F-ERF w.r.t. F-ST RMS [mm]
SLR	t_x	−0.1	0.6	0.3	2.4	0.0	0.3
	t_y	−0.1	0.5	−0.1	2.0	−0.1	0.3
	t_z	−0.4	1.2	−0.3	4.8	−0.3	0.5
	scale	0.2	0.5	−0.1	1.6	0.1	0.2
VLBI	*scale*	−1.1	2.2	0.0	2.9	−0.7	1.1

Table 5.7: ▪Helmert transformation parameters of the single-technique solutions with respect to ITRF2014.

Technique	datum parameter	U-ST Wmean [mm]	U-ST WRMS [mm]	F-ST Wmean [mm]	F-ST WRMS [mm]	Δ [%]
SLR	t_x	−1.6	4.4	−0.9	3.5	−20
	t_y	0.0	3.6	−0.4	2.8	−22
	t_z	2.2	7.7	1.6	5.7	−25
	scale	1.5	3.5	1.4	2.8	−18
VLBI	*scale*	4.8	4.6	4.7	3.1	−31

For the F-ERF solution, we can state that filtering the datum-relevant techniques SLR and VLBI has no systematic effects on the realised datum parameters. The comparison between the U-ST and the F-ST solutions of SLR and VLBI shows no systematic impact on the subnetworks (Tab. 5.6, F-ST w.r.t. U-ST). The same holds for the combination step following filtering, which is seen by a comparison between the F-ERF and the F-ST solutions (Tab. 5.6, F-ERF w.r.t. F-ST). This confirms that the networks are not deformed by the selected LTs [(the mean transformation parameters are below ±0.3 mm for SLR and −0.4 mm for the VLBI scale)].

While the general behaviour of both the F-ERF and the U-ERF solutions is identical (Fig. 5.5, Fig. 5.6), a significant decrease in the WRMS of the transformation parameters with respect to ITRF2014 is observed for the F-ERF solution compared to the U-ERF solution (Tab. 5.8). This is mostly due to a reduced noise of these time series which is caused by the increased network stability achieved in the F-ERF solution. A periodic variation is expected as each ERF solution is realised in an instantaneous CM-

Table 5.8: ▪Helmert transformation parameters of the combined solutions with respect to ITRF2014. In addition, Δ denotes the improvement of the WRMS of the F-ERF solution compared to the U-ERF solution.

Technique	datum parameter	U-ERF Wmean [mm]	U-ERF WRMS [mm]	F-ERF Wmean [mm]	F-ERF WRMS [mm]	Δ [%]
SLR	t_x	−1.6	3.9	−1.1	3.3	−17
	t_y	−0.1	3.3	−0.4	2.7	−19
	t_z	1.5	7.1	1.2	5.4	−24
	scale	1.4	3.0	1.4	2.5	−18
VLBI	t_x	−0.6	4.5	−0.1	3.2	−29
	t_y	3.5	4.1	2.0	3.4	−17
	t_z	1.2	6.1	0.6	4.3	−30
	scale	3.4	3.6	3.5	2.9	−20
GNSS	t_x	0.0	3.5	0.6	2.7	−21
	t_y	0.9	3.1	0.7	2.3	−26
	t_z	−2.0	6.0	−1.7	4.3	−28
	scale	3.3	3.0	2.4	2.6	−15

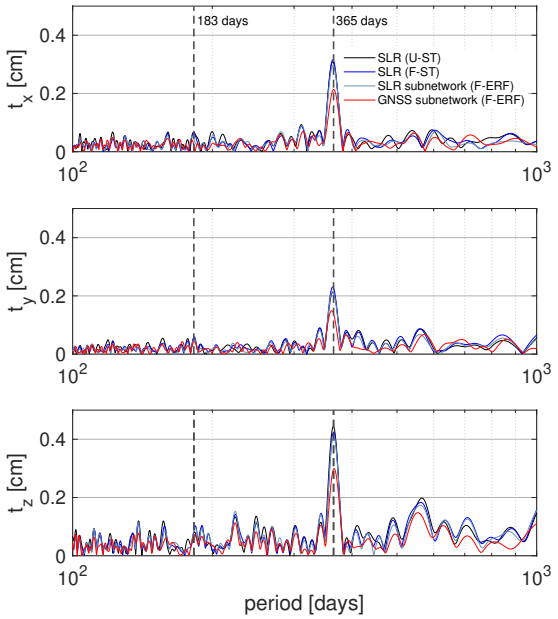

Figure 5.7: ▪Spectra of the translation time series with respect to ITRF2014 of (1) the SLR U-ST solution, (2) the SLR F-ST solution, (3) the SLR subnetwork of the F-ERF solution, and (4) the GNSS subnetwork of the F-ERF solution.

frame, whereas the ITRF2014 is a long-term CM-frame. [Important to note is that also the systematic offsets between the technique-specific subnetworks are reduced, most notably for t_z. The relative offset between the GNSS and the SLR subnetworks in z-direction (i.e., the difference of the network-specific z-translations with respect to ITRF2014) is reduced from 3.5 mm in the U-ERF solution to 2.9 mm in the F-ERF solution, meaning that the GNSS subnetwork inherits the SLR origin with smaller systematic deviation.] This can be related to the better distribution and a larger number of available LTs per week achieved by the filtering. The frequency spectra (Fig. 5.7) of the translations of the SLR solutions (U-ST and F-ST [note: the time series of the SLR F-ST solution is shown in Fig. 5.8]), the SLR subnetwork of the F-ERF solution and the GNSS subnetwork of the F-ERF solution agree in the main frequencies with a decrease in the yearly amplitude for GNSS. This damping may be related to the large and more homogeneously distributed global network (compared to SLR).◂

5.5.2 Discussion of the approach with respect to existing approaches

The previous sections described an approach for filtering and combination of technique-specific networks at the normal equation level in order to realise a geocentric regional epoch reference frame. With the JTRF2014 (Abbondanza et al., 2017), there exists a subsecular geocentric global TRF solution based on a filtering approach. The present section compares the approaches and outlines their similarities and differences.

Table 5.9: Comparison between the combination approaches of JTRF2014 (Abbondanza et al., 2017, 2020) and the F-ERF solution. RMC stands for "rotational minimal constraints" (Abbondanza et al., 2020), NNR for "no-net rotation".

Solution	JTRF2014	F-ERF solution
Combination software	KALREF	DOGS-CS
Combination level	solutions	normal equations
Filtering approach	Kalman filter	information filter
Station motion model	trend, annual, semi-annual	none
Stochastical model	random walk (tuned to NT-L)	implicit scaling of NEQs
Orientation	RMC w.r.t. ITRF2008	NNR w.r.t. ITRF2014

Tab. 5.9 summarises the most important properties of both approaches. The JTRF2014 is a global TRF solution that delivers epoch-wise filtered station positions for SLR, VLBI, GNSS, and DORIS stations. The solution is based on a Kalman filter approach, whereby the dynamical model for the station positions is parameterised by a trend in composition with annual and semi-annual variations. The stochastic model for the station positions is realised by allowing a random walk that is tuned to cover possible station position variations caused by non-tidal loading effects. Co-located sites are constrained by introducing local ties at their measurement epoch in conjunction with co-motion constraints over time. In this way, the JTRF2014 is a reference frame that

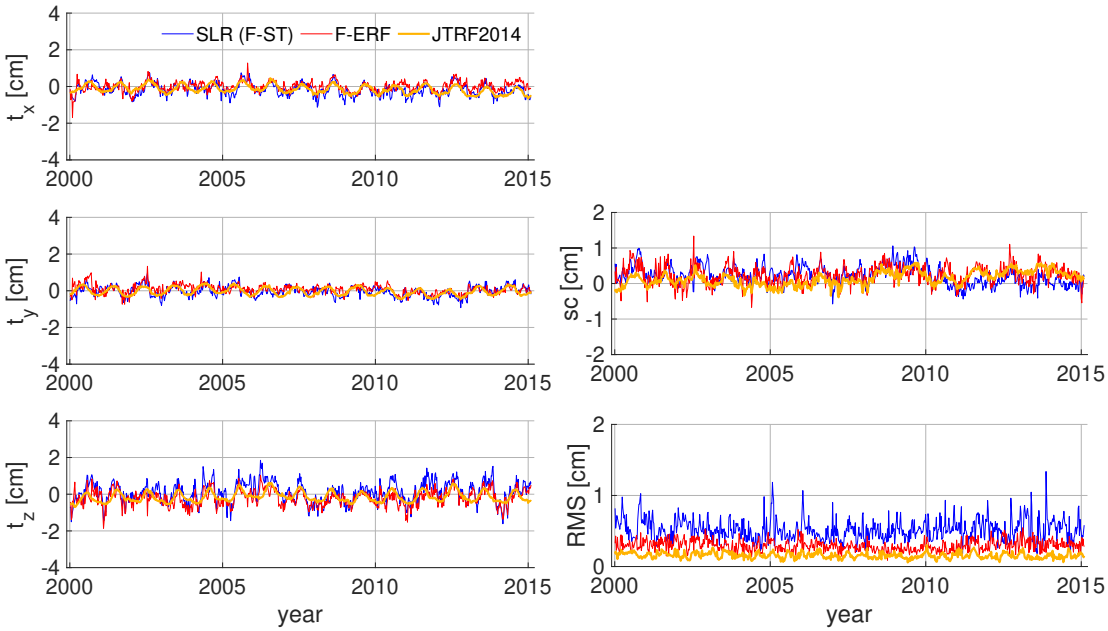

Figure 5.8: Translations (left), scale difference, and RMS of the residuals of the Helmert transformation (right) of (1) the SLR F-ST solution, (2) the GNSS subnetwork of the F-ERF solution, and (3) the JTRF2014 with respect to ITRF2014.

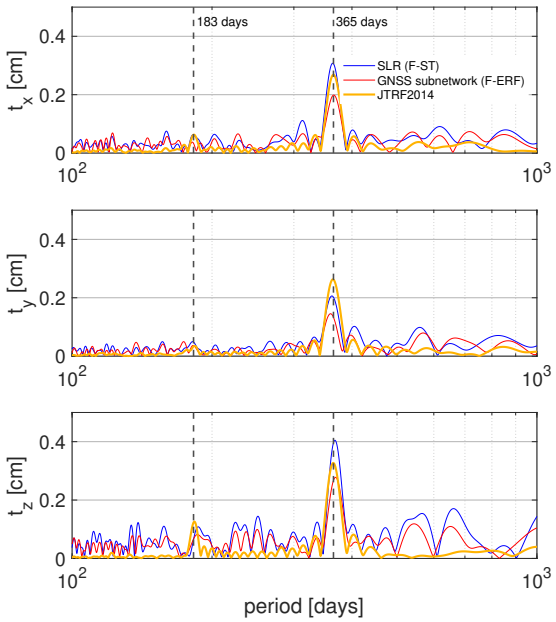

Figure 5.9: Spectra of the translation time series with respect to ITRF2014 of (1) SLR F-ST solution, (2) the GNSS subnetwork of the F-ERF solution and (3) the JTRF2014.

delivers geocentric station positions for global station networks of the four contributing space-geodetic techniques SLR, VLBI, GNSS, and DORIS, whereby all stations are modelled over long periods of time, also outside of their observation period. The stations of regional sub-networks are not available in the JTRF2014.

Our F-ERF solution, on the other hand, is designed to realise a geocentric datum for a regional GNSS network, the datum realisation as well as the estimation of the epoch-wise station positions realised in one common adjustment. The global networks of SLR, VLBI, as well as the globally-distributed IGS sites, only serve for the purpose to realise a *global TRF datum*, while the instantaneous positions of the respective stations are not of interest. Consequently, our approach omits the explicit modelling of station positions for these networks, whereby the filtering approach that is applied at the normal equation level serves to weight the datum-relevant information content of the networks in order to stabilise it over time. We thus realise instantaneous (unfiltered) positions for the Latin American GNSS network that are given in an as-instantaneous-as-possible (filtered) geocentric TRF datum, while we omit to model the station positions of the global SLR and VLBI networks over longer periods of time without observations.

Fig. 5.8 shows the translation time series of the SLR F-ST solution and of the GNSS subnetwork of the F-ERF solution (cf. Fig. 5.6) with respect to the ITRF2014, complemented by the translation time series of the JTRF2014 with respect to the ITRF2014. Fig. 5.9 shows the corresponding spectra. As can be seen, the datum of the SLR F-ST and F-ERF solutions closely follows the JTRF2014 datum, whereby the amplitudes of the annual period of t_x and t_y are damped for the GNSS subnetwork of the F-ERF solution compared to the JTRF2014. This is most probably due to the reason that the datum of the JTRF2014 is much smoother and that the underlying station positions explicitly model semi-annual and annual periods, while our filtering approach realises an origin with variations distributed over a broader range of frequencies. We assume this partially to be noise that is related to remaining network effects caused by our approach of epoch-wise realisation of the datum (i.e., LTs are selected and introduced on an epoch-wise basis), and partially to be actual geophysical signal due to a more instantaneous realisation of the geocentre.

These assumptions are confirmed by the translation time series between the GNSS subnetwork of the F-ERF solution and the JTRF2014. The spectra (Fig. 5.10) do

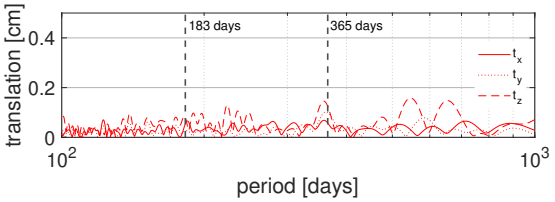

Figure 5.10: Spectra of the translation time series of the GNSS subnetwork of the F-ERF solution with respect to JTRF2014.

Table 5.10: Helmert transformation parameters of the F-ERF solution with respect to JTRF2014.

Technique	datum parameter	F-ERF Wmean [mm]	F-ERF WRMS [mm]
GNSS	t_x	1.0	3.1
	t_y	0.3	3.0
	t_z	−0.7	4.6
	scale	1.8	2.2

not show significant peaks for t_x and t_y, especially not in the semi-annual and annual periods that are explicitly modelled in the JTRF2014. For t_z, an amplitude of about 1.5 mm is visible near the annual band, which is not dominant in the spectrum. The WRMS, i.e., the mostly non-systematic scatter, of the translations between the F-ERF solution and the JTRF2014 is about 3 mm for t_x and t_y and 4.6 mm for t_z, with systematic offsets in the range of ≤ 1.0 mm (Tab. 5.10). We thus conclude that there are only small differences between the datum of the F-ERF solution and of the JTRF2014, with no significant systematic differences in the time evolution of the realised origins.

5.5.3 Validation against geophysical models

Within this section, we present validations by Kehm et al. (2022b■) comparing station-specific time series realised according to our approach to displacement time series derived from geophysical fluid loading site displacement models for non-tidal loading (NT-L) provided by the Earth System Modelling group (ESMGFZ) at the Deutsches GeoForschungsZentrum (GFZ) Potsdam (Dill and Dobslaw, 2013). Thereby, we use the combined effect of the three NT-L components non-tidal atmospheric (NTAL), non-tidal oceanic (NTOL), and hydrological loading (HYDL).

Fig. 5.11 shows the correlations between station-specific displacement time series derived from the F-ERF solution and from the NT-L models in the CM-frame. All time series are positively correlated. Fig. 5.12 shows the RMS differences between these time series. Generally, the RMS differences are larger in the North component (0.40 cm on average) than in the East component (0.26 cm on average). This holds especially for equatorial regions, which can be related to the less reliable realisation of the origin of the z-coordinate of the epoch reference frame solutions (cf. Fig. 5.6). However, the magnitude of the RMS differences confirms that the realised horizontal station displacements and the horizontal displacements derived from the NT-L models agree within a range of several millimetres for most stations. For the Up component, we derive larger RMS differences (0.62 cm on average). In hydrologically active regions like the Amazon basin, the RMS differences in the Up component exceed 1 cm (e.g., for the NAUS site).

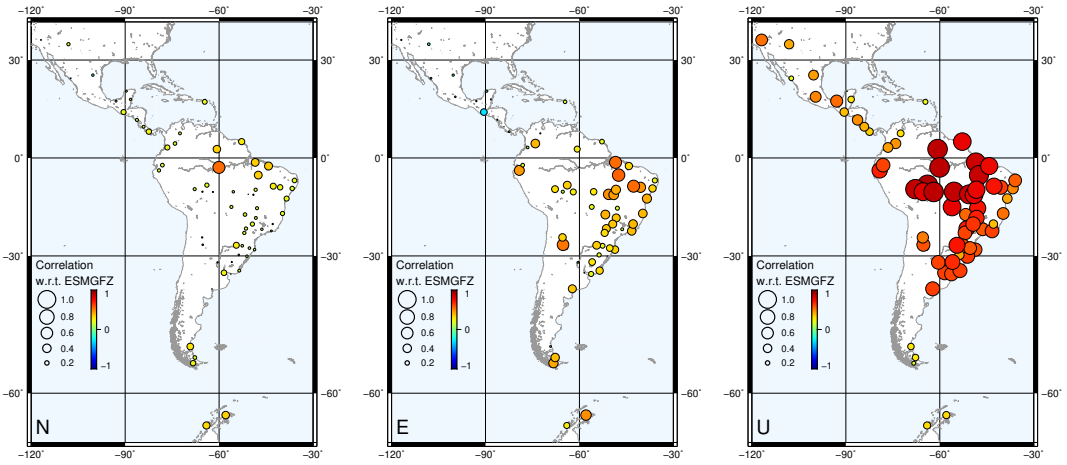

Figure 5.11: ▪Correlations between the site displacement time series derived from the F-ERF solution and the ESMGFZ NT-L time series in CM-frame.

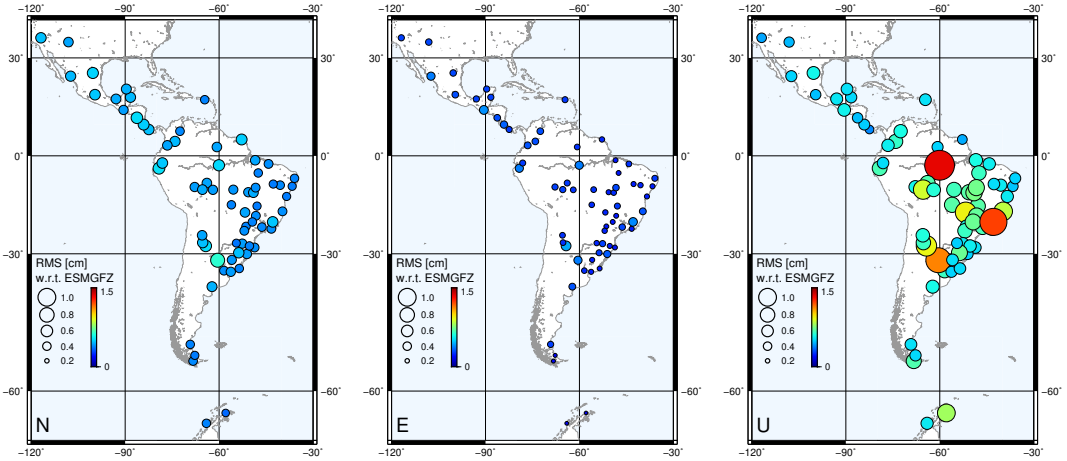

Figure 5.12: ▪RMS differences between the site displacement time series derived from the F-ERF solution and the ESMGFZ NT-L time series in CM-frame.

Within the framework of these studies, the reprocessed GNSS normal equations (Sect. 5.3.1) were also used to calculate a consistently reprocessed SIRGAS-like solution with datum realisation via fiducial points (hereafter called "SIRGAS-repro"). As Kehm et al. (2022b▪) outline, the SIRGAS solutions resemble the datum of the IGS weekly solution including inherent processing-related discontinuities (cf. left panel of Fig. 5.1; for more details, refer to Sect. 2 of Kehm et al., 2022b▪). In Fig. 5.13, we compare selected station-specific time series derived from the SIRGAS-repro solution and from the F-ERF solution to displacement time series derived from the NT-L models. It is visible that the F-ERF solutions rather resemble the CM-related NT-L signals, whereas the SIRGAS-repro time series rather resemble the CF-related NT-L signals. However,

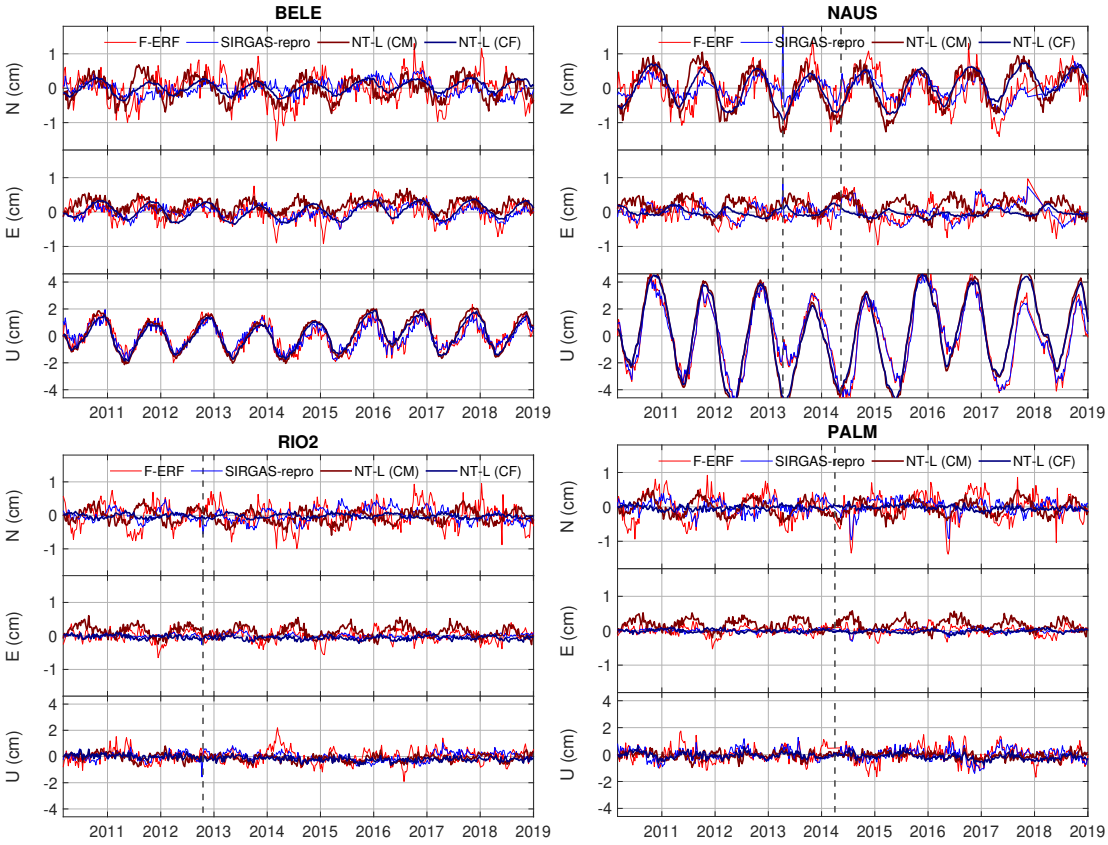

Figure 5.13: Coordinate time series of stations BELE, NAUS, RIO2, and PALM from the SIRGAS-repro and F-ERF solution compared with the ESMGFZ NT-L time series in CM- and CF-frames.

the time series of the F-ERF solution also reflect the larger noise that we obtain in the z-direction of the origin, which is directly mapped into the derived displacement time series. The effect is clearly visible in a larger scatter of the North component of BELE and NAUS, the two stations in the Amazon basin, i.e., close to the equator, and maps into both the North and the Up components of RIO2 and PALM, the two stations located in latitudes further in the South.

Especially for NAUS, a station in the hydrologically active Amazon basin, the East component features a phase shift between the F-ERF solution and the CM-related NT-L time series after a discontinuity in the second quarter of 2014. As the displacements of the F-ERF solution closely follow the pattern visible also for the SIRGAS-repro solution, we assume that this relates to local effects that are not represented by the NT-L model assumptions for the elastic deformation response of the Earth (e.g., Martens et al., 2016). For the North components of both RIO2 and NAUS, we observe a phase shift between the observed F-ERF displacements and the CM-related NT-L values over the full time span, while we observe a periodic variation of the SIRGAS-repro displace-

ments which is not visible in the CF-related NT-L signal. We assume that this effect also is related to local effects which are not covered by the geophysical fluid models.

5.6 Summary and discussion of the results

Within the previous sections, we have outlined our approach to realise a geocentric regional epoch reference frame for the Latin American SIRGAS GNSS network. The realisation of the datum was achieved by combining normal equations of global GNSS, SLR, and VLBI networks. The filter method implemented for SLR and VLBI, the two techniques that are relevant to realise the physically-defined datum parameters origin and scale, significantly improves the stability of the datum realisation. The WRMS deviation (i.e., the scatter) of the epoch-wise Helmert transformation parameters between the F-ERF solution and the ITRF2014 is reduced by up to 21 % in the x-, 26 % in the y-, and 28 % in the z-component, as compared to the corresponding transformation parameters between the U-ERF solution and the ITRF2014. This indicates that the datum of the F-ERF solution is realised more stable with respect to the multi-year secular datum of the ITRF2014. Comparing the F-ERF solution to the JTRF2014, a Kalman-filter-based epoch-wise sub-secular realisation of the ITRS, we do not find systematic differences in the time evolution of the datum parameters realised. Comparing station-specific displacement time series with geophysical models in the CM-frame also indicates that the realised time series are geocentric. This means that the time series allow for a direct interpretation with respect to geophysical processes without having to rely on a transformation between CF-related and CM-related systems.

Our approach exploits global networks for the purpose of datum realisation only, while the coordinates of interest are only those of the instantaneous GNSS subnetwork in the regional network. Consequently, the filter is designed to transfer information content related to the datum over time, whereby a majority of the observational gaps can be bridged with information from the past. Thereby, the filter turns out to be relevant in two ways, namely, first, to stabilise the datum parameters realised from SLR and VLBI, and second, to guarantee a sufficient number of local ties for a reliable datum transfer between the technique-specific networks. The chosen filter approach allows individual epoch-wise determination of the epoch reference frame by relying on space-geodetic observations that are available at short latencies. By limiting the filtering to a restricted time span and to the global SLR and VLBI networks only, our approach is suitable to realise the datum for dense regional networks without running into the problem of too large amounts of observations that would require the processed network to be reduced to a limited number of stations. This is in contrast to the approach of multi-year reference frames like the ITRF or sub-secular frames filtered over long time spans like the JTRF, where the amount of processed data (and with that, the processed station networks) has to be limited for an appropriate handling.

Relying on recent space-geodetic observation data for each epoch-wise solution makes our approach independent from reprocessing campaigns after changes in the conventional models. Moreover, the realisation of the origin and scale of the epoch-wise solutions does not rely on fiducial coordinates, meaning that the realisation of the physical datum parameters origin and scale is independent from reference coordinates in a multi-year reference frame which might decrease in accuracy after the end of its observation period. Consequently, our approach is an opportunity to bridge gaps between ITRF realisations, whereby the independent realisation of the datum guarantees that the geophysical relevance of station-specific displacement time series in the regional network is maintained.

As the approach relies on global networks for the datum realisation, it is conceptually transferable to any other region on the globe by extending a dense regional GNSS station network by the global IGS stations. However, as the approach does not perform an explicit modelling of SLR and VLBI station coordinates over longer observational gaps, single stations in the global SLR and VLBI networks are not suitable to be used as reference points for geodetic applications. In this way, our approach is deliberately developed to realise the datum of dense regional networks at short latencies. Consequently, it complements multi-year reference frames like the ITRF with a global and stable long-term datum that allows to link geodetic observations over several decades, and sub-secular frames like the JTRF that is highly valuable for precise orbit determination in a geocentric frame (Abbondanza et al., 2017, 2020; Rudenko et al., 2018; Zelensky et al., 2018).

As we could demonstrate, a stable epoch-wise realisation of the physical datum parameters origin and scale of the reference frame is highly dependent on the performance and distribution of the datum-relevant space-geodetic networks of SLR and VLBI. In this context, SLR is the technique that is essential to realise the origin with high accuracy. This motivates the studies presented in Chapter 6, which shall investigate which improvements are necessary to enhance the stability of the SLR-derived datum parameters in the context of different geodetic parameter groups related to the Earth system.

6 Satellite Laser Ranging and its relevance for the stable determination of geodetic parameters

6.1 Current status and prospects

SLR is the only space-geodetic technique that allows to determine the geocentre – i.e., the TRF origin – with high accuracy, and it contributes to the realisation of the TRF scale together with VLBI (e.g., Bloßfeld, 2015). Consequently, SLR plays a very important role concerning the evolution of the accuracy and long-term stability of the datum realisation of conventional TRFs. As outlined by Bloßfeld et al. (2014b) and demonstrated in Chapter 5, this is of particular relevance for epoch reference frames. As epoch reference frames are realised for short periods, a good repeatability of the realised TRF datum is crucial and requires a well-distributed high-performance network of observing stations. Since the start of observations in the 1960s, the SLR space and ground segments have undergone a permanent evolution concerning the number of observed satellites, the number and distribution of SLR stations, and technical evolution (Fig. 6.1; Bloßfeld et al., 2018▪; Pearlman et al., 2019).

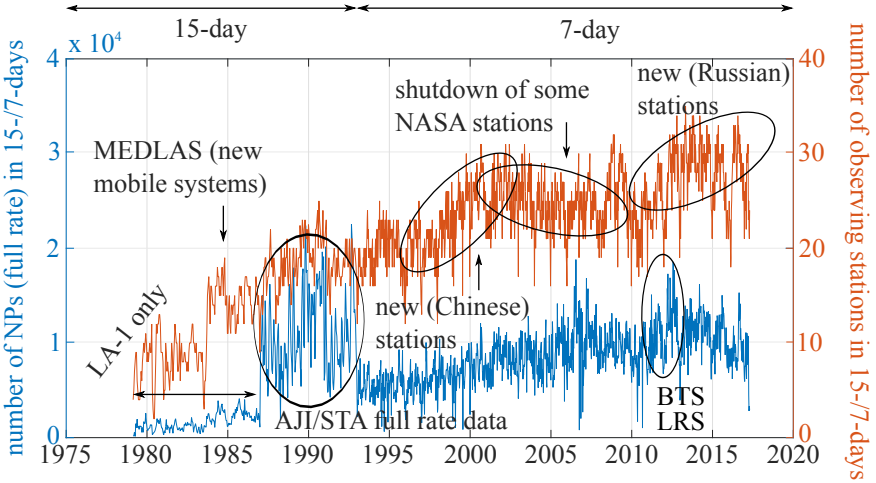

Figure 6.1: ▪Evolution of the number of SLR stations and normal points (NPs) per 15-/7-day interval between 1979 and 2017.

Consequently, one important topic of study is the datum quality of SLR-derived TRFs, especially of the realised origin. Furthermore, SLR contributes to determining the Earth's orientation in space, as SLR observations are sensitive to a subset of the ERPs, namely PM and its rates and LOD, i.e., changes in the Earth's angular velocity. Similar to all satellite techniques, SLR is not sensitive to UT1 – UTC directly as satellite observations cannot separate the Earth's angular velocity from the common precession of the observed satellite constellation. SLR observations are sensitive to low-degree spherical harmonics of the Earth's gravity field model, i.e., the large-area variations in the Earth's gravity field. This includes the fundamental topic of realising a physical TRF orientation, meaning that the sensitivity of SLR observations to the sectoral and tesseral Stokes coefficients of degree 2 is a crucial issue (cf. Sect. 3.1).

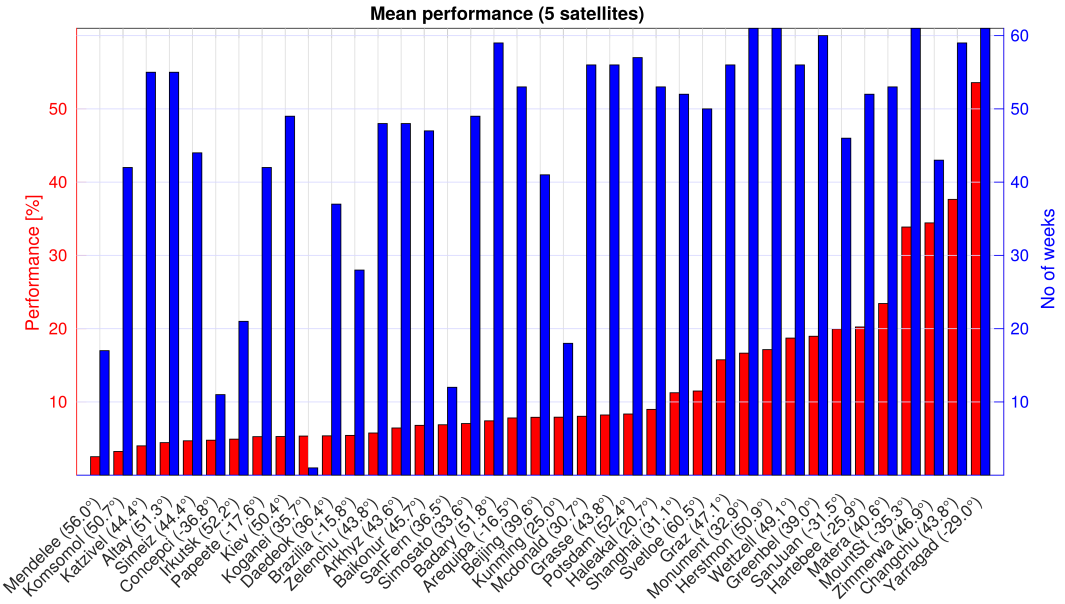

Figure 6.2: Average SLR station performances and number of weeks with observations for the five observed satellites. The stations are sorted by performance. Station names are complemented by the geographical latitude.

Up to now, the global SLR network geometry has been quite inhomogeneous, especially showing a lack of stations on the southern hemisphere with a concentration of stations in Europe and Asia. This inhomogeneous global station distribution is one of the major limiting factors in the datum realisation of TRFs (Collilieux and Altamimi, 2009; Collilieux et al., 2009; Bloßfeld et al., 2014b; Bloßfeld, 2015; Bloßfeld et al., 2015b). In order to solve this problem, additional sites are considered or already planned. Together with the Bureau for Networks and Observations (BNO) of the Global Geodetic Observing System[1] (GGOS), the Directing Board (DB) of the ILRS encouraged different national funding agencies and research institutes to build SLR

[1] `http://www.ggos.org`

systems in strategically valuable places all over the globe.[2] The second important limiting factor is the amount of data produced per station. Lots of the SLR stations are producing only small amounts of data, whereas just a few stations deliver high amounts of data. This raises the question what will be the benefit of improving the performances of these low-performing stations within a future SLR network. For a time span from January 2014 to March 2015, the pass performances, i.e., the number of passes a station has actually observed in relation to the number of passes theoretically observable, range from 3 % to 54 % with an average of 13 % (Fig. 6.2).

Several recent simulation studies investigate the effect of changing network geometries and tracking scenarios on the parameters related to the TRF datum. Pavlis and Kuźmicz-Cieślak (2009) compare different scenarios for possible future SLR networks comprising different numbers of stations, Otsubo et al. (2016) perform covariance analyses with respect to grids of stations distributed equally over the globe, and Glaser et al. (2017, 2019a, b) simulate different space-geodetic networks and also investigate the effect of local ties on the datum realisation. Moreover, further SLR-specific aspects are under consideration, e.g., the impact of the overall ground-/space segment geometry on the SLR solution and the potential of including additional targets like GNSS satellites (Pavlis et al., 2018). The impact of different tracking scenarios on SLR-derived parameters is investigated by Andritsch et al. (2017, 2020), with a special focus on GNSS satellites as SLR targets. Bruni et al. (2018) investigate potential improvements in the SLR network geometry and the tracking of GNSS satellites, whereby space ties are used to evaluate the datum realisation via local ties. The GGOS Committee on Performance Simulations and Architectural Trade-Offs (GGOS-PLATO; cf., e.g., Männel et al., 2018) provides a common framework to coordinate and integrate the simulation studies performed by the various aforementioned groups, including our studies presented later in this chapter.

Within the following subsections, we are going to look deeper into different aspects of SLR. After explaining the measurement principle of SLR (Sect. 6.2), we present studies on possibilities of extending the space and ground segments of SLR and their impact on different geodetic parameter groups related to the TRF datum. We start extending the 4-satellite ILRS constellation to a multi-satellite constellation by processing the already available observations to up to 11 spherical satellites at a time. One major point of that study is related to the potential to decorrelate different parameter groups and to enhance the sensitivity of the SLR observations to the low-degree Stokes coefficients that are in relation with the TRF datum (Sect. 6.3). We continue with simulation studies as a look into a possible future (Sect. 6.4): First, we investigate the impact of an additional satellite in a highly excentric orbit on the estimation of the low-degree Stokes coefficients (Sect. 6.5); afterwards, we take a deeper insight into the potential of extending or improving the SLR ground segment in terms of additional stations or enhanced performance (Sect. 6.6).

[2] cf. 2014 ILRS Governing Board meeting: minutes and slides. URL: `https://ilrs.gsfc.nasa.gov/about/reports/meeting_reports.html` (2022-06-15).

6.2 Analysis of SLR observations

An SLR measurement is influenced by a number of effects which need to be corrected for. Among others, the satellite orbit is affected by the gravity field, the Earth albedo, solar radiation and – in the case of lower orbits – by the atmospheric drag. The Earth itself is deformed by tidal forces from other bodies in space, mainly the Moon and the Sun. These tidal forces also cause ocean tides which have a deforming effect on the Earth as well. Deformations of the Earth's body lead to displacements of the SLR sites which have to be taken into account; moreover, these deformations also change the orbit of the satellite. Furthermore, the SLR laser beam itself is subject to a number of effects when passing through the Earth's atmosphere (e.g. tropospheric delay). Additionally, the EOPs have to be taken into account when setting up the observation equation.

Within the Orbit Computation library of the DGFI Orbit Computation and Geodetic Parameter Estimation Software (DOGS-OC [cf. Sect. 4.2]), the functional model for laser ranging observations is implemented as (Gerstl, 1997; Bloßfeld, 2015)

$$\rho + \epsilon = \|\mathbf{r}_{\mathrm{sat}}(t_{\mathrm{M}} + \delta t) - \mathbf{r}_{\mathrm{sta}}(t_{\mathrm{M}} + \delta t)\| + \delta\rho + c_{\mathrm{trop}}(1 + \delta r) + c_{\mathrm{rel}} + c_{\mathrm{sta}} + c_{\mathrm{masc}} + c_{\mathrm{mesc}}, \quad (6.1)$$

with ρ being the one-way range measurement, ϵ being the measurement error, $\mathbf{r}_{\mathrm{sat}}$ being the 3-dimensional satellite position in the Geocentric Celestial Reference System (GCRS), t_{M} being the approximated epoch of reflexion of the laser pulse at the satellite, δt being the time bias of the measurement, $\mathbf{r}_{\mathrm{sta}}$ being the 3-dimensional position of the station in the ITRS, $\delta\rho$ being the range bias of the measurement, c_{trop} being the tropospheric range correction, δr being the bias of tropospheric refraction, c_{rel} being the relativistic range correction, c_{sta} being the station-dependent SLR correction, c_{masc} being the satellite-specific centre-of-mass correction and c_{mesc} being the SLR-array dependent correction. The EOPs are contained implicitly as the station position is rotated from the Earth-fixed to the space-fixed reference frame. Replacing all modelled systematic errors in Eq. 6.1 by

$$e_{\mathrm{syst,modelled}} = \delta\rho + c_{\mathrm{trop}}(1 + \delta r) + c_{\mathrm{rel}} + c_{\mathrm{sta}} + c_{\mathrm{masc}} + c_{\mathrm{mesc}} \quad (6.2)$$

yields

$$\rho + \epsilon = \|\mathbf{r}_{\mathrm{sat}}(t_M + \delta t) - \mathbf{r}_{\mathrm{sta}}(t_M + \delta t)\| + e_{\mathrm{syst,modelled}}. \quad (6.3)$$

When processing SLR measurements, all the systematic effects mentioned above are either corrected by conventional models or are estimated parameters (with the model values as a priori values; [note: in principle, also the time bias δt can be included into the group of modelled errors, as system-specific a priori values are provided in the ILRS

Table 6.1: Dynamical models for SLR processing.

Force component	model
Earth gravity field	EIGEN-6s static part up to degree/order 120 time variable part up to degree/order 50
Solid Earth tides	IERS 2010 (Petit and Luzum, 2010)
Permanent tide	IERS 2010 (Petit and Luzum, 2010)
Ocean tides	EOT11a (Savcenko and Bosch, 2012) up to degree/order 30 + 62 admittance waves (IERS 2010; Petit and Luzum, 2010)
Atmospheric tides	Biancale and Bode 2003 (Biancale and Bode, 2006)
Solid Earth pole tide	IERS 2010 (Petit and Luzum, 2010)
Ocean pole tide	Desai (2002)
Lunar gravity field	Konopliv et al. (2001) up to degree/order 50
Third body gravity effect	Mercury, Venus, Mars, Jupiter, Saturn, Sun, Moon (DE-421; Folkner et al., 2008)
Solar radiation pressure	constant radiation with eclipse modelling
Earth radiation pressure	albedo and infrared (Knocke et al., 1988)
Atmospheric drag	JB2008 (Bowman et al., 2008; only for LEO satellites)
General relativistic correction	Schwarzschild, de Sitter, Lense-Thirring (IERS 2010; Petit and Luzum, 2010)
Non-tidal gravitational perturbation	not applied
Thermal radiation	not applied

Data Handling File]). The measurement error ϵ represents all unmodelled inconsistencies between the measurement ρ and the modelled (i.e., theoretical) observation on the right-hand side of Eq. 6.3.

For the studies presented in Chapter 5, the SLR observations (in the context of this doctoral thesis, the term "SLR observations" always refers to the so-called *normal points*[3] as they are routinely provided by the stations) to all satellites have been reprocessed using background models that represent the most recent state at the time of the study

[3]Normal points are generated from the original raw observation data by applying a data screening procedure and calculating time averages over certain satellite-dependent time bins. Refer to, e.g., Kehm A. (2019): *Data analysis demonstration – data download and normal point computation.* First One-Day Introductory and Refresher Course on Satellite and Lunar Laser Ranging, Stuttgart, Germany, URL: `https://cddis.nasa.gov/2019_Technical_Workshop/SLR_School/index.html` (2022-06-15).

Table 6.2: Geophysical background models for SLR processing.

Model	description
A priori station coordinates	SLRF2014
Station eccentricities c_{sta}	ILRS Eccentricity File[(a)]
Station discontinuities	ILRS Discontinuities File[(b)]
A priori EOP values	IERS 14C04 (Bizouard et al., 2019) with subdaily corrections (Ray et al., 1994)
Mean pole	UAW 2017 secular pole model (IERS Conventions 2010, v. 1.3.0[(c)])
Precession/nutation	IAU2000A/IAU2006 up to degree 10 (Mathews et al., 2002)
Solid Earth tides	anelastic model (IERS 2010; Petit and Luzum, 2010)
Permanent tide	IERS 2010 (Petit and Luzum, 2010)
Ocean tidal displacement	EOT11a (Savcenko and Bosch, 2012)
Tidal atmospheric loading	S1/S2 tidal model (Ray and Ponte, 2003)
Solid Earth pole tide	UAW2017 secular pole model (IERS Conventions 2010, v. 1.3.0[(c)])
Ocean pole tide loading	Desai (2002)
Non-tidal loading	not applied

[(a)] https://ilrs.gsfc.nasa.gov/network/site_procedures/eccentricity.html (2022-06-15)
[(b)] https://ilrs.gsfc.nasa.gov/network/site_information/data_correction.html (2022-06-15)
[(c)] https://iers-conventions.obspm.fr/conventions_versions.php (2022-06-15)

Table 6.3: SLR measurement corrections.

Correction	description
Tropospheric range correction c_{trop}	Mendes-Pavlis with temperature correction (Mendes and Pavlis, 2004)
Tropospheric scaling factors	(only for LEO satellites)
Centre-of-mass and SLR array corrections c_{masc}, c_{mesc}	station-/satellite-dependent correction models (Otsubo and Appleby, 2003; Otsubo et al., 2015)
Relativistic range correction c_{rel}	IERS 2010 (Petit and Luzum, 2010)
Range and time biases $\delta\rho$, δt	ILRS Data Handling File[(a)]

[(a)] https://ilrs.gsfc.nasa.gov/network/site_information/data_correction.html (2022-06-15)

(IERS Conventions 2010 with updates until v. 1.3.0[4] and updated centre-of-mass correction tables, cf. Rodríguez et al., 2019). The dynamical models (Tab. 6.1) comprise the force components disturbing the satellite orbit ($r_{\mathrm{sat}}(t_{\mathrm{M}} + \delta t)$ in Eq. 6.1 and 6.3) and the geophysical background models (Tab. 6.2) comprise the a priori station coordinates, the a priori models for Earth rotation, and the loading displacement models due to gravitational and non-gravitational effects ($r_{\mathrm{sta}}(t_{\mathrm{M}} + \delta t)$ in Eq. 6.1 and 6.3). Finally, the SLR measurement corrections (Tab. 6.3) comprise all a priori corrections applied to the original SLR observation (Eq. 6.2). For the SLR simulation studies presented in Section 6.4, some of these models have been applied according to earlier standards, being the most recent state at the time of the respective studies. For example, this comprises the IERS 08C04 EOP time series (Bizouard and Gambis, 2009, 2011) or the pre-2017 IERS conventional mean pole model (Petit and Luzum, 2010). This does not have an impact on the interpretation of the results, as these models have been used consistently within the simulation and the analysis steps.

6.3 Multi-satellite SLR: De-correlating essential geodetic parameters

The decision which parameters can be estimated in one common adjustment and their achievable quality are strongly dependent on the sensitivity of the observations to the parameters. Moreover, it depends on the correlations within and between the different parameter groups. Correlations between parameters can thereby be caused by physical or geometrical relation between the estimated quantities (e.g., the correlation between PM and the nutation, or the correlation between the different zonal Stokes coefficients), or by an insufficient distribution of the observations in space and time (e.g., the SLR station network).

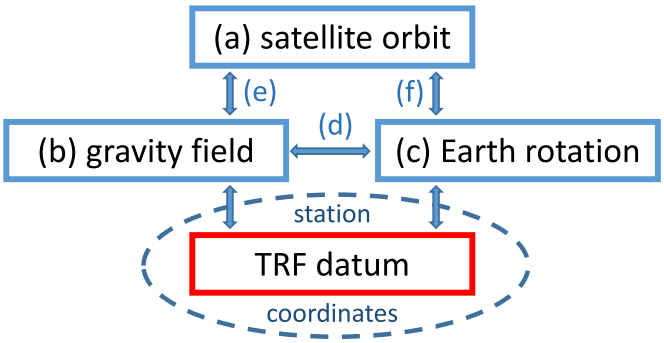

Figure 6.3: Relations between selected SLR-derived parameter groups. The letters refer to the matrix blocks explained in Fig. 6.5.

[4]IERS Conventions 2010, Working Version 1.3.0, URL: `https://iers-conventions.obspm.fr/conventions_versions.php` (2022-06-15).

Fig. 6.3 provides an overview of selected parameter groups that are accessible via SLR. The arrows within the figure show the dependencies between parameter groups which become visible in terms of correlations. While a TRF datum realised from SLR is accessible only implicitly via the estimated station coordinates (of a permanently changing network of observing stations), the correlations within and between the other parameter groups, namely the satellite-dependent orbit and force parameters, the Stokes coefficients of the Earth's gravity field model, and the ERPs, can be thoroughly investigated. The less the parameter groups or individual parameters are correlated, the more reliable are their estimates resulting from a common adjustment. These parameters are relevant in the context of observables describing key properties of the Earth. A list of these parameters is compiled by the GGOS Committee on Essential Geodetic Variables (EGVs; cf. Sect. 2.2 of Angermann et al., 2022).

Bloßfeld et al. (2018▪) process observations to all past and present spherical satellites, extending the basic ILRS 4-satellite constellation step-wise to a constellation comprising up to 11 satellites at a time. The following subsections outline the results with respect to the impact of an extended space segment on the parameter correlations (Sect. 6.3.1), the sensitivity of the observations to the Earth's gravity field coefficients (Sect. 6.3.2) and their improvement (Sect. 6.3.3).

6.3.1 Correlations between the parameter groups

To date, the official ILRS products comprise only observations to four satellites, namely the Laser Geodynamics Satellite (LAGEOS) -1 and -2 (LA-1/2), and Etalon-1 and -2 (ET-1/2). Within the nearer future, this constellation shall be extended by a fifth satellite, the Laser Relativity Satellite (LARES; LRS). While LAGEOS-1/-2 and Etalon-1/-2 are Medium Earth Orbit (MEO) satellites, LARES will complement the constellation by a Low Earth Orbit (LEO). As shown by Bloßfeld et al. (2018▪), this will significantly improve the sensitivity of the SLR solution to higher-degree Stokes coefficients, i.e., it will allow a higher spatial resolution of the Earth's gravity field than possible with the current 4-satellite constellation, while other satellites would be more beneficial to decorrelate the different parameter groups.

However, it has to be noted that many more spherical SLR satellites are in orbit that are routinely observed by the stations but are not used to generate the operational ILRS products. Besides LARES, this group of satellites comprises various LEO and MEO satellites out of which we will take into account Ajisai (AJI), Starlette (STA; Satellite de Taille Adaptée avec Réflecteurs pour les Etudes de la Terre), WESTPAC (WP1; Western Pacific Laser Tracking Network), BLITS (BTS; Ball Lens In The Space), Stella (STE), and Larets (LTS). Fig. 6.4 indicates the observation periods of all satellites that have been processed within this study.

To study the correlations among the different parameter groups, we investigated multi-satellite SLR solutions that were combined from five selected constellations, namely

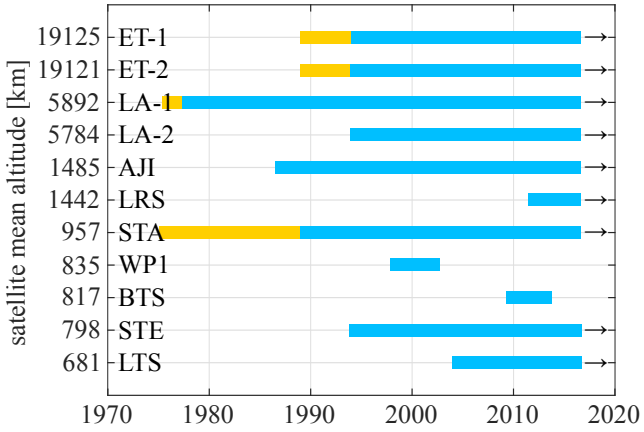

Figure 6.4: Time intervals of used SLR observations (blue boxes) to different spherical satellites. The orange boxes indicate time intervals of unused observations with lower accuracy.

(1) the ILRS 4-satellite standard setup (LAGEOS-1/2 and Etalon-1/2),

(2) the ILRS standard setup plus Ajisai,

(3) the ILRS standard setup plus LARES,

(4) the ILRS standard setup plus Stella,

(3) a solution comprising up to 11 spherical satellites at a time.

Figure 6.5 shows the average correlation matrices for 218 weekly solutions between January 13, 2013 and March 18, 2017 (GPS weeks 1723–1940), for five selected SLR constellations.

For a better understanding, we subdivide the correlation matrix into different blocks. The first three blocks represent the correlations within one parameter group each [(cf. Fig. 6.3; the order of the parameters is according to the parameterisation in DOGS-CS)]:

(a) Earth's radiation pressure scaling factor p_{albe} and satellite-specific orbital (Keplerian) elements (LAGEOS-1 only).

(b) Stokes coefficients (selected coefficients up to degree 6, [see Fig. 5 of Bloßfeld et al., 2018]).

(c) x/y-pole coordinates, solar radiation pressure scaling factor p_{rad} and LOD parameters.

The second three blocks give information on the correlations between different parameter groups:

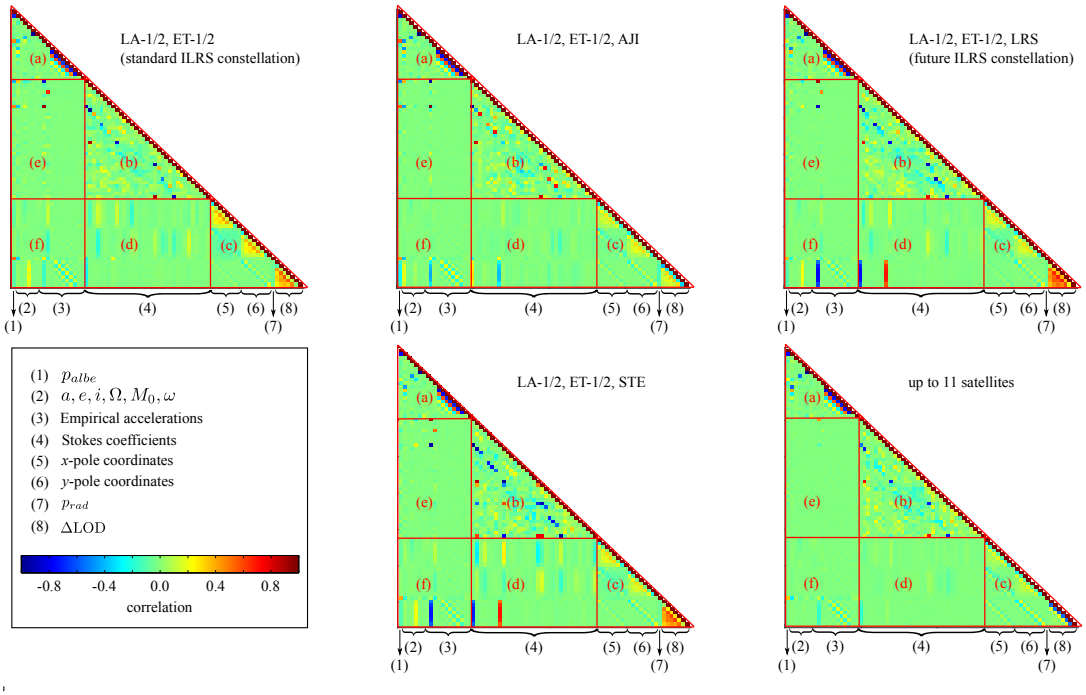

Figure 6.5: Correlation matrices of different constellation-specific SLR solutions. The orbit-related block is limited to LAGEOS-1 only. The station-related rows and columns have been omitted due to the varying station network.

(d) Correlations between the Stokes coefficients and the x/y-pole coordinates and LOD parameters.

(e) Correlations between the LAGEOS-1 orbit parameters and the Stokes coefficients.

(f) Correlations between the LAGEOS-1 orbit parameters and the x/y-pole coordinates and LOD parameters.

Block (a) For a 4-satellite solution, the largest correlations can be found between the empirical accelerations themselves (extrema $\rho = -0.77$ and $\rho = 0.61$) as well as between the mean anomaly $M_{0,\mathrm{LA1}}$ and the argument of perigee ω_{LA1} which are highly correlated with a factor of $\rho = -0.96$ due to the very small eccentricity of the LAGEOS-1 orbit. Significant correlations are also visible between p_{albe} and the semi-major axis a_{LA1} ($\rho = -0.69$) as well as the sine component of the cross-track empirical acceleration ($\rho = 0.46$). The latter is also significantly correlated with a_{LA1}. In a 5-satellite solution adding Ajisai (or Starlette, not shown in the plot), the correlation pattern within this block remains similar. If LARES or Stella is added, a significant reduction in the correlations of the sine component of the cross-track acceleration with p_{albe} and a_{LA1} can be achieved. This holds also for Larets (not shown in the plot). The reason for this might be the fact that p_{albe} is determined by the observations of several satellites at different inclinations [and in different orbital heights] than those of the 4-satellite

solution which decorrelates the Earth radiation pressure acceleration from offsets in a_{LA1} (radial orbit errors). In the 11-satellite solution, no additional parameters can be decorrelated in this block of parameters. [...]

Block (b) Visible are correlations between certain Stokes coefficients, most notably between $C_{2,0}$ and $C_{4,0}$ [(for a detailed investigation of the correlation behaviour, refer to Sect. 3.2 of Bloßfeld et al., 2018)]. As it can be seen, numerous of these correlations remain equal for all solutions as most of these correlations are due to the fact that there is no satellite which is sensitive to only one of the correlated Stokes coefficients (e.g., $C_{2,0}$ or $C_{4,0}$) and strong mathematical correlations due to their parameterisation exist between the even low-degree zonal Stokes coefficients.

Block (c) The daily LOD values are correlated with each other (up to $\rho = 0.60$). This holds also for the daily x/y-pole coordinates (up to $\rho = 0.43$). Here as well, the investigated 5-satellite solutions can be divided into two groups: While the pole coordinates are decorrelated in any case, the correlations between the LOD parameters are getting smaller in case of the inclusion of Ajisai or Starlette, whereas they increase in case of the inclusion of LARES, Larets or Stella. Again, this behaviour might be caused by the inclinations of the satellites. Within the 11-satellite solution, all correlations are reduced significantly.

Block (d) For a 4-satellite solution, only a small correlation between the $C_{2,0}$ and the LOD parameters is visible. If Ajisai or Starlette is added to the solution, these correlations remain small. However, additional correlations between $C_{4,0}$ and the LOD parameters (up to $\rho = 0.38$) become visible. In contrast to this, adding LARES, Larets or Stella in the solutions increases the correlations between the LOD parameters and the sine component of the cross-track acceleration (up to $\rho = -0.76$), $C_{2,0}$ (up to $\rho = -0.75$) and $C_{4,0}$ (up to $\rho = -0.71$). Consequently, the determination of LOD should always be based on satellites with orbit inclinations which cause prograde and retrograde precessions of the orbital plane.

Block (e) Significant correlations are visible between p_{albe} and $C_{2,0}$ ($\rho = -0.39$) as well as $C_{4,0}$ ($\rho = 0.48$). The sine component of the cross-track empirical acceleration is highly correlated with $C_{2,0}$ ($\rho = -0.82$) and $C_{4,0}$ ($\rho = 0.95$). This fact was previously discussed by Bloßfeld et al. (2014a) who studied in detail the correlations within an estimation of orbital parameters and Stokes coefficients together with LOD. The cosine component of the along-track empirical acceleration is correlated with $C_{3,0}$ ($\rho = 0.69$). In the 11-satellite solution, all these correlations between the orbit parameters and the Stokes coefficients are reduced. A crucial issue is the correlation between the longitude of the ascending node Ω_{LA1} and the low-degree even zonal Stokes coefficients (especially $C_{2,0}$), which has already been investigated in detail by Bloßfeld et al. (2015a). In a single-satellite solution, these parameters cannot be distinguished. With the 11-satellite constellation setup, these two parameters are nearly totally decorrelated.

Block (f) A significant correlation is visible between p_{albe} and p_{rad} ($\rho = 0.54$). In addition, small correlations are seen between all LOD parameters and Ω_{LA1} (up to

$\rho = 0.25$) as well as the sine component of the cross-track acceleration (up to $\rho = 0.14$) and $C_{2,0}$ (up to $\rho = -0.25$). If Ajisai or Starlette is added to the solution, the correlations between LOD and the sine component of the cross-track acceleration are getting slightly higher up to $\rho = 0.42$. In contrast, adding LARES, Larets or Stella increases these correlations significantly up to a value of $\rho = -0.76$. The 11-satellite solution minimises most of these correlations; the correlations between p_{rad} and p_{albe} remain in any case, as well as small correlations between LOD and the empirical accelerations.

To conclude, the investigated 5-satellite solutions can be subdivided into two groups. Whereas the first group (Ajisai and Starlette) reduces the correlations between the LOD parameters, the orbital elements and the Stokes coefficients, respectively, the second group (LARES, Larets and Stella) increases them. This is, most probably, due to the specific inclinations of the satellites resulting in a different precession period. As the satellites of the first group have lower inclinations and therefore a higher precession rate of their orbital planes (cf. Eq. 2 in Bloßfeld et al., 2014a), they can better distinguish between LOD and orbital parameters. This behaviour results in a higher sensitivity to variations in LOD and $C_{2,0}$ which causes higher correlations. On the other hand, the second group decreases correlations between the sine component of the cross-track empirical acceleration and a_{LA1} as well as p_{albe}, respectively.

A solution including up to 11 satellites can remove nearly all correlations between different parameter groups. Remaining are only correlations among the Stokes coefficients themselves and within the block of satellite-specific orbit parameters which are due to mathematical-physical reasons (due to the parameterisation). The correlation between ω_{LA1} and $M_{0,\mathrm{LA1}}$ cannot be solved as the LAGEOS-1 orbit is nearly circular, which means that these two parameters cannot be separated properly.◂

6.3.2 Sensitivity of the observations to the coefficients of the Earth's gravity field

▸Solutions computed using SLR observations to different satellite constellations allow it to estimate different sets of the Earth's gravity field coefficients. Generally, the more satellites with different orbit characteristics are used, the more reliably (small correlations) can the low-degree spherical harmonic coefficients be estimated. The possibility to freely estimate a parameter includes two aspects: First, the observations should be sensitive to the parameter, and second, the parameter should not be highly correlated with other estimated parameters. Thus, the impact of a satellite on the SLR constellation solution can be analysed regarding its contribution to the sensitivity of the solution to a specific Earth's gravity field coefficient and regarding its contribution to the decorrelation of the parameters. [...]

For this analysis, we use the approach by Floberghagen (2001): the free normal equation matrix of a constellation reflects the contribution of observations to each parameter

included in this NEQ. This allows us to quantify this contribution for all parameters of interest using the respective NEQ:

$$\mathbf{C_x} = (\mathbf{N} + \alpha\mathbf{K})^{-1}\mathbf{N}, \tag{6.4}$$

where the diagonal elements of $\mathbf{C_x}$ are a vector of the length of the parameter list $\mathbf{x}$, $\mathbf{N}$ is the free normal equation matrix and $\alpha\mathbf{K}$ is a diagonal regularisation matrix. The diagonal elements of the K-matrix were all the same. The value of α was chosen empirically under the condition that it should, on the one hand, repair the singularities of the initial normal matrix and allow us to invert it, and, on the other hand, it should not be too big to avoid the over-regularisation, with the contribution of the observations to all the parameters fully replaced by the constraint. In our case, the value was 10^{-8}.

The computation of the main diagonal elements of $\mathbf{C_x}$ gives us a value of observation contribution for each parameter between 0 and 1. The value 1 means that the solution is sensitive to the parameter and it can be estimated based on the observations. The value 0 means that the observations do not contribute to the parameter at all, the solution is insensitive to it, and thus the parameter cannot be estimated.

Some examples are given in Fig. 6.6. In the upper panel, the sensitivity of the basic SLR solution based on observations to 4 satellites for the GPS week 1773 (December 29, 2013, until January 5, 2014) to the gravity field coefficients up to degree and order 60 (to avoid omission errors) is shown. As it can be seen, the solution is sensitive to most spherical harmonic coefficients up to degree and order 3. When one satellite is added to the basic 4-satellite solution, the sensitivity changes dramatically, depending on the orbital characteristics of the added satellite. The middle panel of Fig. 6.6 shows a solution for the same week with the gravity field coefficients set up to degree and order 60, where LARES was added to the basic configuration. This solution shows a much higher sensitivity to the Earth's gravity field coefficients.

When up to 11 satellites are included in the solution (see Fig. 6.6, lower panel), the sensitivity of the SLR constellation shows its maximum with a sensitivity of up to degree and order 20 for the tesseral coefficients and up to degree and order 6 for the zonal coefficients, among the cases studied here. The orbital resonances derived in Table 1 [of Bloßfeld et al. (2018▪)] are clearly identified in Fig. 6.6 (lower panel).◂

The results lead us to the conclusion that the 11-satellite SLR constellation allows a reliable determination of Stokes coefficients up to degree and order 6, while a reliable estimation of the higher-degree Stokes coefficients is not possible from this SLR constellation.

▸The sensitivity tests show if observations included in a solution allow us to separate information of specific Stokes coefficients. Thus, if the contribution is zero, the respective coefficient cannot be reliably estimated using these observations. The opposite statement, that a contribution equal or close to 1 means that a coefficient can be reliably estimated, is not always true. This is due to the existing correlations between

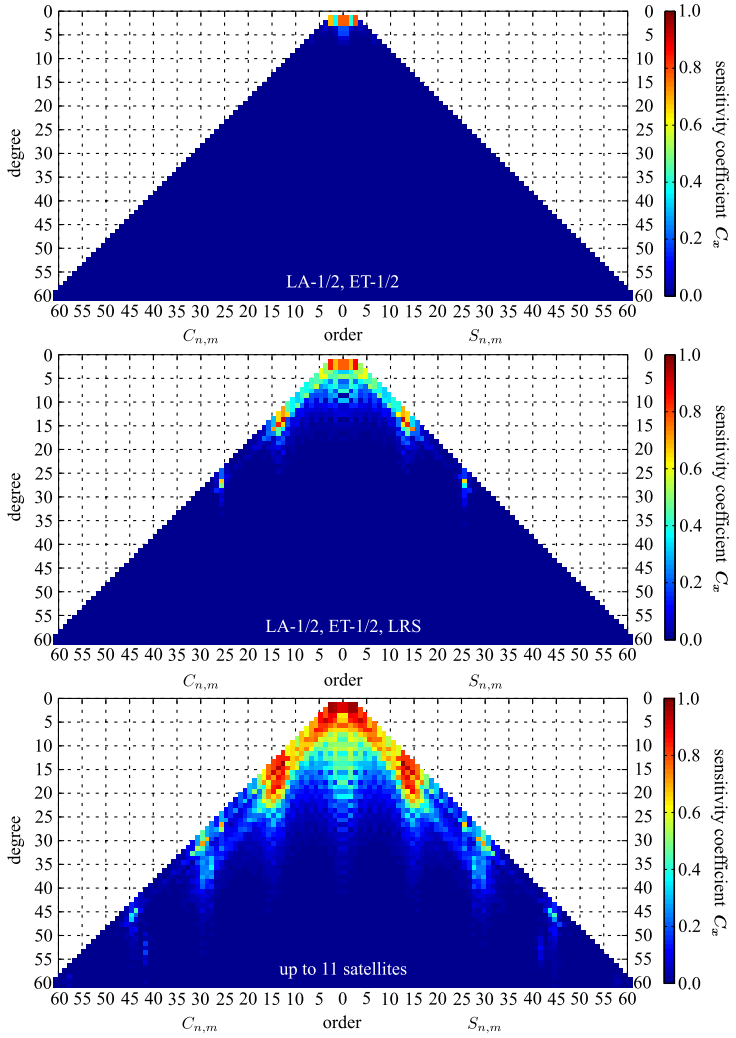

Figure 6.6: Sensitivity of SLR observations of 4 satellites (LAGEOS-1/2 and Etalon-1/2; upper panel), 5 satellites (4 satellites + LARES; middle panel) and up to 11 satellites (lower panel) to the Earth's gravity field coefficients.

different gravity field coefficients, which are not reflected by the sensitivity tests. If two parameters are correlated one-to-one, the sensitivity of the solution may be very high for both of them, but it would not be possible to estimate them together in one solution. At the same time, adding observations of different satellites may help to decorrelate some gravity field parameters.

6.3.3 Improvement of selected gravity field coefficients

This section is dedicated to investigating the scatter (in terms of WRMS values) of time series of low-degree Stokes coefficient estimates. The smaller the derived WRMS

is, the smaller is the scatter of the solutions. This means that a smaller WRMS indicates a better repeatability of the results, which means that we consider a smaller WRMS of a Stokes coefficient as an improvement of the repeatability of the estimated parameter. Thereby, we take the 4-satellite solution as basis and look at the magnitude of improvement of the scatter of the time series when the constellation is extended.

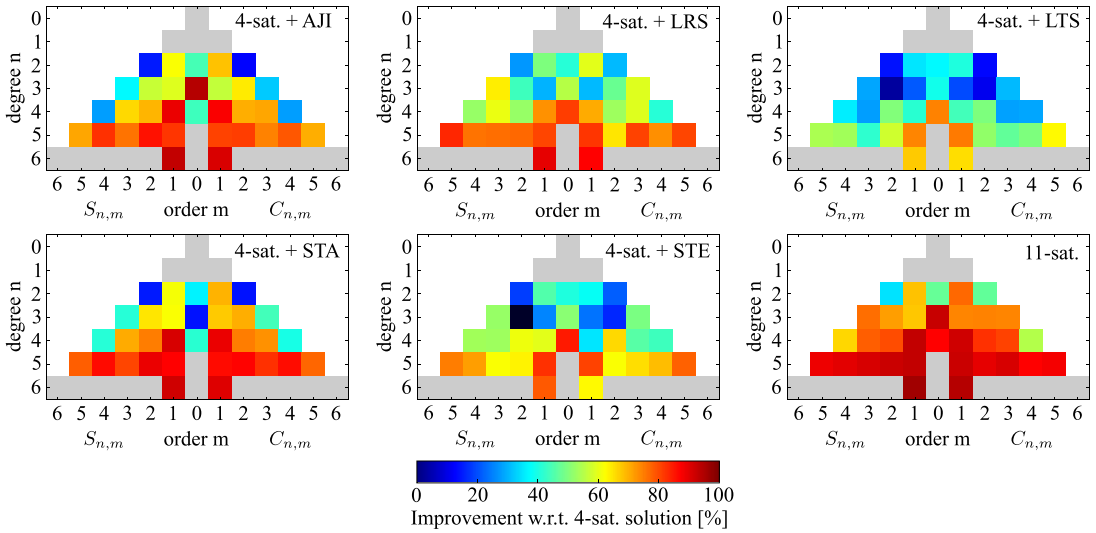

Figure 6.7: Improvements in the WRMS over the weekly SLR gravity field coefficient solutions w.r.t. the 4-satellite solution. Coefficients marked in grey have not been estimated. Note: In the solution 4-sat. + STE, $S_{3,2}$ is degraded by 13 % (coefficient marked in black).

An overview about the achieved WRMS improvements w.r.t. the 4-satellite solution is given in Fig. 6.7. Looking at the different 5-satellite solutions, one can observe a different pattern of improvement, especially for the gravity field coefficients up to order 3. The WRMS of $C_{2,0}$ (and also of $C_{2,1}$ and $S_{2,1}$) is improved by all satellites with maximum values of over 40 % for Ajisai, LARES and Stella. Striking is the improvement behaviour of the WRMS of $C_{3,0}$. Whereas this coefficient is improved extremely by Ajisai (94.3 % improvement) and still by ≥ 50 % by LARES and Stella, Starlette and Larets yield improvements ≤ 40 % with a minimum of only 14.5 % for Starlette. The WRMS of $C_{4,0}$ is mainly improved by LARES and Stella by ≥ 80 %, respectively, and Larets by 74.5 %. All these three satellites have inclinations > 60°. In contrast, Ajisai and Starlette improve this coefficient by < 50 %. The smallest improvements in WRMS of the tesseral gravity field coefficients are visible for Larets and Stella (inclinations of ≥ 98°), followed by LARES (medium inclination of i_{LRS} = 69.5°). The biggest improvements in these coefficients can be determined for Ajisai and Starlette (inclinations around 50°). All the sectoral GFCs are most improved by LARES. In the 11-satellite solution, all coefficients are significantly improved by at least 40 % and reaching almost 100 % for degree 5, as well as degree 4, 6, and order 1 coefficients. Therein, each satellite contributes to specific coefficients based on the geometry of Earth's gravitational

field and satellite orbital plane. This means, each coefficient is, to a certain extent, improved by a specific satellite (e.g., $C_{3,0}$ by Ajisai) or by a combination of satellites.

6.4 Simulation of potential future scenarios

DOGS-OC includes a simulation modus that has been made operational for the studies presented hereafter. It allows to simulate SLR observations from existing or fictional stations to existing or fictional satellites. The software allows to set the observation rate (i.e., the normal point bin size), the satellite's centre-of-mass correction, and a minimum elevation angle as global parameters for all stations. Additionally, performance (percentage of observed passes), measurement noise, range and time biases, or coordinate offsets can be defined for each station individually. While the simulations are performed independently for all satellites, additional post-processing scripts have been developed to reduce the simulated observations to certain observation patterns and to remove "simultaneous" observations of a single station to different satellites at a time via a satellite priority list.

In the following, Sections 6.4.1 to 6.4.3 outline the simulation and solution workflow and the underlying assumptions.

6.4.1 Simulation procedure

Based on orbital elements solved from real observations, the simulation, combination, and solution workflow is implemented according to Fig. 6.8 and comprises five steps, namely

(1) simulate observations for all stations,

(2) estimate the initial orbital elements from the simulated observations,

(3) generate normal equations based on the simulated observations and the initial orbital elements from step (2),

(4) calculate single-satellite solutions, and

(5) calculate a 5-satellite combined solution.

In step (1), observations are simulated for all stations with 100 % performance based on a dynamically-integrated satellite orbit from previously-estimated initial elements. Afterwards, the simulated observations are reduced according to the station-specific performances and the satellite priority list. Steps (2) to (5) are identical to the workflow to process real observation data: Step (2) delivers better initial values for the parameters that shall be determined in step (5), step (4) is required to determine the relative weights of the satellite-specific contribution in the combined solution in step (5). These weights are calculated based on the a posteriori variance factors of the

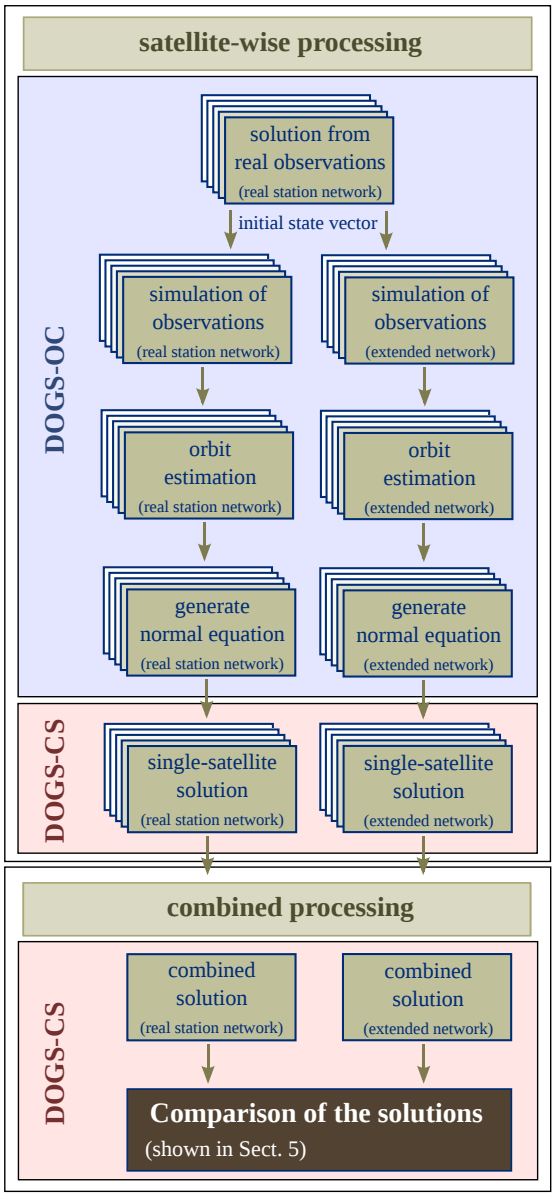

Figure 6.8: SLR simulation and solution process for one week.

single-satellite solutions from step (4). The single-satellite processing steps (1) to (3) are performed with DOGS-OC, while the combination and solution steps (4) and (5) are performed with DOGS-CS.

To ensure comparability of the results, the different scenarios are simulated under the assumption of an observation scheduling of three normal points at the beginning, mid, and end of each observed pass. This is in accordance with the tracking scheme recommended by the ILRS for orbit determination.

Within the following sections, we analyse time series of weekly SLR solutions for different geodetic parameters. The solutions are processed from observations that have been simulated according to different scenarios. Our criterion of interest is the WRMS deviation between the a priori values of the parameters and their solutions. To quantify the datum repeatability of ERFs, this means to compute the WRMS over time series of Helmert transformation parameters between the ERF solutions and the a priori TRF. To quantify the repeatability of the ERPs or the Stokes coefficients, this means to calculate the WRMS over the difference time series between their estimates and their a priori values. Consequently, the WRMS delivers us a measure for the *repeatability of the solution* and gives a hint how well the assumed scenario (satellite constellation, network geometry, performances and observation errors) allows us to re-determine the a priori values of the geodetic parameters from the simulated observations.

6.4.2 Representation of the measurement error

SLR observations are simulated by calculating a theoretical observation, which is the geometrical distance between an SLR station and a satellite at a given epoch corrected by all modelled effects according to Eq. 6.1. To guarantee realistic conditions, this theoretical observation has to be "degraded" in quality in order to take into account potential errors of systematic and non-systematic nature. We thus divide the measurement error ϵ (Eq. 6.3) into two parts

$$\epsilon = e_{\text{syst,unmodelled}} + e_{\text{err}}, \tag{6.5}$$

namely one part $e_{\text{syst,unmodelled}}$ representing systematic model deficiencies (i.e., remaining inaccuracies of the models that cover $e_{\text{syst,modelled}}$ in Eq. 6.3), and another part e_{err} representing remaining errors of unknown source and magnitude.

To account for the systematic model deficiencies $e_{\text{syst,unmodelled}}$, we vary some of the geophysical background models between the simulation step, i.e., the generation of simulated observations, and the orbit recovery step, i.e., the processing of these simulated observations. ▸Within this study, we have limited this modification to the Earth gravity field model, the ocean tide model, and the ocean loading model. The gravity field model has been switched between EIGEN-6s (Förste et al., 2011) for the simulation step and GGM05S (Tapley et al., 2013; Ries et al., 2016) for the orbit recovery step. The ocean tide and ocean loading models have been switched accordingly from EOT11a (Savcenko and Bosch, 2012) to FES2004 (Lyard et al., 2006). Studies investigating the impact of different ocean tide and gravity field models on the orbit RMS of real-data processing have determined an average variation of up to 1.3 mm for ocean tide models (Sośnica, 2015) and a variation of up to about 0.2 mm caused by switching between different recent gravity field models from the post-CHAMP era (Sośnica et al., 2012).

The second measurement error component e_{err} has been assumed to behave like white noise. It is represented by a simulation noise with a standard deviation of σ_{sim} added to

the simulated SLR observations. This error component contains the measurement noise or the normal point (NP) precision as well as remaining unmodelled errors, respectively. It can thus be represented as

$$\sigma_{\text{sim}} = \sqrt{\sigma_{\text{sta}}^2 + \sigma_{\text{other}}^2}, \tag{6.6}$$

with σ_{sta} denoting the normal point precision ($\leq$ 1 mm) and σ_{other} referring to all other errors. Clearly, σ_{sim} is dominated by the σ_{other} contribution, rather than the NP precision, which is not a limiting factor.◂ As standard case, we have chosen a simulation noise of σ_{sim} = 1 cm, as this value closely approximates the average orbit RMS derived from real observations with estimating station coordinates, range biases (for certain stations only), EOPs, empirical forces and atmospheric drag coefficients.

▸The issue of the station-dependent range biases in the existing SLR network (e.g., Coulot et al., 2008; Appleby et al., 2016) has not been taken into account in the present simulations. As this study is focused on the impact of additional stations [or satellites] (geometry) or an increasing amount of data (performance), the range biases have been omitted for all stations – existing and future – as they are unknown for potential future stations.◂

6.4.3 Station performances and observed satellite constellation

All of our simulations take as reference case the future ILRS 5-satellite constellation comprising LAGEOS-1/-2, Etalon-1/-2, and LARES, observed by the existing network of SLR stations. Thereby, the station (pass) performances of the network are chosen such that they reflect the actual performance of each individual station over a chosen time span excluding longer periods of inactivity. This means that the performance of existing stations has been determined for those weeks in which the station has actually delivered observation data. In the simulations, the stations of the existing network have, consequently, either been simulated with their determined average performance (within weeks where the station has actually been active), or they have been omitted (within weeks where the station has actually been inactive). The assumed minimum elevation angle for simulated observations has been set to 10° for all stations. The reference case is then compared to other scenarios where either additional satellites are added to the space segment, or additional stations are added to the ground segment, or the existing stations of the ground segment are enhanced in performance. Details about the performance assumptions for existing and additional stations are provided in the following subsections that describe the different simulated scenarios.

6.5 Extending the SLR space segment

In the coming years, the SLR space segment shall undergo significant changes due to the launch of additional satellites. The 2016 call for proposals for the ESA Earth Explorer Opportunity Mission EE-9 led to a proposal for a mission called European Geodetic Reference Antenna in Space (E-GRASP)/European Reference Antenna of Space Geodetic Techniques Enhancing Earth Science (Eratosthenes). The E-GRASP/Eratosthenes mission proposed a satellite co-locating all space-geodetic techniques on one platform, with one major goal being to achieve millimetric TRF precision by co-locations in space (Biancale et al., 2017). Besides these aforementioned advantages, a satellite in an E-GRASP-like orbit would extend the current SLR constellation – featuring only nearly circular orbits in different heights – by a highly excentric orbit with heights varying between 700 and 7000 km (Fig. 6.9).

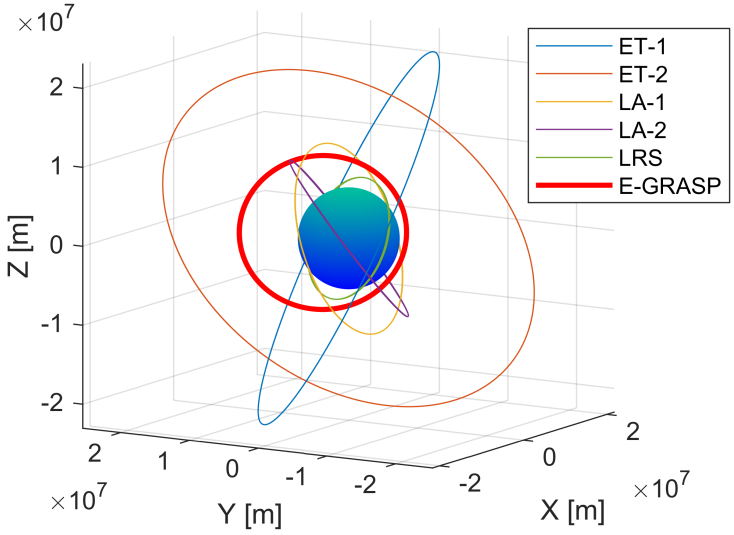

Figure 6.9: The future ILRS 5-satellite constellation extended by an E-GRASP-like orbit as assumed for the simulation study.

Simulation studies conducted within the framework of the E-GRASP/Eratosthenes proposal investigate the impact of enhanced SLR space and ground segments on the estimation of low-degree spherical harmonics of the Earth's gravitational field model and on the correlations between different parameter groups. The study compares a 5-satellite solution combining LAGEOS-1/2, Etalon-1/2, and LARES (future ILRS setup) to a 6-satellite solution including a satellite in an E-GRASP-like orbit. For the purpose of this study, the satellite has been assumed as a spherical satellite with SLR retro-reflectors only. In order to determine which parameter improvements can be related directly to the improved orbit constellation, the study also contrasts simulations with the existing SLR station network against a scenario with eight additional stations as assumed by Kehm et al. (2018▪, cf. Sect. 6.6.1). Tab. 6.4 summarises the simulation conditions.

Table 6.4: Simulation assumptions for an SLR space segment extended by an E-GRASP-like orbit.

Statistics and performance assumptions	
Pass performances of the existing network	station-specific average for GPS weeks 1773 (2013-12-29) to 1833 (2015-02-28)
Average network performance	13 %
Maximum performance	54 % (Yarragadee)
Additional stations	13 % (La Plata), 15 % (Colombia, Canary Islands, Ny-Ålesund, Ponmudi, Mount Abu), 20 % (Nigeria, Malindi)
Solution setup	
Sampling	weekly
Time span	week 1773 (2013-12-29) to 1833 (2015-02-28)
Constellation	5 satellites (Etalon-1, Etalon-2, LAGEOS-1, LAGEOS-2, LARES)
Observation scheme	each pass simulated with 3 NPs at the beginning, middle, and end (simultaneous observations of a station to multiple satellites removed)
Noise/error assumptions	
Observation (NP) noise	1 cm
Systematic errors	switch of gravity field model (EIGEN6s to GGM05S) and ocean tide and ocean loading models (EOT11a to FES2004)

The assumed E-GRASP/Eratosthenes initial state vector at epoch 2012/01/01 00:00 UTC has been chosen as:

- semi-major axis: $a = 10488.277\,\text{km}$,
- eccentricity: $e = 0.32$,
- inclination: $i = 116.6°$,
- longitude of the ascending node: $\Omega = 131.803°$,
- argument of perigee: $\omega = 180.0°$,
- mean anomaly: $M = 180.0°$.

As Fig. 6.10 (left panel) shows, an SLR satellite in an E-GRASP-like orbit reduces the standard deviations of the estimated low-degree harmonic coefficients by up to 30 %. The largest improvements are seen in $C_{2,0}$, $C_{4,0}$, and in tesseral and sectoral terms of degrees 3 and 5 (coefficients marked in grey were not estimated).

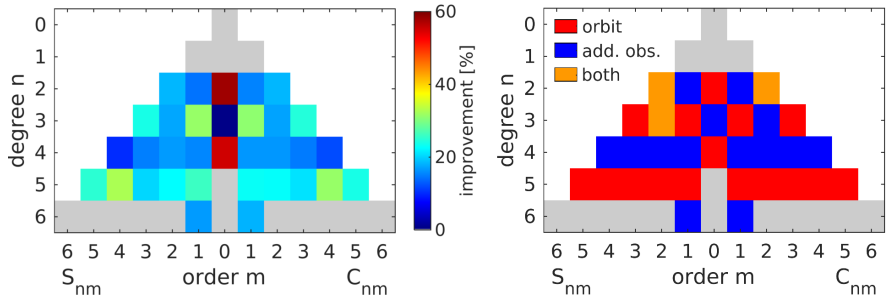

Figure 6.10: Impact of an E-GRASP-like orbit on the estimated standard deviations of SLR-derived low-degree gravity field coefficients. Improvement by the E-GRASP-like orbit (left), dominance of the additional orbit vs. dominance of the improved ground segment (right).

Table 6.5: Correlation coefficients ρ between $C_{2,0}$ and the right ascension of the ascending node of LAGEOS-1 (Ω_{LA1}). Taken from Bloßfeld et al. (2015a), extended by values determined for an additional E-GRASP-like orbit (lines in bold script).

Solution	satellite constellation	ρ
LA1	LA1	1.00
2-sat.	LA1/2	0.44
4-sat.	LA1/2, ET1/2 (current ILRS setup)	0.44
4-sat. + BTS	LA1/2, ET1/2, BTS	0.43
4-sat. + LTS	LA1/2, ET1/2, LTS	0.41
4-sat. + EGR	**LA1/2, ET1/2, EGR**	**0.39**
4-sat. + STE	LA1/2, ET1/2, STE	0.31
4-sat. + STA	LA1/2, ET1/2, STA	0.28
4-sat. + AJI	LA1/2, ET1/2, AJI	0.24
4-sat. + LRS	LA1/2, ET1/2, LRS (future ILRS setup)	0.24
6-sat. (1)	LA1/2, ET1/2, AJI, STE	0.24
6-sat. (2)	**LA1/2, ET1/2, LRS, EGR**	**0.23**
7-sat.	LA1/2, ET1/2, AJI, STE, STA	0.22
8-sat.	LA1/2, ET1/2, AJI, STE, STA, BTS	0.21
9-sat.	LA1/2, ET1/2, AJI, STE, STA, BTS, LTS	0.21
10-sat.	LA1/2, ET1/2, AJI, STE, STA, BTS, LTS, LRS	0.08

In order to separate the impact of the additional number of observations – which results from adding the satellite or adding stations to the solutions – from the impact of improved observation geometry on the solution, scaling the resulting standard deviations by the $\sqrt{n}$ law allows to assess which of the aspects is dominant for the improvement of the standard deviation of each Stokes coefficient. Fig. 6.10 (right panel) summarises the results from this comparison. We conclude that the tesseral and sectoral Stokes coefficients of degrees 3 and 5, $C_{2,0}$, and $C_{4,0}$ benefit directly from the observation geometry improved by the E-GRASP orbit. In contrast, $C_{3,0}$ and the tesseral and

sectoral coefficients of degrees 2 and 4 mainly benefit from the additional amount of observations to an additional satellite or from additional SLR stations.

For orbits with inclinations $\geq 50\,\text{deg}$, $C_{2,0}$ is highly correlated with the right ascension of the ascending node. The two parameters can be decorrelated by combining satellites with different inclinations. Thus, the correlation is a measure for the impact of the additional satellite on the estimated Stokes coefficients. Tab. 6.5 shows the contribution of an E-GRASP-like satellite to decorrelating the right ascension of the ascending node of LAGEOS-1, Ω_{LA1}, from the gravity field coefficient $C_{2,0}$, within the context of results from previous studies by Bloßfeld et al. (2015a). The results indicate that adding an E-GRASP-like satellite to the current 4-satellite or the future 5-satellite constellation would significantly decorrelate $C_{2,0}$ and the right ascension of the ascending node Ω_{LA1}.

6.6 Improving the SLR ground segment

This section is dedicated to two possible ways to improve the SLR ground segment, namely either the inclusion of additional stations into the network or the improvement of the performance of the stations in the existing network.

Predicting the impact of additional SLR stations on the SLR-derived parameters is highly relevant as the findings can help to decide which regions should be prioritised to host new SLR systems. Fig. 6.11 shows an overview about the studies presented in the following sections. Thereby, *Study A* is one part of a study published by Kehm et al.

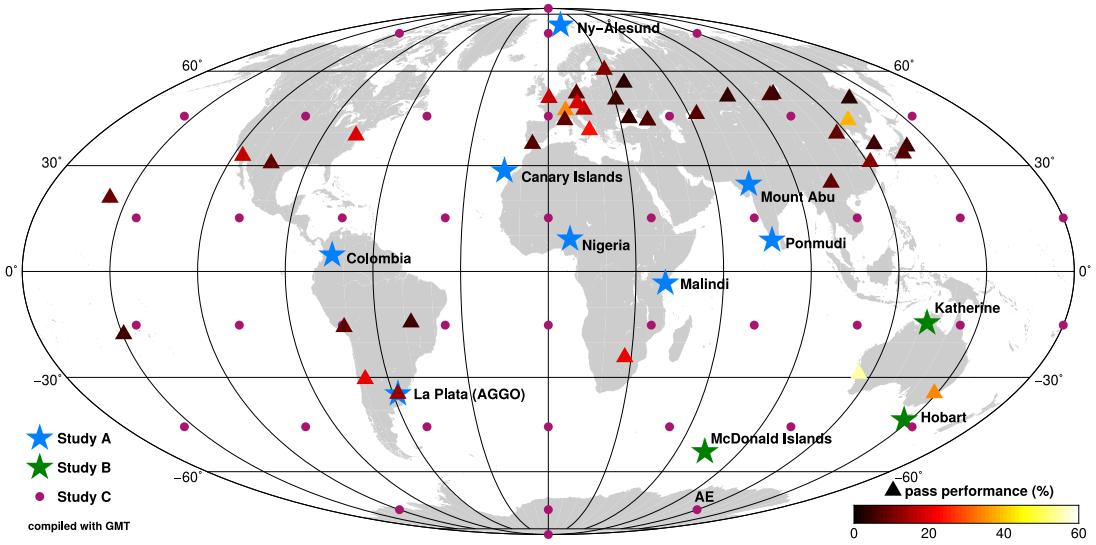

Figure 6.11: Overview about the different simulation studies on SLR network extensions. The triangles denote the stations of the existing network and are colour-coded according to their average pass performances between 2012-12-28 and 2015-02-28 (cf. Fig. 6.2).

(2018), investigating the impact of a network extended by eight globally-distributed additional stations, and comparing the results to a network that has enhanced station performances (Sect. 6.6.1). Afterwards, *Study B* puts the focus on three potential stations in the Australian network that could improve the SLR network geometry on the southern hemisphere (Sect. 6.6.2). Finally, free from any geographical or administrative constraints, *Study C*, published by Kehm et al. (2019), aims to determine the best locations for additional SLR stations with respect to different TRF datum parameters and EOPs (Sect. 6.6.3). Section 6.7 concludes with a summary of the results.

6.6.1 Study A: Extending the global SLR network

One part of the study by Kehm et al. (2018) is to investigate the impact of an SLR network extended by eight globally-distributed additional stations. The simulation conditions are summarised in Tab. 6.6. We assume the calculation of week-wise SLR-only-derived epoch reference frames over a time span of 61 weeks between the end of December 2013 and February 2015. We estimate the station coordinates, the ERPs, and the initial state vector of the satellite. The NNR condition to realise the TRF orientation is applied to the whole network in order to determine a direct effect of the improved network geometry on the epoch-wise realisation of the orientation (omitting differentiation between core and non-core stations). We simulate four different scenarios that assume observation noises of 1 cm (reference case), 7 mm, 4 mm, and finally 1 mm, respectively, for all stations and all satellites. The station-specific minimum station performances of the existing network are set to the average performance values determined for the chosen time span (cf. Sect. 6.4.3). In case of future stations, the performance values are chosen as 13 % (the average performance of the existing network) for La Plata (Argentina), 15 % (the rounded average performance of the existing network) for Colombia, the Canary Islands, Ny-Ålesund (Spitsbergen), Ponmudi and Mount Abu (India), and 20 % for the stations in Nigeria and Malindi (Kenya). We intend the chosen performances to reflect the operating conditions of a station at the time when it might be established, without a significant technological improvement compared to the existing systems. To investigate the impact of enhanced performances due to a technical improvement, we perform simulation runs assuming minimum network performances of 20 %, 40 %, 60 %, and 80 %.

With respect to the influence of additional stations, the results suggest a relative improvement of the WRMS values of all parameters that is rather independent from the chosen minimum network performance or the chosen measurement noise. While the TRF datum parameters improve by about 15 % for t_z and about 20 % for t_x, t_y, and the scale, the ERPs improve to a smaller extent by about 3–5 % on average. We relate the small effect on the ERPs to the fact that the station clusters in Europe and East Asia do already cover the two axis directions of x_{pole} and y_{pole} comparably well. A significant improvement is also visible for the condition number of the normal equation matrix – a measure for the overall solution quality – which is reduced by about 13 %.

Table 6.6: Simulation assumptions for a global SLR network extension.

Statistics and performance assumptions	
Pass performances of the existing network	station-specific average for GPS weeks 1773 (2013-12-29) to 1833 (2015-02-28)
Average network performance	13 %
Maximum performance	54 % (Yarragadee)
Additional stations	- minimum: 13 % (La Plata), 15 % (Colombia, Canary Islands, Ny-Ålesund, Ponmudi, Mount Abu), 20 % (Nigeria, Malindi) - runs with step-wise increased performance for the whole network (existing and new stations; cf. Kehm et al., 2018▪)
Solution setup	
Sampling	weekly
Time span	week 1773 (2013-12-29) to 1833 (2015-02-28)
Constellation	5 satellites (Etalon-1, Etalon-2, LAGEOS-1, LAGEOS-2, LARES)
Observation scheme	each pass simulated with 3 NPs at the beginning, middle, and end (simultaneous observations of a station to multiple satellites removed)
Noise/error assumptions	
Observation (NP) noise	1 cm, 7 mm, 4 mm, 1 mm
Systematic errors	switch of gravity field model (EIGEN6s to GGM05S) and ocean tide and ocean loading models (EOT11a to FES2004)

From simulation runs varying the minimum performance of the SLR network, we find that enhanced station performances significantly improve the derived TRF datum parameters and the condition number of the normal equation matrix, while the ERPs are less improved, yet significantly more than by the improved network geometry. Assuming a (theoretical) network performance of 80 % for all stations, the WRMS of the TRF datum parameters can be improved by up to more than 70 % (depending on the parameter), while the ERPs can be improved by up to 48 %. The condition number of the normal equation matrix can be reduced from the order 10^8 by over 95 %, meaning a reduction by two orders of magnitude. For the datum realisation of ERFs, these results indicate that a theoretical high-performing SLR network could significantly stabilise the epoch-wise realised datum. For more details, refer to Fig. A.1 in the Appendix and the original publication by Kehm et al. (2018▪).

Table 6.7: Improvement of the WRMS of the Helmert parameters and of the RMS of the transformation residuals due to technical improvement, improved network geometry, and combined effect for a minimum global SLR network performance of 20 %. Values taken from Tab. 2 in (Kehm et al., 2018).

	ΔWRMS				ΔRMS
	t_x	t_y	t_z	scale	of residuals
Technical improvement	10 %	27 %	14 %	49 %	44 %
Network geometry	18 %	20 %	24 %	20 %	7 %
Combined effect	26 %	41 %	35 %	59 %	48 %

Table 6.8: Improvement of the WRMS of the ERPs due to technical improvement, improved network geometry, and combined effect for a minimum global SLR network performance of 20 %. Values taken from Tab. 2 in (Kehm et al., 2018).

	ΔWRMS		
	x_{pole}	y_{pole}	LOD
Technical improvement	10 %	10 %	4 %
Network geometry	4 %	5 %	2 %
Combined effect	13 %	15 %	6 %

The question that arises is: Which of the scenarios is most likely for the nearer future? Performances of 80 % do not only require the administrative and technical conditions allowing the stations to be permanently operational (e.g., automatisation of the ground systems). Also the weather conditions at the site need to be appropriate in order to perform measurements. Thus, we assume that it will not be possible to increase the minimum performance of the network to more than 20 % in the foreseeable future. For about one third of the existing stations, this would mean a performance value two to three times as high as presently. Tab. 6.7 and 6.8 summarise the effect of technical improvement (increased performance), the effect of the improved network geometry, and the combined effect for the simulated case assuming a minimum network performance of 20 %. For all Helmert parameters, it turns out that the effect of an improved network performance and of an improved network geometry are equally important. A significant improvement is visible for the translation components, where the effect of the improved network geometry dominates for t_z and t_x while the effect of the improved performance dominates for t_y, the scale, and also for the overall RMS of the transformation residuals. As outlined above, the quality of the ERPs is mainly improved by a higher network performance, as the station distribution is already well-adjusted to the axes of polar motion.

The improved datum stability achieved by extending the SLR network and by enhancing the performance of the stations also has an impact on the station position residuals resulting from the Helmert transformation on the a priori reference frame and are shown

in Fig. A.2 in the Appendix. ▸Especially for the high-performant stations located in regions with a low network density on the southern hemisphere, the benefit from an improved network geometry and the indirect effect of a higher network performance are of equal importance (remember, the performance has not been improved any further for stations whose value is already above 20 %). The WRMS values are improved by up to 20 % by each effect leading to a combined improvement of up to about 40 %. This holds for Mt. Stromlo, Yarragadee (both Australia), and Hartebeesthoek (South Africa), but also for certain Central European stations like Graz (Austria; East component), Zimmerwald (Switzerland; East and height component), and Wettzell (Germany; East component). For stations in regions with a high network density (Europe, East Asia, North America, Arequipa/Peru), the performance is the dominant factor (15 %–50 % WRMS reduction). For these stations, the effect of an improved network geometry reduces the WRMS by up to about 15 %. Especially for the stations in North America and East Asia, no improvement in the North coordinate WRMS value can be seen. An increased WRMS, as can be seen for a small number of stations, can result from indirect effects via the estimated orbit – when performances of surrounding stations are improved or additional stations are added to the network – in combination with increased weights due to the larger number of observations for a number of weekly solutions, even if the coordinate residuals themselves are not getting significantly larger w.r.t. the reference solution.◂

6.6.2 Study B: Extending the SLR network on the southern hemisphere

In order to figure out the value of additional SLR stations in the Australian subnetwork, we simulated the existing network and different scenarios for an extended network over a time span of approximately 4.5 years between 12/2014 and 07/2019. The assumptions taken are summarised in Tab. 6.9. The results are based on an SLR-only weekly epoch reference frame solution. The assumed average pass performance of 22.5 % for each additional SLR station has been chosen as a conservative guess, as the minimum performance of current Australian SLR systems is already 29 % (Mt. Stromlo).

Eight scenarios have been simulated (Tab. 6.10): Scenario 0) simulates the existing network only, Scenarios 11)–13) each add one out of three potential stations (green stars in Fig. 6.11) to the existing network, Scenarios 21)–23) each add two of these stations at a time, and Scenario 31) adds all three stations together.

Tab. 6.11 provides the relative improvements derived for the TRF datum (in terms of reduced WRMS values) and Tab. 6.12 provides the relative improvements of the ERPs, whereby the given improvements are calculated as an average of the two simulation runs with 15 % and 30 % performance (cf. Tab. 6.9). We conclude that McDonald is the most beneficial site for both the TRF origin and the ERPs, which confirms that this station fills a significant gap in the current SLR network. McDonald and Hobart both yield improvements in the TRF origin, predominantly, which is due to the currently weak observation geometry for this parameter. McDonald, Hobart and Katherine all

Table 6.9: Simulation assumptions for an extension of the Australian SLR network.

Statistics and performance assumptions	
Pass performances of the existing network	station-specific average for GPS weeks 1825 (2014-12-28) to 2060 (2019-07-06)
Average network performance	11 %
Maximum performance	56 % (Yarragadee)
Additional stations	22.5 % generated as average from two simulation runs: - run with 15 % performance (cf. Kehm et al., 2019); this value is slightly above the average performance of the network but is reasonable as a lowest assumption for modern SLR) - run with 30 % performance (as the minimum performance of both current Australian SLR systems is close to 30 %)
Solution setup	
Sampling	weekly
Time span	week 1825 (2014-12-28) to 2060 (2019-07-06)
Constellation	5 satellites (Etalon-1, Etalon-2, LAGEOS-1, LAGEOS-2, LARES)
Observation scheme	each pass simulated with 3 NPs at the beginning, middle, and end (simultaneous observations of a station to multiple satellites removed)
Noise/error assumptions	
Observation (NP) noise	1 cm
Systematic errors	switch of gravity field model (EIGEN6s to GGM05S) and ocean tide and ocean loading models (EOT11a to FES2004)

yield improvements in LOD (for Katherine, this effect can be seen mostly in the 30 % performance run, with $\Delta\mathrm{WRMS(LOD)} = -1,7\,\%$; not shown in Tab. 6.12). Adding all three stations together (Katherine, McDonald and Hobart) yields the largest improvement in the TRF scale; for the translations, the results from both simulation runs differ (seen in the uncertainties, especially for the translations). The 15 % performance run yields the largest improvement of 7 % in t_z and 2 % in the scale, the 30 % run yields improvements of 6 % in t_x and 4 % in the scale.

Table 6.10: Scenarios for additional Australian SLR systems.

Scenario	existing network	Katherine	Hobart	McDonald
0)	■			
11)	■	■		
12)	■		■	
13)	■			■
21)	■	■	■	
22)	■	■		■
23)	■		■	■
31)	■	■	■	■

Table 6.11: Improvement of the WRMS of the Helmert parameters for different scenarios of additional Australian SLR systems.

Scenario	t_x	t_y	t_z	sc
0)	–	–	–	–
11)	-0.6 ± 0.6	$+0.7 \pm 0.3$	$+0.1 \pm 0.5$	-1.3 ± 0.7
12)	-1.5 ± 0.2	-1.4 ± 0.2	-3.4 ± 0.0	$+2.1 \pm 0.2$
13)	-2.6 ± 1.1	-2.9 ± 1.0	-7.7 ± 1.1	-0.7 ± 0.8
21)	-0.6 ± 0.9	$+0.7 \pm 0.3$	-3.3 ± 1.2	-0.8 ± 1.3
22)	-0.7 ± 0.8	-0.1 ± 0.4	-6.3 ± 1.1	-0.7 ± 0.7
23)	-1.3 ± 1.3	-3.2 ± 0.8	-8.9 ± 0.1	-0.6 ± 0.8
31)	-3.1 ± 3.1	-1.0 ± 0.8	-3.2 ± 4.7	-2.9 ± 1.9

Table 6.12: Improvement of the WRMS of the ERPs for different scenarios of additional Australian SLR systems.

Scenario	x_{pole}	y_{pole}	LOD
0)	–	–	–
11)	$+0.1 \pm 0.6$	$+1.5 \pm 0.3$	-0.2 ± 1.0
12)	-0.8 ± 0.4	$+1.0 \pm 0.4$	-0.9 ± 0.3
13)	-1.7 ± 0.3	-4.0 ± 0.8	-2.3 ± 1.3
21)	-1.3 ± 0.3	$+1.2 \pm 0.2$	-3.1 ± 1.3
22)	-2.6 ± 0.2	-2.5 ± 0.6	-2.5 ± 2.3
23)	-2.7 ± 0.1	-3.1 ± 1.0	-3.4 ± 1.0
31)	-2.5 ± 0.8	-2.6 ± 1.0	-0.9 ± 0.9

6.6.3 Study C: Best location for a future SLR station

The study conducted by Kehm et al. (2019) aims to determine the regions where one station added to the existing SLR network would be most beneficial for the accuracy of the estimated datum parameters and ERPs. The simulation study is again based on a weekly SLR-only-derived epoch reference frame and has been performed as contribution to GGOS-PLATO.

Within this study, we assume 42 different potential sites. The sites are equal-area distributed on a global grid, including the poles. We calculate 43 different solutions out of which one comprises the present SLR network (marked as triangles in Fig. 6.11) while each of the remaining 42 solutions comprises the present network plus one additional station located at one of the grid points (magenta dots in Fig. 6.11). As in the previous simulation studies, we calculate weekly solutions. In contrast to *Study A*, the simulated period of time has been extended to a time span of five years from 2012-12-30 to 2018-01-06.

The simulation conditions and performance assumptions have been chosen similar to *Study A*, but with some modifications: As the SLR system at the Argentinean-German Geodetic Observatory (AGGO; Häfner, 2019) is expected to be operational in the near future, it has been considered to be part of the already operational network and has been assigned a performance of 15 % (a value close to the average performance of the existing network of 13 %). For each of the other simulated additional stations (i.e., each of the equal-area distributed sites), a common performance of 20 % has been assigned. This common value has been chosen on purpose: We are assuming further improvement of the systems in the foreseeable future; i.e., automated stations equipped with, e.g., kilohertz lasers, fast-slewing telescopes, improved daytime tracking, being able to exploit a much larger amount of the (sometimes short) phases where a satellite is trackable. This would presumably also increase the number of measured passes during predominantly bad weather conditions. Our assumption stands in contrast to simulations using station performances derived from the basis of a total cloud coverage (TCC), [an approach chosen by some of the simulation studies mentioned in Sect. 6.1]. As, e.g., pointed out by Glaser et al. (2019a), the TCC alone is not the only aspect that has an effect on the performance of a station and would – neglecting all other performance-relevant aspects – allow for a performance higher than 20 % for all of the existing stations (Fig. 3 in Glaser et al., 2019a).

Free of these imponderables, we thus decided to assign a common performance value of 20 % to each of the additional stations. This could be defined as our "minimum performance goal" for modern laser systems. With a latitude-dependent minimum of 4 and 5 passes per week on the LARES and LAGEOS satellites, resp., each of the assumed sites would fulfil the ILRS Pass Performance Standard[5] defining a fixed minimum number of 3500 observed passes per year on all satellites, among them 600

[5] ILRS Pass Performance Standard, Revision 2015. URL: `https://ilrs.gsfc.nasa.gov/network/system_performance/index.html` (2022-06-15).

passes on the LAGEOS-class (LAGEOS-1, LAGEOS-2, LARES) satellites (i.e., 4 passes per week on each LAGEOS-class satellite). The aim of the present study is to define potential sites for additional stations given the precondition of comparable conditions at each of these sites.

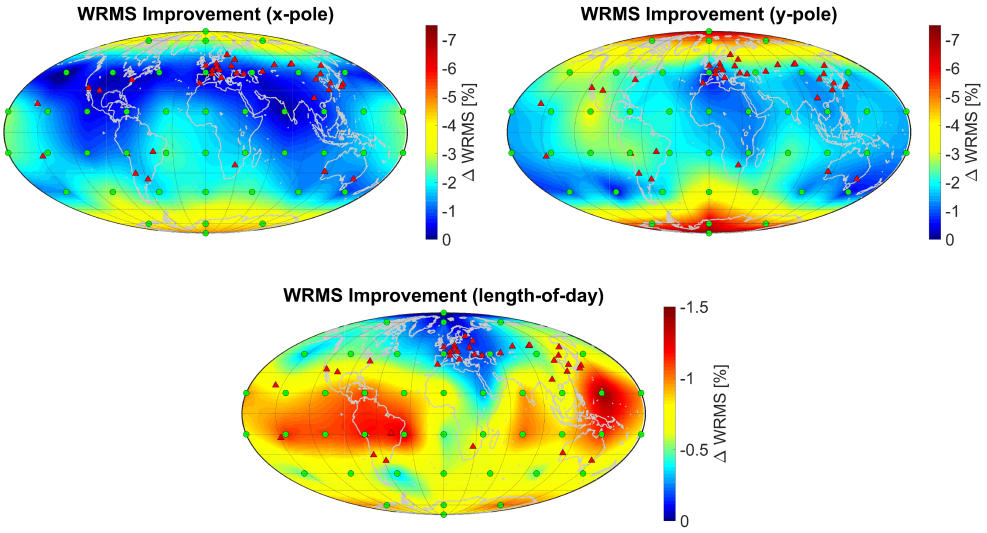

Figure 6.12: Improvement of the WRMS of the ERPs by one additional SLR station (note the different scales; for visualisation a triangulation-based natural neighbour interpolation was applied between the grid points). Red triangles mark the existing network, green circles the additional stations.

Figure 6.12 shows the results for the improvement of the estimated ERPs. It can be clearly seen that the impact of an additional station is systematically affected by the geographical dependence of the sensitivity to a certain ERP which is related to the axes along which the pole coordinates are defined. The maximum improvements for the pole coordinates could be achieved with stations in the polar regions (improvements up to 4.5 % and 7 % for x_{pole} and y_{pole}, respectively) as well as in equatorial regions along the planes through 30° W and 180° longitude for x_{pole} (defined in the direction of the zero meridian) and through 90° E and 90° W for y_{pole} (defined in the direction of 90° W) with a maximum of about 3 % for both pole coordinates. LOD is predominantly improved by stations in the equatorial region (maximum effect of Earth's rotation), but to a smaller extent by up to 1.5 % (note the different scaling of the colour bars in Figure 6.12). It is clearly visible that the potential for improvement is largest for y_{pole} with up to 7 % WRMS improvement, as the x_{pole} plane is already covered by a large number of stations in Europe (close to 0° longitude). This is also the reason why the improvement in the plane of 0° longitude is reduced and shifted towards the West into the Atlantic ocean, the "gap" between the European/African and American sub-networks. LOD is already well determined due to a distribution of the existing SLR stations in West-East direction. In general, an additional station in the southern

hemisphere has a larger potential to improve the estimated ERPs. Moreover, especially sites in the polar regions could help to improve the pole coordinates.

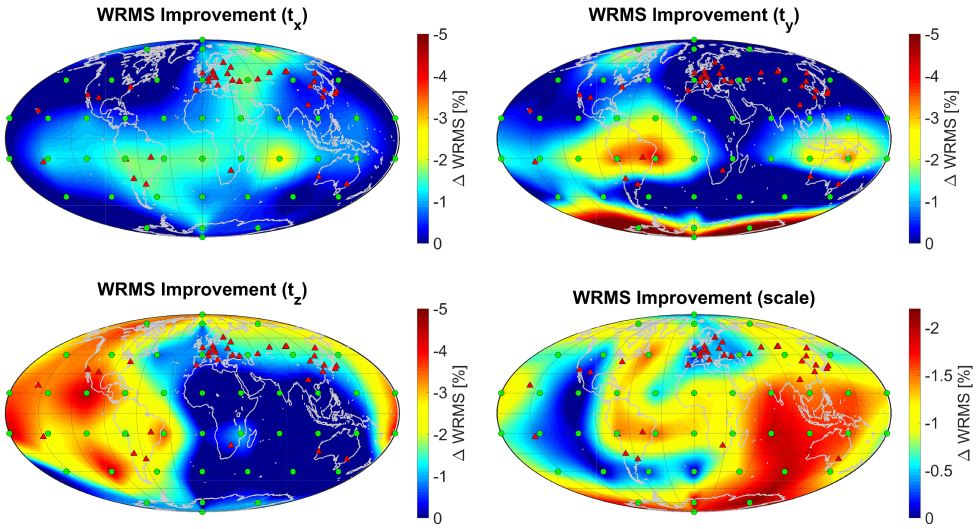

Figure 6.13: Improvement of the WRMS of the Helmert parameters by one additional SLR station (note the different scales; for visualisation a triangulation-based natural neighbour interpolation was applied between the grid points). Red triangles mark the existing network, green circles the additional stations.

Figure 6.13 shows the geographical dependence of the impact of an additional SLR station on the estimated datum parameters. The results follow a less systematic pattern than the ones obtained for the ERPs. Whereas the potential for improvement of the x-translation t_x is a WRMS reduction of up to 2.5 %, larger improvements can be achieved for the y-translation t_y by additional sites in the North of South America and the northern parts of the Australian continent (WRMS reduced by up to 4 %), as well as in Antarctica (WRMS reduction ≥ 5–7 %). The z-translation t_z is mainly improved by stations in the Pacific Ocean region, America, and around the Arctic (WRMS reduction up to 4.5 %). The WRMS of the scale can be improved significantly by up to 2.2 % by stations in America, the Indian Ocean, Australia and Antarctica, as well as to a smaller extent (WRMS reduction up to 1.5 %) by sites in Canada, the Pacific Ocean and the North of South America. The rough pattern of these results coincides with the results obtained by Otsubo et al. (2016), especially the large impact of additional stations in Antarctica on t_y and in South America on all three translations as well as the generally lower potential of improvement for the scale.

One of our conclusions from the study is that an additional SLR site in or close to the Antarctic should be one of the priorities for further investigation on an extended SLR ground segment. However, due to the exterior conditions like a rather high cloud coverage and snow and ice particles transported by katabatic winds, the actual tracking capability of an SLR site at these locations might be lower than the 20 % station

performance assumed here. In order to be able to give a measure for the impact of worse tracking conditions on our results, we performed an additional simulation for the grid point located at 75° S, 120° E, in an area located between the existing Syowa and McMurdo sites already being equipped with VLBI. [The site is marked with "AE" in Fig. 6.11.] We assigned a performance of 7 % (half of the average performance of the existing network) and re-performed the analysis for this grid point. With on average 3 passes per week on LAGEOS-1 and LARES and 2 passes per week on LAGEOS-2, this station would perform below the ILRS Pass Performance Standard.

Table 6.13: WRMS improvement [%] of the ERPs for an additional SLR site in Antarctica ("AE" in Fig. 6.11) with assumed performances of 20 % and 7 %.

Performance	x_{pole}	y_{pole}	LOD
20 %	−4.3	−4.8	−1.0
7 %	−1.5	−1.4	−0.3

As to be expected, the resulting improvements of the WRMS of the weekly solutions w.r.t. the a priori parameters get smaller. For the datum parameters, this is significantly visible for the y-translation t_{y} where the improvement decreases from 6.4 % to 2.3 %, i.e., by a factor of 2.8. The x- and z- translations and the scale are not largely affected as their improvements have already been rather small for this station. In case of the ERPs, the improvements decrease by a factor of 3.3 on average (cf. Tab. 6.13). Thus, if a single station is added to the network but achieves only about one third of the performance we aim at, a significant reduction in the WRMS improvement will be seen; however, the improvements of about 2.3 % (t_{y}) and 1.5 % (pole coordinates) by one single station are still significant, keeping in mind that the maximum values that can be obtained by adding a single station with 20 % performance are at a level of 2–7 % for the TRF-defining parameters as well as for the pole coordinates. This is due to the large improvement of the network and observation geometry by an SLR site in such a location.

6.7 Summary and discussion of the results

Within the previous sections, we investigated scenarios to improve the sensitivity of SLR to geodetic parameter groups related to the datum of terrestrial reference frames. Thereby, we could show that extending the SLR space segment by processing more observations to satellites that are already tracked would have two significant impacts, namely

(1) a decorrelation of various geodetic parameter groups estimated from SLR, and

(2) an improved sensitivity of the observations to the low-degree Stokes coefficients.

Both aspects in combination significantly improve the combined estimation of geodetic parameters. Consequently, including all spherical SLR satellites available into the ILRS products is crucial to achieve the goal of a fully physical realisation of a TRF datum including its orientation, or to study the variation of the Earth's principal axes of inertia with respect to the conventional TRF datum. In this context, as updated centre-of-mass correction tables currently are available only for selected satellites (Rodríguez et al., 2019), we consider it essential that these tables be extended for the remaining spherical satellites. Outreaching beyond the current situation, we simulated an additional satellite in a highly elliptic orbit, as it has been proposed within the framework of the E-GRASP/Eratosthenes mission proposal. Our simulation results indicate that such an orbit would significantly contribute to a more stable estimation of certain low-degree Stokes coefficients. Adding such an orbit to the constellation would especially help to decorrelate $C_{2,0}$ and the right ascensions of the ascending nodes of the satellite orbits, meaning that the geodetic parameters describing the physics of the Earth can be more reliably separated from those describing the constellation-related celestial mechanics.

Further simulation studies put focus on potential extensions or improvements of the SLR ground segment. Thereby, especially the repeatability of epoch-wise derived TRF datum parameters and ERPs have been our focus. We conclude that two components contribute to improving the realisation of SLR-derived TRFs and ERPs: First, improving the performance of the existing stations, and second, improving the geometry of the network. While the relative improvement of all parameters with respect to the current situation is highly dependent on the network performance (with a very high impact in case of very high performances, which is, however, unrealistic), it turns out to be crucial to fill gaps in the observational network of SLR. While the ERPs are already determined quite well by the existing network, the TRF datum parameters can be improved significantly by additional stations, especially in the Southern hemisphere. Our results indicate that an enhancement of the station-specific pass performances from 13 % on average to a minimum performance goal of 20 %, for example by automatisation of the systems, should go hand in hand in hand with establishing new stations in selected regions.

Going more into detail, we see that the optimal place for an additional SLR station is strongly dependent on the parameter of interest. We conclude that a reliable estimation of ERPs requires the SLR stations to be systematically distributed around the TRF axes' pierce points. To realise the TRF datum parameters, it turns out to be most valuable to fill gaps in the existing global station distribution, i.e., in and around the Pacific and Indian Oceans, Southeast Asia, and the polar regions. Consequently, the future station at Ny-Ålesund (cf. Pearlman and Noll, 2018) should be complemented by an additional station in the Antarctic region, as both prove valuable for both the ERPs and the TRF datum parameters. Such a station could be established at an existing VLBI site, as it is under investigation in case of the Japanese site Syowa (cf. Aoyama et al., 2017), and – as investigated in an additional scenario – also proves to be significant even if the local conditions do not allow to meet the performance goal of 20 %.

One main limiting factor of the performance of SLR stations are the actual, and potentially changing, local weather conditions, while our simulation studies relied on performance assumptions that have been kept constant over the simulation period. Consequently, any location for an additional SLR site should undergo a thorough investigation before a decision to erect a new system is taken. First of all, one should consider co-location sites with other techniques that allow for a better linking of the different space-geodetic observing networks via local ties, as their availability and distribution are very important factors that impact the reliability of the datum realisation for combined networks (Chapt. 5). In this context, Glaser et al. (2019a, b) confirm that the availability of well distributed and precisely measured local ties is crucial to be able to realise a consistent datum for all space-geodetic techniques contributing to a multi-technique reference frame. The focus of the simulation studies presented here has been on SLR-derived TRF datum parameters and ERPs only. Thus, in view of precise orbit determination, also other locations for additional SLR sites might turn out to be valuable.

Taking into account the aforementioned results and bearing in mind the increasing cost, we draw the following conclusions: First of all, the ILRS ACs should aim to include observations to all available spherical satellites into their routine products in order to exploit these observations for the determination of reliable geodetic parameters. Second, one should focus on improving the performances of the stations in the existing SLR network. This could be done by automated systems that do no longer rely on permanent on-site staff. Third, one should consider establishing new SLR stations in regions with low coverage. While we could demonstrate that filling the gaps in the observational network is highly beneficial for the SLR-derived geodetic parameters, the first priority should be to establish additional co-location sites with other space-geodetic techniques to enhance the distribution of local ties.

7 Conclusion and Outlook

This doctoral thesis presents a strategy to integrate currently available observation data of SLR, VLBI, and GNSS to realise an epoch-wise stable datum for a regional epoch reference frame. The datum is realised from global networks, whereby the goal parameters are the station coordinates from a regional network, in our case the Latin American SIRGAS GNSS station network. In this context, Chapter 5 addresses our first research question, namely

> **RQ 1** To what extent do currently available space-geodetic observations allow to realise a regional reference frame that is geocentric at any epoch, epoch-wise for short periods, and has a stable datum?

The implemented strategy compensates for the network effects of SLR and VLBI in order to achieve a reliable epoch-wise realisation of the origin and scale of the epoch reference frame. Thereby, the information content of the technique-specific normal equations of SLR and VLBI is filtered prior to the combination with GNSS. The filtering approach is designed to bridge observational gaps of individual stations up to several weeks, whereby only the stochastic model is modified in order to omit introducing external information about potential station motions. Comparisons with the JTRF2014 and geophysical models indicate that the realised station position time series reflect motions in a geocentric frame (cf. Sect. 5.5). The chosen filtering approach allows to bridge approximately 75 % of the observational gaps of both SLR and VLBI. This means that the approach achieves both a stabilisation of the datum parameters realised from SLR and VLBI and a more reliable datum transfer between the technique-specific networks due to an improved availability and distribution of local ties. Reflecting geocentric motions, the approach is suitable to study regional geophysical effects on short and long time scales. Avoiding the alignment of the datum to a global multi-year TRF, the approach does not rely on external and, in the extrapolation period of the multi-year TRF potentially degrading, information for the datum parameters origin and scale. With that, the approach can serve as independent reference for various applications in geosciences.

The results are based on a reprocessing of the available observations resulting in normal equation input data that are, or soon could, similarly be routinely provided by the IAG Scientific Services and the regional network analysis centres. Thereby, the realisation of the origin and scale relies on a fully reprocessed SLR constellation according to the future ILRS setup comprising five satellites and on a reprocessed VLBI contribution

according to the most recent standards and conventions. These global networks have been combined with a fully reprocessed globally-extended GNSS network that comprises all stations of the Latin American SIRGAS network plus the globally-distributed IGS sites in order to exploit all co-locations and to have a homogeneous network to apply a NNR constraint to realise the orientation. These global networks have been combined via local ties in order to transfer the datum information from SLR and VLBI (i.e., origin and scale) to the GNSS network and vice-versa (i.e., the orientation). As the approach relies on global networks and does not necessarily require local ties (or, in the classical sense, fiducial points) in the region of interest, the concept can be transferred to any other global region, including regions that have high geophysical activity limiting the number of locally available co-location sites with precisely measured local ties.

The results show that the space-geodetic techniques SLR, VLBI, and GNSS can be integrated to determine a reliable and epoch-wise datum, provided that the data undergo a filtering for the sake of datum stability issues caused by deficiencies of the networks. Thereby, it clearly turns out that the reliability of the realised origin is fully dependent on the SLR contribution. In this context, Chapter 6 addresses the second of our two research questions, namely

> **RQ 2** To what extent can further enhancements in the SLR space and ground segments improve the reliability of SLR-derived geodetic parameters with relation to the TRF datum?

While it is well known that SLR is crucial to determine the TRF origin, the results indicate that the potential of this space-geodetic technique, to date, is not fully exploited. Calculating multi-satellite solutions that integrate observations to up to 11 spherical satellites into one common solution, it can be shown that it is possible to decorrelate the different parameter groups to which SLR observations are sensitive, namely the satellite orbit parameters from the gravity field coefficients and the ERPs. This is an essential prerequisite for the integrated realisation of gravity and geometrical reference frames (having in mind that the TRF datum and the low-degree Stokes coefficients of the Earth's gravity field model are interdependent, cf. Sect. 3.1) as well as ERP time series, i.e., the different parameter groups to be integrated by GGOS (cf. Sect. 6.3). Simulation studies point out the relevance of further extensions and enhancements of the SLR space and ground segments. While a satellite in a highly elliptic orbit could be highly beneficial to improve the tesseral and sectoral low-degree coefficients of the Earth's gravity field model (cf. Sect. 6.5) – a crucial issue with respect to the physical realisation of the TRF orientation – a more homogeneous distribution of the global network of observing stations is indispensable to stabilise the derived geodetic parameters and should go hand in hand with a further enhancement of the station performances. Simulations of possible future scenarios show that the WRMS of the Helmert parameters can be reduced by up to 24 % if the station network is extended by eight globally-distributed stations, and by up to 41 % if, in addition, the station performances are increased to $\geq 20\,\%$ (cf. Sect. 6.6).

Having answered the two research questions posed in the beginning leads to the following conclusion:

Reliable epoch-wise short-term realisations of the ITRS require high-performing space-geodetic networks with homogeneous global coverage. This is of special relevance for the SLR network as this is the only technique allowing to realise the TRF origin with high accuracy.

The results demonstrate that the performance of the observational network has a significant impact on the reliability of the datum parameters realised. While observers should aim to avoid gaps in the observation time series and enhance the performances of the existing stations, analysts can try to compensate for remaining gaps through an appropriate filtering of the data. Both steps are essential to improve the long-term stability of the geodetic parameter estimates. Extending the ground and space segments of SLR further decorrelates the geodetic parameter groups related to the TRF datum and further improves the sensitivity of the observations to the low-degree Stokes coefficients that represent the physical realisation of the TRF datum. Finally, establishing new co-location sites with other space-geodetic techniques is essential to guarantee a reliable realisation of the geodetic datum in multi-technique combined reference frames.

In the future, SLR will gain relevance within the context of millimetric TRF realisation. Although investigations on exploiting other satellite techniques, mainly GNSS, do already deliver promising results, for the foreseeable future there is no alternative to SLR as the only space-geodetic technique realising the TRF origin with high accuracy. On the long term, a high-performing global SLR network will be a central contribution to the combined multi-satellite technique realisation of the TRF datum. While these solutions are developed, SLR will have the central role to provide the reference for validation of the datum realisation performed by the other satellite techniques.

In the context of exploiting existing and potential co-location sites, a review of the current non-standardised procedures of providing local ties should be considered, as it would be valuable if local ties would be re-measured and provided on a standardised regular basis. Moreover, the issue of using space ties for a more rigorous combination of the space-geodetic techniques should be investigated. In this context, the processing of SLR observations to GNSS satellites could be valuable to strengthen the link between those two space-geodetic networks, which could be a significant step towards meeting the ambitious goals of GGOS, namely the realisation of TRFs at sub-millimetre level.

Geocentric regional epoch reference frames available in (near-)real time with a stable datum have the potential to serve as a common reference to integrate different observation types from geodesy and geophysics in order to study local geophysical effects at low latencies. In this way, they can be a valuable complement to multi-year reference frames like the ITRF and sub-secular reference frames like the JTRF, which will remain the benchmarks for high-precision positioning and navigation relating to a stable reference over long time spans or for the precise determination of satellite orbits.

Acronyms

AC	Analysis Centre.
AGGO	Argentinean-German Geodetic Observatory.
BASH	Bourne-Again Shell.
BIH	Bureau International de l'Heure.
BKG	Bundesamt für Kartographie und Geodäsie/Federal Agency for Cartography and Geodesy.
BLITS	Ball Lens In The Space.
BNO	Bureau for Networks and Observations.
BTS	Bureau International de l'Heure Terrestrial System.
Caltech	California Institute of Technology.
CF	centre-of-figure.
CM	centre-of-mass.
CRF	celestial reference frame.
CRS	celestial reference system.
DB	Directing Board.
DGFI-TUM	Deutsches Geodätisches Forschungsinstitut at the Technical University of Munich.
DIGERATI	DIrect GEocentric Realisation of the American reference frame by combination of geodetic observation TechnIques.
DOGS	DGFI Orbit and Geodetic Parameter estimation Software.
DOGS-CS	— Combination and Solution library.
DOGS-RI	— Radio Interferometry software.
DOGS-OC	— Orbit Computation software.
DORIS	Doppler Orbitography and Radiopositioning Integrated by Satellite.
E-GRASP	European Geodetic Reference Antenna in Space.
EOP	Earth orientation parameter.
ERF	epoch reference frame.
ERP	Earth rotation parameter.
ESA	European Space Agency.

ESMGFZ	Earth System Modelling group at the Deutsches GeoForschungsZentrum Potsdam.
ETRS89	European Terrestrial Reference System 89.
EUREF	Reference Frame Sub Commission for Europe.
GCRS	geocentric celestial reference system.
GFC	gravity field coefficient (Stokes coefficient).
GFZ	Deutsches GeoForschungsZentrum Potsdam/GFZ German Research Centre for Geosciences.
GGOS	Global Geodetic Observing System.
GGOS-PLATO	— Committee on Performance Simulations and Architectural Trade-Offs.
GNSS	Global Navigation Satellite Systems.
HEO	High Earth Orbit.
IAG	International Association of Geodesy.
IAU	International Astronomical Union.
ICRF	International Celestial Reference Frame.
ICRS	International Celestial Reference System.
IDS	International DORIS Service.
IERS	International Earth Rotation and Reference Systems Service.
IGN	Institut national de l'information géographique et forestrière.
IGS	International GNSS Service.
ILRS	International Laser Ranging Service.
ITRF	International Terrestrial Reference Frame.
ITRS	International Terrestrial Reference System.
IUGG	International Union of Geodesy and Geophysics.
IVS	International VLBI Service for Geodesy and Astrometry.
JPL	Jet Propulsion Laboratory.
LAGEOS	Laser Geodynamics Satellite.
LARES	Laser Relativity Satellite.
LEO	Low Earth Orbit.
LOD	length-of-day.
LT	local tie.
MEO	Medium Earth Orbit.
NASA	National Aeronautics and Space Administration.

NEQ	normal equation.
NNR	no-net rotation.
NNS	no-net scale.
NNT	no-net translation.
NP	normal point.
NT-L	non-tidal loading.
PM	polar motion.
RMC	rotational minimal constraints.
RMS	root mean square.
RQ	research question.
SINEX	Solution INdependent EXchange format.
SIRGAS	Sistema de Referencia Geodésico para las Américas.
SLR	Satellite Laser Ranging.
Starlette	Satellite de Taille Adaptée avec Réflecteurs pour les Etudes de la Terre.
TCC	total cloud coverage.
TCG	Temps Coordonné Géocentrique.
TRF	terrestrial reference frame.
TRS	terrestrial reference system.
TUM	Technische Universität München/Technical University of Munich.
UT1	Universal Time (No. 1).
UTC	Coordinated Universal Time.
VLBI	Very Long Baseline Interferometry.
WESTPAC	Western Pacific Laser Tracking Network.
WRMS	weighted root mean square.

Bibliography

Abbondanza C., Chin T. M., Gross R. S., Heflin M. B., Parker J. W., Soja B. S., van Dam T., and Wu X. (2017). *JTRF2014, the JPL Kalman filter and smoother realization of the International Terrestrial Reference System.* Journal of Geophysical Research: Solid Earth, 122(10):8474–8510, DOI: 10.1002/2017JB014360.

Abbondanza C., Chin T. M., Gross R. S., Heflin M. B., Parker J. W., Soja B. S., and Wu X. (2020). *A sequential estimation approach to terrestrial reference frame determination.* Advances in Space Research, 65(4):1235–1249, DOI: 10.1016/j.asr.2019.11.016.

Altamimi Z., Rebischung P., Métivier L., and Collilieux X. (2016). *ITRF2014: A new release of the International Terrestrial Reference Frame modeling nonlinear station motions.* Journal of Geophysical Research: Solid Earth, 121(8):6109–6131, DOI: 10.1002/2016JB013098.

Altamimi Z. (2018). *EUREF Technical Note 1: Relationship and Transformation between the International and the European Terrestrial Reference Systems.* Technical report, Institut National de l'Information Géographique et Forestière (IGN), http://etrs89.ensg.ign.fr/pub/EUREF-TN-1.pdf.

Andritsch F., Grahsl A., Dach R., and Jäggi A. (2017). *Comparing tracking scenarios to LAGEOS and Etalon by simulating realistic SLR observations.* Geophysical Research Abstracts, 19(EGU2017-16642), http://www.bernese.unibe.ch/publist/2017/post/poster_fa.pdf.

Andritsch F., Grahsl A., Dach R., Schildknecht T., and Jäggi A. (2020). *Simulation of tracking scenarios to LAGEOS and Etalon satellites.* Journal of Geodesy, 94(40), DOI: 10.1007/s00190-019-01327-w.

Angermann D., Bloßfeld M., Seitz M., Kwak Y., Rudenko S., and Glomsda M. (2020). *ITRS Combination Centres: Deutsches Geodätisches Forschungsinstitut der TU München (DGFI-TUM).* In Dick W. R. and Thaller D. (Eds.), *IERS Annual Report 2018*, pages 162–166. Verlag des Bundesamtes für Kartographie und Geodäsie, Frankfurt am Main, Germany, ISBN: 978-3-86482-136-3, https://www.iers.org/IERS/EN/Publications/AnnualReports/AnnualReport2018.html.

Angermann D., Gruber T., Gerstl M., Heinkelmann R., Hugentobler U., Sánchez L., Steigenberger P., Gross R., Heki K., Marti U., Schuh H., Sehnal M., and Thomas M. (2022). *GGOS Bureau of Products and Standards: Description and promotion of geodetic products.* In *IAG 2021 Symposium Series (accepted).* Springer, DOI: 10.1007/1345_2022_144.

Aoyama Y., Doi K., Fukuda Y., Ikeda H., Hayakawa H., Fukuzaki Y., Sekido M., Otsubo T., Nogi Y., and Shibuya K. (2017). *Geodetic activities at Syowa Station, East Antarctica.* IAG-IASPEI Joint Scientific Assembly, Kobe, Japan, https://confit.atlas.jp/guide/event/iagiaspei2017/subject/G07-4-02/advanced.

Appleby G., Rodríguez J., and Altamimi Z. (2016). *Assessment of the accuracy of global geodetic satellite laser ranging observations and estimated impact on ITRF scale: estimation of systematic errors in LAGEOS observations 1993–2014*. Journal of Geodesy, 90(12):1371–1388, DOI: 10.1007/s00190-016-0929-2.

Arias E. F., Charlot P., Feissl M., and J.-F. L. (1995). *The extragalactic reference system of the International Earth Rotation Service, ICRS*. Astronomy and Astrophysics, 303:604–608.

Assimakis N., Adam M., and Douladiris A. (2012). *Information filter and kalman filter comparison: Selection of the faster filter*. In *Information Engineering*, volume 2, pages 1–5.

Bachmann S., Hellmers H., Schneider-Leck S., Geist S., Thaller D., Bloßfeld M., and Seitz M. (2021). *BKG/DGFI-TUM Combination Center 2019+2020 Biennial Report*. In Behrend D., Armstrong K. L., and Baver K. D. (Eds.), *International VLBI Service for Geodesy and Astrometry 2019+2020 Biennial Report. NASA/TP–20210021389*, pages 195–198. National Aeronautics and Space Administration, Goddard Space Flight Center, Greenbelt, MD, USA.

Barkin Y. V. and Ferrandiz J. M. (2000). *The motion of the Earth's principal axes of inertia, caused by tidal and rotational deformations*. Astronomical and Astrophysical Transactions, 18(4):605–620, DOI: 10.1080/10556790008208165.

Berger H. (1880). *Die geographischen Fragmente des Eratosthenes: Neu gesammelt, geordnet und besprochen von Dr. Hugo Berger*. Teubner, Leipzig, Germany.

Bevis M., Alsdorf D., Kendrick E., Fortes L. P., Forsberg B., Smalley Jr R., and Becker J. (2005). *Seasonal fluctuations in the mass of the Amazon River system and Earth's elastic response*. Geophysical Research Letters, 32(16), DOI: 10.1029/2005GL023491.

Biancale R. and Bode A. (2006). *Mean annual and seasonal atmospheric tide models based on 3-hourly and 6-hourly ECMWF surface pressure data. GeoForschungsZentrum Potsdam Scientific Technical Report STR06/01*. Technical report, GeoForschungsZentrum Potsdam (GFZ), Potsdam, Germany, DOI: 10.2312/GFZ.b103-06011.

Biancale R., Pollet A., Coulot D., and Mandea M. (2017). *E-GRASP/Eratosthenes: a mission proposal for millimetric TRF realization*. Geophysical Research Abstracts, 19(EGU2017-8752).

Bizouard C. and Gambis D. (2009). *The Combined Solution C04 for Earth Orientation Parameters Consistent with International Terrestrial Reference Frame 2005*. In Drewes H. (Ed.), *Geodetic Reference Frames. IAG Symposia 134*, pages 265–270. Springer, DOI: 10.1007/978-3-642-00860-3_41.

Bizouard C. and Gambis D. (2011). *The Combined Solution C04 for Earth Orientation Parameters Consistent with International Terrestrial Reference Frame 2008*. IERS notice, http://hpiers.obspm.fr/iers/eop/eopc04/C04.guide.pdf.

Bizouard C., Lambert S., Gattano C., Becker O., and Richard J.-Y. (2019). *The IERS EOP 14C04 solution for Earth orientation parameters consistent with ITRF 2014*. Journal of Geodesy, 93(5):621–633, DOI: 10.1007/s00190-018-1186-3.

Bloßfeld M., Gerstl M., Hugentobler U., Angermann D., and Müller H. (2014a). *Systematic effects in LOD from SLR observations*. Advances in Space Research, 54(6):1049–1063, DOI: 10.1016/j.asr.2014.06.009.

Bloßfeld M., Seitz M., and Angermann D. (2014b). *Non-linear station motions in epoch and multi-year reference frames.* Journal of Geodesy, 88(1):45–63, DOI: 10.1007/s00190-013-0668-6.

Bloßfeld M., Müller H., Gerstl M., Stefka V., Bouman J., Göttl F., and Horwath M. (2015a). *Second-degree Stokes coefficients from multi-satellite SLR.* Journal of Geodesy, 89(9):857–871, DOI: 10.1007/s00190-015-0819-z.

Bloßfeld M., Seitz M., and Angermann D. (2015b). *Epoch Reference Frames as Short-Term Realizations of the ITRS. Datum Stability versus Sampling.* In Rizos C. and Willis P. (Eds.), *IAG 150 Years. IAG Symposia 143*, pages 27–32. Springer, DOI: 10.1007/1345_2015_91.

Bloßfeld M. (2015). *The key role of Satellite Laser Ranging towards the integrated estimation of geometry, rotation and gravitational field of the Earth.* PhD Thesis. Deutsche Geodätische Kommission (DGK) Reihe C, 745. Verlag der Bayerischen Akademie der Wissenschaften in Kommission beim Verlag C. H. Beck, München (Munich), Germany, ISBN: 978-3-7696-5157-7.

Bloßfeld M., Seitz M., Angermann D., and Moreaux G. (2016). *Quality assessment of IDS contribution to ITRF2014 performed by DGFI-TUM.* Advances in Space Research, 58(12):2505–2519, DOI: 10.1016/j.asr.2015.12.016.

Bloßfeld M., Rudenko S., Kehm A., Panafidina N., Müller H., Angermann D., Hugentobler U., and Seitz M. (2018▪). *Consistent estimation of geodetic parameters from SLR satellite constellation measurements.* Journal of Geodesy, 92(9):1003–1021, DOI: 10.1007/s00190-018-1166-7.

Bloßfeld M. and Kehm A. (2020). *ILRS Analysis Activities. DGFI-TUM (Deutsches Geodätisches Forschungsinstitut – Technische Universität München), Germany.* In Noll C. and Pearlman M. (Eds.), *International Laser Ranging Service 2016–2019 Report. NASA/TP-20205008530*, pages 7-10–7-13. National Aeronautics and Space Administration, Goddard Space Flight Center, Greenbelt, MD, USA.

Bloßfeld M., Glomsda M., Kehm A., Gerstl M., and Müller H. (2021). *DOGS-CS 5.1 – File Format. Version 2.6.* Technical report, Deutsches Geodätisches Forschungsinstitut (DGFI-TUM), Technical University of Munich, Munich, Germany.

Böckmann S., Artz T., and Nothnagel A. (2010). *VLBI terrestrial reference contributions to ITRF2008.* Journal of Geodesy, 84(3):201–219, DOI: 10.1007/s00190-009-0357-7.

Boucher C. and Altamimi Z. (1985). *Towards an improved realization of the BIH terrestrial frame.* In Mueller I. I. (Ed.), *The MERIT/COTES Report on Earth Rotation and Reference Frames*, volume 2. Department of Geodetic Science, Ohio State University, Columbus, OH, USA.

Bouguer P. (1749). *La figure de la terre, Déterminée par les Observations de Messieurs Bouguer, & de la Condamine, de l'Académie Royale des Sçiences, envoyés par ordre du Roy au Pérou, pour observer aux environs de l'Equateur.* Charles-Antoine Jombert, Paris, France.

Bowman B. R., Tobiska W. K., Marcos F. A., Huang C. Y., Lin C. S., and Burke W. J. (2008). *A New Empirical Thermospheric Density Model JB2008 Using New Solar and Geomagnetic Indices. AIAA 2008-6438.* AIAA/AAS Specialist Conference and Exhibit. Honolulu, HI, USA, DOI: 10.2514/6.2008-6438.

Bruni S., Rebischung P., Zerbini S., Altamimi Z., Errico M., and Efisio S. (2018). *Assessment of the possible contribution of space ties on-board GNSS satellites to the terrestrial reference frame.* Journal of Geodesy, 92(3):383–399, DOI: 10.1007/s00190-017-1069-z.

Bruns H. (1878). *Die Figur der Erde. Ein Beitrag zur Europäischen Gradmessung.* P. Stankiewicz, Berlin, Germany.

Chen J. L., Wilson C. R., and Ries J. C. (2016). *Broadband assessment of degree-2 gravitational changes from GRACE and other estimates, 2002–2015.* Journal of Geophysical Research: Solid Earth, 121(3):2112–2128, DOI: 10.1002/2015JB012708.

Chin T. (2001). *On Kalman filter solution of space-time interpolation.* IEEE Transactions on Image Processing, 10(4):663–666, DOI: 10.1109/83.913601.

Clairaut A. C. (1743). *Théorie de la figure de la terre : tirée des principes de l'hydrostatique.* David Fils, Paris, France.

Collilieux X. and Altamimi Z. (2009). *Impact of the network effect on the origin and scale: case study of satellite laser ranging.* In Sideris M. G. (Ed.), *Observing our Changing Earth. Proceedings of the 2007 IAG General Assembly, Perugia, Italy, July 2–13, 2007*, pages 31–37. Springer, ISBN: 978-3-540-85426-5.

Collilieux X., Altamimi Z., Ray J., van Dam T., and Wu X. (2009). *Effect of the satellite laser ranging network distribution on geocenter motion estimation.* Journal of Geophysical Research: Solid Earth, 114(B4), DOI: 10.1029/2008JB005727.

Copernicus N. (1543). *De revolutionibus orbium cœlestium, Libri VI.* Ioh. Petreius, Norimbergæ (Nuremberg), Holy Roman Empire.

Couhert A., Bizouard C., Mercier F., Chanard K., Greff M., and Exertier P. (2020). *Self-consistent determination of the Earth's GM, geocenter motion and figure axis orientation.* Journal of Geodesy, 94(113), DOI: 10.1007/s00190-020-01450-z.

Coulot D., Berio P., Bonnefond P., Exertier P., Féraudy D., Laurain O., and Deleflie F. (2008). *Satellite Laser Ranging Biases and Terrestrial Reference Frame Scale Factor.* In Sideris M. G. (Ed.), *Observing our Changing Earth. IAG Symposia 133*, pages 39–46. Springer, DOI: 10.1007/978-3-540-85426-5_5.

Dach R., Lutz S., Walser P., and Fridez P. (2015). *Bernese GNSS Software Version 5.2.* Technical report, Astronomical Institute, University of Bern, Berne, Switzerland.

Desai S. D. (2002). *Observing the pole tide with satellite altimetry.* Journal of Geophysical Research, 107(C11):7-1–7-13, DOI: 10.1029/2001JC001224.

Dill R. and Dobslaw H. (2013). *Numerical simulations of global-scale high-resolution hydrological crustal deformations.* Journal of Geophysical Research: Solid Earth, 118(9):5008–5017, DOI: 10.1002/jgrb.50353.

Dill R., Dobslaw H., Hellmers H., Kehm A., Bloßfeld M., Thomas M., Seitz F., Thaller D., Hugentobler U., and Schönemann E. (2020). *Evaluating Processing Choices for the Geodetic Estimation of Earth Orientation Parameters with Numerical Models of Global Geophysical Fluids.* Journal of Geophysical Research: Solid Earth, 125(9):e2020JB02002, DOI: 10.1029/2020JB020025.

Dong D., Yunck T., and Heflin M. (2003). *Origin of the International Terrestrial Reference Frame.* Journal of Geophysical Research: Solid Earth, 108(B4), DOI: 10.1029/2002JB002035.

Drewes H., Angermann D., and Seitz M. (2013). *Alternative Definitions of the Rerrestrial Reference System and its Realization in Reference Frames.* In *Reference frames for applications in geosciences*, pages 39–44. Springer, DOI: 10.1007/978-3-642-32998-2_7.

Drewes H., Adám J., and Poutanen M. (2020). *The International Association of Geodesy. Historical Overview.* The Geodesist's Handbook 2020. Journal of Geodesy, 94(11):7–15, DOI: 10.1007/s00190-020-01434-z.

Einstein A. (1916). *Die Grundlage der allgemeinen Relativitätstheorie.* Annalen der Physik, 354(7):769–822, DOI: 10.1002/andp.19163540702.

Floberghagen R. (2001). *The Far Side: Lunar Gravimetry into the Third Millenium.* PhD Thesis. Technische Universiteit Delft, Delft, The Netherlands, ISBN: 90-9014693-8.

Folkner W. M., Williams J. G., and Boggs D. H. (2008). *The planetary and lunar ephemeris DE421. Memorandum IOM 343R-08-003.* Jet Propulsion Laboratory, California Institute of Technology. Pasadena, CA, USA.

Förste C., Bruinsma S., Shako R., Marty J.-C., Flechtner F., Abrykosov O., Dahle C., Lemoine J.-M., Neumayer K.-H., Biancale R., and EIGEN Team (2011). *EIGEN-6 – A new combined global gravity field model including GOCE data from the collaboration of GFZ-Potsdam and GRGS-Toulouse.* Geophysical Research Abstracts, 13(EGU2011-3242-2).

Gauss C. F. (1823). *Theoria combinationis observationum erroribus minimis obnoxiae.* In *Commentationes Societatis Regiae Scientiarum Gottingensis recentiores – Classis Physicae*, volume 5, pages 33–90. Henricus Dieterich, Gottingae (Göttingen), Kingdom of Hanover.

Gerstl M. (1997). *Parameterschätzung in DOGS-OC. DGFI Interner Bericht MG/01/1996/DGFI, 2. Auflage.* Technical report, Deutsches Geodätisches Forschungsinstitut (DGFI), Munich, Germany.

Gerstl M., Kelm R., Müller H., and Ehrnsperger W. (2008). *DOGS-CS – Kombination und Lösung großer Gleichungssysteme. DGFI Interner Bericht MG/01/1995/DGFI, Version 01.10.2008.* Technical report, Deutsches Geodätisches Forschungsinstitut (DGFI), Munich, Germany.

Glaser S., König R., Ampatzidis D., Nilsson T., Heinkelmann R., Flechtner F., and Schuh H. (2017). *A Global Terrestrial Reference Frame from simulated VLBI and SLR data in view of GGOS.* Journal of Geodesy, 91(7):723–733, DOI: 10.1007/s00190-017-1021-2.

Glaser S., König R., Neumayer K. H., Balidakis K., and Schuh H. (2019a). *Future SLR station networks in the framework of simulated multi-technique terrestrial reference frames.* Journal of Geodesy, 93(11):2275–2291, DOI: 10.1007/s00190-019-01256-8.

Glaser S., König R., Neumayer K. H., Nilsson T., Heinkelmann R., Flechtner F., and Schuh H. (2019b). *On the impact of local ties on the datum realization of global terrestrial reference frames.* Journal of Geodesy, 93(5):655–667, DOI: 10.1007/s00190-018-1189-0.

Glaser S., Michalak G., Männel B., König R., Neumayer K. H., and Schuh H. (2020). *Reference system origin and scale realization within the future GNSS constellation "Kepler".* Journal of Geodesy, 94(117), DOI: 10.1007/s00190-020-01441-0.

Glomsda M., Seitz M., Gerstl M., Kehm A., Bloßfeld M., and Angermann D. (2020). *Impact of new models for the ITRF2020 in VLBI analysis at DGFI-TUM.* In *AGU Fall Meeting 2020.* https://mediatum.ub.tum.de/?id=1586328.

Glomsda M., Bloßfeld M., Seitz M., and Seitz F. (2021a). *Correcting for site displacements at different levels of the Gauss-Markov model – A case study for geodetic VLBI.* Advances in Space Research, 68(4):1645–1662, ISSN: 0273-1177, DOI: https://doi.org/10.1016/j.asr.2021.04.006.

Glomsda M., Seitz M., Angermann D., and Gerstl M. (2021b). *DGFI-TUM Analysis Center Biennial Report 2019+2020.* In Behrend D., Armstrong K. L., and Baver K. D. (Eds.), *International VLBI Service for Geodesy and Astrometry 2019+2020 Biennial Report. NASA/TP–20210021389*, pages 201–205. National Aeronautics and Space Administration, Goddard Space Flight Center, Greenbelt, MD, USA.

Göttl F. (2013). *Kombination geodätischer Raumbeobachtungen zur Bestimmung von geophysikalischen Anregungsmechanismen der Polbewegung.* PhD Thesis. Deutsche Geodätische Kommission (DGK) Reihe C, 714. Verlag der Bayerischen Akademie der Wissenschaften in Kommission beim Verlag C. H. Beck, München (Munich), Germany, ISBN: 978-3-7696-5126-3.

Günther C. (2018). *Kepler – Satellite Navigation without Clocks and Ground Infrastructure.* In *Proceedings of the 31st International Technical Meeting of the Satellite Division of The Institute of Navigation (ION GNSS+ 2018)*, pages 849–856. Institute of Navigation (ION), ISBN: 0-936406-10-0, DOI: 10.33012/2018.15997.

Häfner M. (2019). *The Satellite Laser Ranging System of AGGO.* International Workshop for the Implementation of the Global Geodetic Reference Frame (GGRF) in Latin America, Buenos Aires, Argentina, https://www.sirgas.org/fileadmin/docs/GGRF_Wksp/49_Haefner_2019_AGGO-SLR.pdf.

Heath T. L. (Ed.) (1897). *The Works of Archimedes, Edited in Modern Notation with Introductory Chapters.* The University Press, Cambridge, United Kingdom.

Hellmers H., Thaller D., Bloßfeld M., Kehm A., and Girdiuk A. (2019). *Combination of VLBI Intensive Sessions with GNSS for generating Low Latency Earth Rotation Parameters.* Advances in Geosciences, 50:49–56, DOI: 10.5194/adgeo-50-49-2019.

Helmert F. R. (1880). *Die mathematischen und physikalischen Theorieen der höheren Geodäsie. Einleitung und I. Teil: Die mathematischen Theorieen.* Teubner, Leipzig, Germany.

Helmert F. R. (1884). *Die mathematischen und physikalischen Theorieen der höheren Geodäsie. II. Teil: Die physikalischen Theorieen, mit Untersuchungen über die mathematische Erdgestalt auf Grund der Beobachtungen.* Teubner, Leipzig, Germany.

Hofmann-Wellenhof B. and Moritz H. (2006). *Physical Geodesy. Second Edition.* Springer, Wien, Austria, ISBN: 978-3-211-33544-4.

Johnston G., Riddell A., and Hausler G. (2017). *The International GNSS Service.* In Teunissen P. J. G. and Montenbruck O. (Eds.), *Springer handbook of global navigation satellite systems*, pages 967–982. Springer, DOI: 10.1007/978-3-319-42928-1.

Kalman R. E. (1960). *A New Approach to Linear Filtering and Prediction Problems.* Transactions of the ASME–Journal of Basic Engineering, 82(Series D):35–45.

Kehm A., Bloßfeld M., Pavlis E. C., and Seitz F. (2018▪). *Future global SLR network evolution and its impact on the terrestrial reference frame.* Journal of Geodesy, 92(6):625–635, DOI: 10.1007/s00190-017-1083-1.

Kehm A., Bloßfeld M., König P., and Seitz F. (2019▪). *Future TRFs and GGOS–where to put the next SLR station?* Advances in Geosciences, 50:17–25, DOI: 10.5194/adgeo-50-17-2019.

Kehm A., Hellmers H., Bloßfeld M., Dill R., Angermann D., Seitz F., Hugentobler U., Dobslaw H., Thomas M., Thaller D., Böhm J., Schönemann E., Mayer V., Springer T., Otten M., Bruni S., and Enderle W. (2022a). *Combination strategy for consistent final, rapid and predicted Earth rotation parameters.* Submitted to Journal of Geodesy.

Kehm A., Sánchez L., Bloßfeld M., Seitz M., Drewes H., Angermann D., and Seitz F. (2022b▪). *Combination Strategy for the Geocentric Realization of Regional Epoch Reference Frames.* Journal of Geophysical Research: Solid Earth, 127(10):e2021JB023880, DOI: 10.1029/2021JB023880.

Kepler J. (1609). *Astronomia Nova Αιτιολογητος, Seu Physica Coelestis, tradita commentariis De Motibus Stellae Martis, Ex observationibus G. V. Tychonis Brahe.* Rudolphus II. Romanorum Imperator &c (Ed.), [Gotthard Vögelin], [Heidelberg], Holy Roman Empire.

Kepler J. (1619). *Harmonices mundi libri V.* Godofredus Tampachius Bibl. Francof. (Ed.), Ioannes Plancus, Lincii Austriae (Linz), Holy Roman Empire.

Knocke P. C., Ries J. C., and Tapley B. D. (1988). *Earth radiation pressure effects on satellites. AIAA 88-4292.* AIAA/AAS Astrodynamics Conference. Minneapolis, MN, USA, DOI: 10.2514/6.1988-4292.

Koch K.-R. (2004). *Parameterschätzung und Hypothesentests in linearen Modellen. Vierte, bearbeitete Auflage.* Ehemals Ferd. Dümmlers Verlag, Bonn, Germany, http://www.geod.uni-bonn.de.

Konopliv A. S., Asmar S. W., Carranza E., Sjogren W. L., and N. Y. D. (2001). *Recent gravity models as a result of the Lunar Prospector Mission.* Icarus, 150(1):1–18, DOI: 10.1006/icar.2000.6573.

Kotsakis C. (2012). *Reference frame stability and nonlinear distortion in minimum-constrained network adjustment.* Journal of Geodesy, 86(9):755–774, DOI: 10.1007/s00190-012-0555-6.

Kovalevsky J., Mueller I. I., and Kolaczek B. (Eds.) (1989). *Reference Frames in Astronomy and Geophysics.* Kluver Academic Publishers, Dordrecht, The Netherlands, ISBN: 0-7923-0182-X.

Kwak Y., Gerstl M., Bloßfeld M., , Angermann D., Schmid R., and Seitz M. (2017). *DOGS-RI: new VLBI analysis software at DGFI-TUM.* In Haas R. and Elgered G. (Eds.), *Proceedings of the 23rd European VLBI Group for Geodesy and Astrometry Working Meeting*, pages 212–215. Chalmers, ISBN: 978-91-88041-09-8.

Liu H. S. and Chao B. F. (1991). *The Earth's equatorial principal axes and moments of inertia.* Geophysical Journal International, 106(3):699–702, DOI: 10.1111/j.1365-246X.1991.tb06341.x.

Lyard F., Lefevre F., Letellier T., and Francis O. (2006). *Modelling the global ocean tides: modern insights from FES2004.* Ocean Dynamics, 56:394–415, DOI: 10.1007/s10236-006-0086-x.

Männel B. and Rothacher M. (2017). *Geocenter variations derived from a combined processing of LEO- and ground-based GPS observations.* Journal of Geodesy, 91(8):933–944, DOI: 10.1007/s00190-017-0997-y.

Männel B., Thaller D., Rothacher M., Böhm J., Müller J., Glaser S., Dach R., Biancale R., Bloßfeld M., Kehm A., Herrera Pinzón I., Hofmann F., Andritsch F., Coulot D., and Pollet A. (2018). *Recent Activities of the GGOS Standing Committee on Performance Simulations and Architectural Trade-Offs (PLATO).* In Freymueller J. and Sánchez L. (Eds.), *International Symposium on Advancing Geodesy in a Changing World. IAG Symposia 149*, pages 161–164. Springer, DOI: 10.1007/1345_2018_30.

Martens H. R., Simons M., Owen S., and Rivera L. (2016). *Observations of ocean tidal load response in South America from subdaily GPS positions.* Geophysical Journal International, 205(3):1637–1664, ISSN: 0956-540X, DOI: 10.1093/gji/ggw087.

Mathews P. M., Herring T. A., and Buffett B. A. (2002). *Modeling of nutation and precession: New nutation series for nonrigid Earth and insights into the Earth's interior.* Journal of Geophysical Research, 107(B4):2068, DOI: 10.1029/2001JB000390.

Mendes V. B. and Pavlis E. C. (2004). *High-accuracy zenith delay prediction at optical wavelengths.* Geophysical Research Letters, 31(14):L14602, DOI: 10.1029/2004GL020308.

Modiri S. (2021). *On the improvement of earth orientation parameters estimation: using modern space geodetic techniques.* PhD Thesis. Scientific Technical Report STR 21/10. GFZ German Research Centre for Geosciences, Potsdam, Germany, DOI: 10.48440/GFZ.b103-21107.

Newton I. (1687). *Philosophiæ naturalis principia mathematica.* Societatis Regiæ (Ed.), Joseph Streater, Londini (London), England.

Niemeier W. (2008). *Ausgleichungsrechnung. Statistische Auswertemethoden. 2. Auflage.* Walter de Gruyter, Berlin, Germany.

Nothnagel A., Artz T., Behrend D., and Malkin Z. (2017). *International VLBI service for geodesy and astrometry – Delivering high-quality products and embarking on observations of the next generation.* Journal of Geodesy, 91(7):711–721, DOI: 10.1007/s00190-016-0950-5.

Otsubo T. and Appleby G. M. (2003). *System-dependent center-of-mass correction for spherical geodetic satellites.* Journal of Geophysical Research, 108(B4):2201, DOI: 10.1029/2002JB002209.

Otsubo T., Sherwood R. A., Appleby G. M., and Neubert R. (2015). *Center-of-mass corrections for sub-cm-precision laser-ranging targets: Starlette, Stella and LARES.* Journal of Geodesy, 89(4):303–312, DOI: 10.1007/s00190-014-0776-y.

Otsubo T., Matsuo K., Aoyama Y., Yamamoto K., Hobiger T., Kubo-oka T., and Sekido M. (2016). *Effective expansion of satellite laser ranging network to improve global geodetic parameters.* Earth, Planets and Space, 68(1):1–7, DOI: 10.1186/s40623-016- 0447-8.

Pavlis E. C. and Kuźmicz-Cieślak M. (2009). *SLR and the next generation global geodetic networks.* Proceedings of the 16th International Workshop on Laser Ranging, https://cddis.nasa.gov/lw16/docs/papers/ggo_5_Pavlis_p.pdf.

Pavlis E. C., Kuzmicz-Cieslak M., and Evans K. (2018). *Expanded SLR Target Constellation for Improved Future ITRFs.* 21st International Workshop on Laser Ranging, Canberra, Australia, https://cddis.nasa.gov/lw21/docs/2018/posters/A4_Pavlis_Poster.pdf.

Pearlman M. R. and Noll C. (2018). *ILRS Central Bureau Report.* ILRS Governing Board Meeting, 21st International Workshop on Laser Ranging, Canberra, Australia, https://cddis.nasa.gov/lw21/docs/2018/presentations/ilrsgb_presentations_20181104.pdf.

Pearlman M. R., Noll C. E., Pavlis E. C., Lemoine F. G., Combrink L., Degnan J. J., Kirchner G., and Schreiber U. (2019). *The ILRS: approaching 20 years and planning for the future.* Journal of Geodesy, 93(11):2161–2180, DOI: 10.1007/s00190-019-01241-1.

Petit G. and Luzum B. (2010). *IERS Conventions (2010). IERS Technical Note 36, v 1.3.0.* Technical report, International Earth Rotation and Reference Systems Service, Frankfurt am Main, Germany, ISBN: 3-89888-989-6.

Plag H.-P. and Pearlman M. (Eds.) (2009). *Global Geodetic Observing System.* Springer, Berlin, Germany, ISBN: 978-3-642-02687-4.

Ptolemaeus C. (1482). *Cosmographia.* Transl.: Jacobus Angelus. Nicolaus Germanus (Ed.), Lienhart Holle, Ulm, Holy Roman Empire. Mainz, GM (Ink. 1062).

Ray R. D., Steinberg J., Chao B. F., and Cartwright D. E. (1994). *Diurnal and Semidiurnal Variations in the Earth's Rotation Rate Induced by Oceanic Tides.* Science, 264(5160):830–832, DOI: 10.1126/science.264.5160.830.

Ray R. D. and Ponte R. M. (2003). *Barometric tides from ECMWF operational analyses.* Annales Geophysicae, 21:1897–1910, DOI: 10.5194/angeo-21-1897-2003.

Rebischung P., Schmid R., and Herring T. (2016). *Upcoming switch to IGS14/igs14.atx.* https://lists.igs.org/pipermail/igsmail/2016/001233.html.

Ries J., Bettadpur S., Eanes R., Kang Z., Ko U., McCullough C., Nagel P., Pie N., Poole S., Richter T., Save H., and Tapley B. (2016). *Development and Evaluation of the Global Gravity Model GGM05. CSR-16-02.* Technical report, Center for Space Research, The University of Texas at Austin, Austin, TX, USA.

Rodríguez J., Appleby G., and Otsubo T. (2019). *Updated modelling for the determination of centre of mass corrections of geodetic SLR satellites: impact on key parameters of the terrestrial reference frame.* Journal of Geodesy, 93(12):2553–2568, DOI: 10.1007/s00190-019-01315-0.

Rosat S., Gillet N., Boy J.-P., Couhert A., and Dumberry M. (2020). *Interannual variations of degree 2 from geodetic observations and surface processes.* Geophysical Journal International, 225(1):200–221, DOI: 10.1093/gji/ggaa590.

Rudenko S., Bloßfeld M., Müller H., Dettmering D., Angermann D., and Seitz M. (2018). *Evaluation of DTRF2014, ITRF2014, and JTRF2014 by Precise Orbit Determination of SLR Satellites.* IEEE Transactions on Geoscience and Remote Sensing, 56(6):3148–3158, DOI: 10.1109/TGRS.2018.2793358.

Rudenko S., Bloßfeld M., and Zeitlhöfler J. (2021). *DGFI-TUM Associate Analysis Center.* In Soudarin L. and Ferrage P. (Eds.), *International DORIS Service Activity Report 2019–2020*, pages 71–76. International DORIS Service, Central Bureau, https://ids-doris.org/documents/report/IDS_Report_2019-2020.pdf.

Rummel R. (2000). *Global Integrated Geodetic and Geodynamic Observing System (GIGGOS).* In Rummel R., Drewes H., Bosch W., and Hornik H. (Eds.), *Towards an Integrated Global Geodetic Observing System (IGGOS). IAG Symposia 120*, pages 253–260. Springer, DOI: 10.1007/978-3-642-59745-9_53.

Sánchez L., Drewes H., Brunini C., Mackern M., and Martínez-Díaz W. (2016). *SIRGAS core network stability.* In Rizos C. and Willis P. (Eds.), *IAG 150 Years. IAG Symposia 143*, pages 183–191. Springer, DOI: 10.1007/1345_2015_143.

Sánchez L. and Drewes H. (2016). *Crustal deformation and surface kinematics after the 2010 earthquakes in Latin America.* Journal of Geodynamics, 102:1–23, DOI: 10.1016/j.jog.2016.06.005.

Sánchez L. and Drewes H. (2020). *Geodetic monitoring of the variable surface deformation in Latin America.* In Freymueller J. and Sánchez L. (Eds.), *IAG Symposia 152.* DOI: 10.1007/1345_2020_91.

Sánchez L. and Kehm A. (2021). *SIRGAS Regional Network Associate Analysis Centre (IGS RNAAC SIRGAS) Technical Report.* In Villiger A. and Dach R. (Eds.), *International GNSS Service Technical Report 2020 (IGS Annual Report)*, pages 135–146. IGS Central Bureau and University of Bern; Bern Open Publishing, DOI: 10.48350/156425.

Savcenko R. and Bosch W. (2012). *EOT11A – Empirical Ocean Tide model from multi-mission satellite altimetry. Report No. 89.* Technical report, Deutsches Geodätisches Forschungsinstitut (DGFI), Munich, Germany.

Schön S. and Kutterer H. (2007). *A comparative analysis of uncertainty modelling in GPS data analysis.* In Tregoning P. and Rizos R. (Eds.), *Dynamic Planet: Monitoring and Understanding a Dynamic Planet with Geodetic and Oceanographic Tools. IAG Symposia 130*, pages 137–142. Springer, DOI: 10.1007/978-3-540-49350-1_22.

Schön S. and Brunner F. K. (2008). *A proposal for modelling physical correlations of GPS phase observations.* Journal of Geodesy, 82(10):601–612, DOI: 10.1007/s00190-008-0211-3.

Seitz F. and Krügel M. (2009). *Inverse model approach for vertical load deformations in consideration of crustal inhomogeneities.* In Drewes H. (Ed.), *Geodetic Reference Frames. IAG Symposia 134*, pages 23–29. Springer, DOI: 10.1007/978-3-642-00860-3_4.

Seitz M., Angermann D., Bloßfeld M., Drewes H., and Gerstl M. (2012). *The 2008 DGFI realization of the ITRS: DTRF2008.* Journal of Geodesy, 86(12):1097–1123, DOI: 10.1007/s00190-012-0567-2.

Seitz F., Hedman K., Meyer F. J., and Lee H. (2014). *Multi-sensor space observation of heavy flood and drought conditions in the Amazon region.* In Rizos C. and Willis P. (Eds.), *Earth on the Edge: Science for a Sustainable Planet. IAG Symposia 139*, pages 311–317. Springer, DOI: 10.1007/978-3-642-37222-3_41.

Seitz M., Angermann D., Gerstl M., Bloßfeld M., Sánchez L., and Seitz F. (2015). *Geometrical Reference Systems.* In Freeden W., Nashed M. Z., and Sonar T. (Eds.), *Handbook of Geomathematics. Second Edition*, pages 1995–3034. Springer, ISBN: 978-3-642-54550-4.

Seitz M., Bloßfeld M., Angermann D., and Seitz F. (2022). *DTRF2014: DGFI-TUM's ITRS realization 2014.* Advances in Space Research, 69(6):2391–2420, DOI: 10.1016/j.asr.2021.12.037.

Sośnica K., Thaller D., Jäggi A., Dach R., and Beutler G. (2012). *Sensitivity of Lageos Orbits to Global Gravity Field Models.* Artificial Satellites, 47(2):47–65, DOI: 10.2478/v10018-012-0013-y.

Sośnica K. (2015). *LAGEOS Sensitivity to Ocean Tides.* Acta Geophysica, 63(4):1181–1203, DOI: 10.1515/acgeo-2015-0032.

Sośnica K., Jäggi A., Meyer U., Thaller D., Beutler G., Arnold D., and Dach R. (2015). *Time variable Earth's gravity field from SLR satellites.* Journal of Geodesy, 89(10):945–960, DOI: 10.1007/s00190-015-0825-1.

Steigenberger P., Rothacher M., R. S., Rülke A., Fritsche M., Dietrich R., and Tesmer V. (2009). *Effects of Different Antenna Phase Center Models on GPS-Derived Reference Frames.* In Drewes H. (Ed.), *Geodetic Reference Frames. IAG Symposia 134*, pages 83–88. Springer, DOI: 10.1007/10.1007/978-3-642-00860-3_13.

Stocks J. L. (Ed.) (1922). *De caelo.* The Clarendon Press, Oxford, United Kingdom. Original work by Aristoteles (c. 350 BC).

Tapley B. D., Flechtner F., Bettadpur S. V., and Watkins M. M. (2013). *The Status and Future Prospect for GRACE After the First Decade.* American Geophysical Union Fall Meetings, 2013(G32A-01).

Torge W. (2001). *Geodesy. 3rd Edition.* Walter de Gruyter, Berlin, Germany; New York, USA, ISBN: 3-11-017072-8.

Villiger A., Dach R., Schaer S., Prange L., Zimmermann F., Kuhlmann H., Wübbena G., Schmitz M., Beutler G., and Jäggi A. (2020). *GNSS scale determination using calibrated receiver and Galileo satellite antenna patterns.* Journal of Geodesy, 94(93), DOI: 10.1007/s00190-020-01417-0.

Willis P., Lemoine F. G., Moreaux G., Soudarin L., Ferrage P., Ries J., Otten M., Saunier J., Noll C., Biancale R., and Luzum B. (2015). *The International DORIS Service (IDS): Recent Developments in Preparation for ITRF2013.* In Rizos C. and Willis P. (Eds.), *IAG 150 Years. IAG Symposia 143*, pages 631–640. Springer, DOI: 10.1007/1345_2015_164.

Zelensky N. P., Lemoine F. G., Beckley D. B., Chinn D. S., and Pavlis D. E. (2018). *Impact of ITRS 2014 realizations on altimeter satellite precise orbit determination.* Advances in Space Research, 61(1):45–73, DOI: 10.1016/j.asr.2017.07.044.

List of Figures

List of Tables

Scientific environment

The scientific studies presented within this doctoral thesis have primarily been conducted within the framework of the project *DIrect GEocentric Realisation of the American reference frame by combination of geodetic observation TechnIques* (DIGERATI) funded by the German Research Foundation (DFG) under grant no. SE 1916/5-1, which is gratefully acknowledged. The work has been performed at the Deutsches Geodätisches Forschungsinstitut (DGFI-TUM) at the Technical University of Munich (TUM) and included a research stay at the NASA Jet Propulsion Laboratory (JPL) at the California Institute of Technology (Caltech).

SLR observation data are provided by the International Laser Ranging Service (ILRS) and were accessed via the EUROLAS Data Centre hosted at DGFI-TUM (EDC, `https://edc.dgfi.tum.de/en/`; 2022-06-15). VLBI observation data are provided by the International VLBI Service for Geodesy and Astrometry (IVS) and were accessed via NASA's Crustal Dynamics Data Information System (CDDIS, `https://cddis.nasa.gov`; 2022-06-15). GNSS data of the global IGS stations are provided by the International GNSS Service (IGS) and were accessed via NASA's CDDIS. The GNSS data of the SIRGAS stations are provided by the SIRGAS Data Centres to DGFI-TUM in its function as IGS Regional Network Associate Analysis Centre for SIRGAS (`https://www.sirgas.org`; 2022-06-15).

Appendix

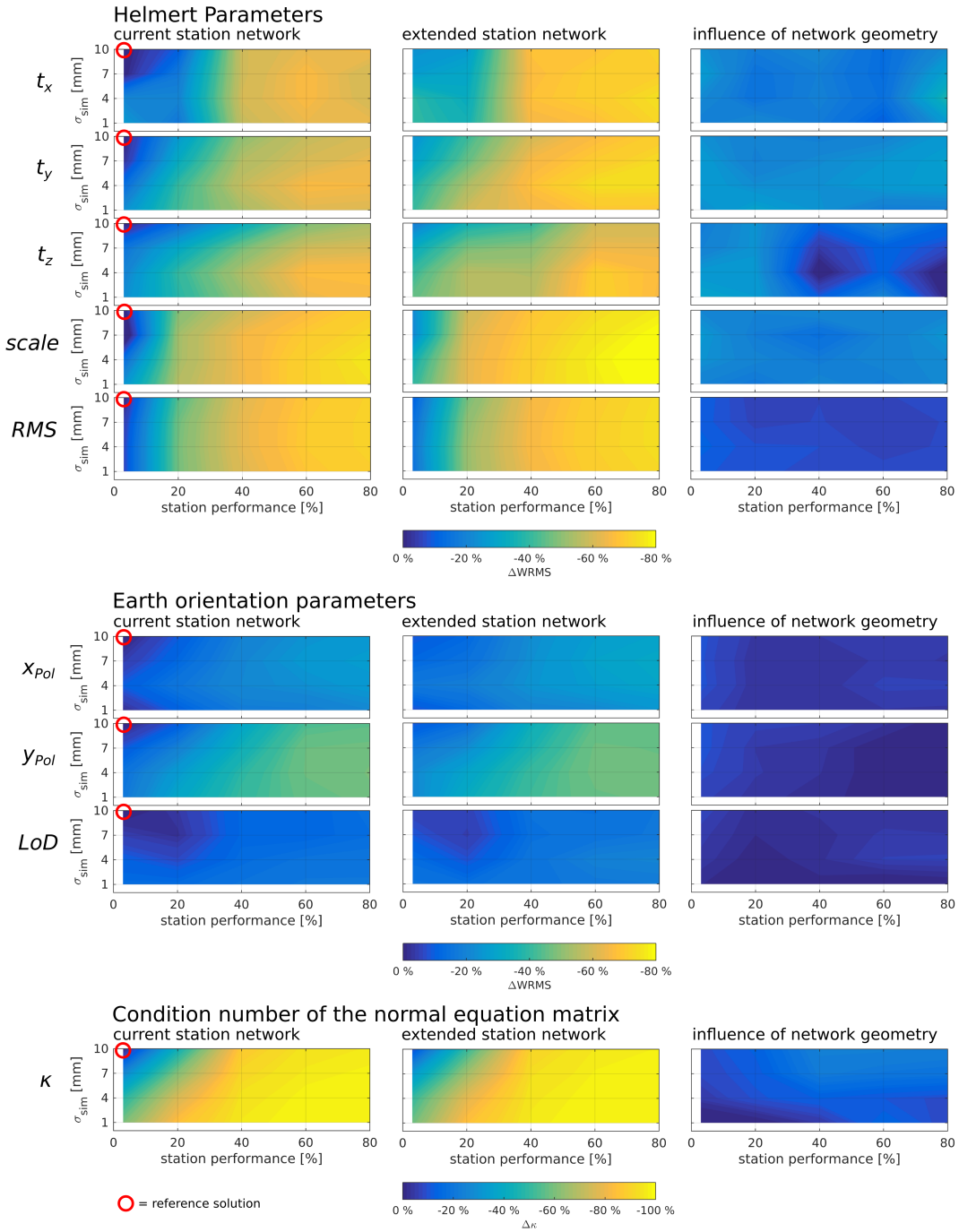

Figure A.1: Solutions from *Study A*. The x-axes represent the minimum station performance, the y-axes represent the simulation noise of a scenario. First column: relative WRMS improvement w.r.t. reference scenario (σ_{sim} = 10 mm, real performances), starting with 0 % improvement in the upper left of a plot (red circles). Second column: same as before but with extended station network, i.e., combined effect of technical improvement and network geometry. Third column: effect of network geometry only, i.e., relative improvement between scenarios with current and the extended station networks assuming the same noise and performance conditions.

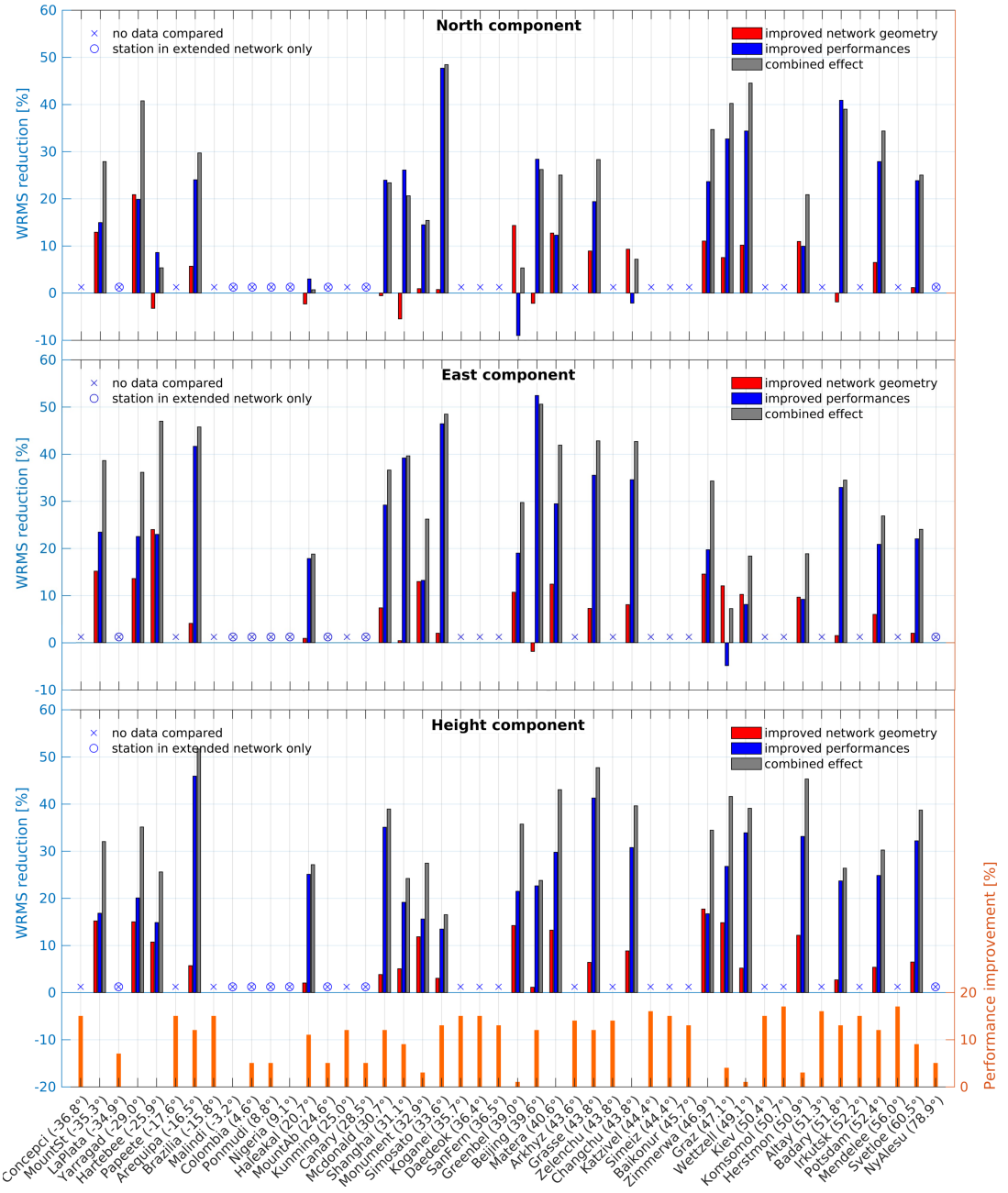

Figure A.2: Improvement of the WRMS of the station coordinates from *Study A*. Only stations present in the solutions within the same number of weeks are compared. Shown is the average WRMS improvement due to an improved network geometry (red) and due to improved station performances (blue). WRMS reductions given in percentage w.r.t. the WRMS of the reference solution. The sum of the red and blue bars reflects the combined effect (grey). The indicated performance improvement (bottom, orange) is the difference between a station's real performance and its improved performance of 20 % at minimum. If it is zero, the station's performance has already been equal to or higher than 20 % in the reference scenario. Stations sorted by latitude from South to North.

Danksagung

Mein Dank gilt zuallererst meinem Doktorvater und Erstgutachter Herrn Prof. Dr.-Ing. habil. Florian Seitz dafür, dass er mir die Arbeit am Deutschen Geodätischen Forschungsinstitut der Technischen Universität München (DGFI-TUM) sowie den wissenschaftlichen Austausch im internationalen Umfeld ermöglicht, meine Arbeit über den gesamten Zeitraum hervorragend betreut und auf diese Weise wesentlich zur Motivation und zum Gelingen dieser Arbeit beigetragen hat.

Außerdem gilt mein Dank den Gutachtern Prof. Dr. Urs Hugentobler und Adjunct Prof. Dr. Richard Gross für die sorgfältige fachliche Begutachtung der Arbeit. Richard Gross möchte ich darüber hinaus dafür danken, dass er mir einen Forschungsaufenthalt am NASA Jet Propulsion Laboratory möglich gemacht hat. Die hierbei gewonnenen Erfahrungen sind von unschätzbarem Wert!

Mein besonderer Dank gilt Dr.-Ing. Laura Sánchez, ohne deren Beitrag – die Diskussion der Methodik sowie eine vollständige Reprozessierung der Beobachtungsdaten des regionalen südamerikanischen SIRGAS-Stationsnetzes als Eingangsdatensatz – diese Arbeit nicht möglich gewesen wäre. Darüber hinaus gilt mein besonderer Dank meinem Mentor Dr.-Ing. Mathis Bloßfeld, dem Leiter des Forschungsbereichs Referenzsysteme am DGFI-TUM Dr.-Ing. Detlef Angermann sowie meiner Kollegin Dr.-Ing. Manuela Seitz. Sie alle haben mich bei den Problemen, die sich mir im Rahmen dieser Arbeit in den Weg stellten, unterstützt und hatten stets ein offenes Ohr für meine Fragen.

Ebenso möchte ich mich bei allen aktuellen und ehemaligen Kolleginnen und Kollegen an unserem Institut bedanken. Es sind das fruchtbare wissenschaftliche und das angenehme private Umfeld an unserem Institut, die wertvolle Impulse zur Erstellung dieser Arbeit beigetragen haben. Hervorheben möchte ich hierbei insbesondere meine Mitpromovenden Dr.-Ing. Felix Müller, Christian Schwatke und Matthias Glomsda, die mich – teils vom ersten Tag an – über die Zeit der Promotion hinweg begleitet und unterstützt haben.

Mein Dank gilt ebenso allen institutsfremden Kolleginnen und Kollegen, mit denen ich im Rahmen verschiedener Projekte zusammenarbeiten und auf nationalen und internationalen Konferenzen wissenschaftlichen Austausch betreiben durfte. Auch sie alle haben wertvolle Impulse für diese Arbeit geliefert.

Zu guter Letzt möchte ich mich auch bei meinen Eltern dafür bedanken, dass sie mir Studium und Promotion überhaupt erst ermöglicht und meinen Weg mitgetragen haben.